

# **NPL REPORT OP5**

# **CONTROLS Deliverable 10:**

Measurement report CEOS WGCV pilot comparison of techniques and instruments used for the vicarious calibration of land surface imaging through a ground reference standard test site 2009

Irina Behnert, Andrew Deadman, Nigel Fox, Peter Harris, NPL Selime Gürol, Hilal Özen, TU (Tubitak Space Technologies Research Institute, Turkey)

Martin Bachmann, DLR (German Remote Sensing Data Centre) Yannick Boucher, ONERA (French Aerospace Lab) Sophie Lachérade, CNES (French National Aerospace Agency)

February 2011













# Measurement report CEOS WGCV pilot comparison of techniques and instruments used for the vicarious calibration of land surface imaging through a ground reference standard test site 2009

Irina Behnert, Andrew Deadman, Nigel Fox, Peter Harris\* National Physical Laboratory, Engineering Measurement Division and \*Mathematics and Scientific Computing

Selime Gürol, Hilal Özen, TU (Tubitak Space Technologies Research Institute, Turkey)

Martin Bachmann, DLR (German Remote Sensing Data Centre)

Yannick Boucher, ONERA (French Aerospace Lab)

Sophie Lachérade, CNES (French National Aerospace Agency)

# **ABSTRACT**

This report presents the procedures and results of the 2009 Committee of Earth Observation Systems (CEOS) pilot land comparison of techniques and instruments used for the vicarious calibration of optical remote sensors over a reference standard test site Tuz Gölü, Turkey. The principal objective of this pilot comparison was to evaluate and optimise the procedures needed for a full CEOS comparison to be held at the same site in 2010. The measurement campaign participants were: CNES (French National Aerospace Agency), DLR (German Remote Sensing Data Centre), ONERA (French Aerospace Lab), TU (Tubitak Space Technologies Research Institute, Turkey) and NPL (National Physical Laboratory, UK), where NPL was the pilot of this comparison. The report contains a detailed description of the instrumentation used by each participant, the instrumentation calibration and traceability to SI standards, techniques used to characterise the site and the comparison of the results obtained by different teams. The results of 2009 CEOS pilot land comparison demonstrated that the four days of field measurements were not enough to assess all sources of uncertainty.

# © Crown copyright 2011 Reproduced with the permission of the Controller of HMSO and Queen's Printer for Scotland

# ISSN 1754-2944

National Physical Laboratory Hampton Road, Teddington, Middlesex, TW11 0LW

Extracts of this report may be reproduced provided the source is acknowledged and the extract is not taken out of the context.

Approved on behalf of the Managing Director, NPL by Ian Severn, Engineering Measurement, Business Leader

# **Contents**

1	Intro	oduction	6
	1.1	Scope	6
	1.2	Summary of outcomes	
	1.3	Structure of this report	8
2	CEC	OS pilot land comparison 2009 Turkey	9
	2.1	Participants	10
	2.2	Schedule	11
	2.3	Instrumentation	13
3	Cros	ss-comparison of instrumentation	14
	3.1	Laboratory measurements: Cross-comparison against TSARS	14
	3.1.1	Radiance and reflectance factor	15
	3.1.2	Data	16
	3.1.3	Combined standard uncertainty	16
	3.1.4	Calibration against TSARS	19
	3.1.5	Calibration checks	22
	3.1.6	Correction of measured radiance values	25
	3.2	Field measurements: Cross-comparison against reference panels	
	3.2.1	1 2	
	3.2.2		
	3.2.3		
	3.2.4	Results of cross-comparison against reference panels	31
	3.2.5		
	3.3	Field measurements: Cross-comparison against NPL reference panel	
	3.3.1	1 0	
	3.3.2		
	3.3.3	v v i	
	3.3.4		
4	Site	surface characterisation	
	4.1	Reflectance factor	45
	4.1.1		
	4.1.2		
	4.1.3		
	4.1.4		
	4.1.5		
	4.1.6		
		BRDF	
	4.2.1		
	4.2.2		
	4.2.3	····································	
	4.2.3 4.2.4	<i>y y</i> 1 0	
	4.2.5		
5		ospheric characterisation	
J		-	
	5.1	Aerosols optical properties and Water Vapour	
	5.1.1	1	
	5.1.2	Sources of uncertainty	II

	5.1.	3 Data	71
	5.1.		
	5.2	Meteorological data	73
6	Uno	ertainty estimation	75
	6.1	Experimental standard deviation for measured values of radiance	75
	6.2	Calibration checks	
	6.3	Correcting measured radiance values	
	6.4	Characterization of the site	79
7	Cor	nclusions	83
A	ppendi	x A: Instrumentation	85
	ASD I	FieldSpec3 spectroradiometer	85
		RAdiometric Spectrometer System (GRASS)	
	CIME	L automatic sunphotometer	88
	MICR	OTOPS handheld sunphotometer	89
	Transf	er Standard Absolute Radiance Source (TSARS)	90
A	ppendi	x B: Definition of terms	92
A	ppendi	x C: Participants' reported data	93
A	ppendi	x D: BRDF data	94
A	ppendi	x E: BRDF Type A standard uncertainty	105
A	ppendi	x F : Airborne hyperspectral data	109
R	eferen	ces	110

### 1 Introduction

# 1.1 Scope

One of the principal aims of the 2009 Committee of Earth Observation Systems (CEOS) pilot land comparison was to evaluate, and optimise, the procedures to be used for a full CEOS Comparison in 2010. These comparisons are designed to evaluate instruments and techniques used in the post-launch calibration of optical remote sensors. The Tuz Gölü, Turkey, reference test site provides a convenient location for these comparisons.

The objectives were sub-divided into the following [1]:

- 1) Evaluate differences in field instrument primary calibrations
  - a. Reference standard source used and traceability (based on "Laboratory calibration")
  - b. In-situ calibrations and validations of instrumentation
- 2) Evaluate differences in methods for characterising and assigning a radiometric value or a reflectance value to the site
  - a. Small area 100 m x 300 m for high-resolution imagers
  - b. Large area 1 km x 1 km for medium-resolution imagers
- 3) Establish formal traceability of the Tuz Gölü reference test site based on an evaluation of all comparison results
- 4) Establish best practice guidance for the above and/or knowledge of the differences between methodologies
- 5) Undertake a multi-sensor (satellite and aircraft) comparison linked to the ground calibration derived from the multi-team comparison
- 6) Identify the minimum and ideal specifications for characterisation/instrumentation for a CEOS "reference standard"

# 1.2 Summary of outcomes

The 2009 CEOS pilot land comparison took place between 23rd August 2009 and 29<sup>th</sup> August 2009 and had five participants: CNES (French National Aerospace Agency), DLR (German Remote Sensing Data Centre), ONERA (French Aerospace Lab), TU (Tubitak Space Technologies Research Institute, Turkey) and NPL (National Physical Laboratory, UK), where NPL was the pilot of this comparison. Variability in weather conditions meant that the planned timescale (two days for laboratory crosscomparisons and four days for field measurements) was not enough to fulfil all the objectives listed above. A longer period of time is thus planned for the 2010 CEOS Comparison.

1) The laboratory cross-comparisons of instrumentation followed the schedule as planned. However, it was not possible to assess the importance of the influence of the ambient conditions in the Ankara University laboratory (temperature and humidity), as these were not monitored during the calibration activities. The scheduled field cross-comparisons were limited by the presence of cirrus, which influenced the illumination conditions. The variable meteorological conditions found at Tuz Gölü and the importance of the CEOS comparison led us to the

conclusion that a significant contingency in available time was required to ensure a satisfactory conclusion in the future.

2) A number of factors produced differences in the measured radiometric value or reflectance factor of the site. Whilst not all have been fully evaluated at the time of writing of this report they fall into three main categories: i/ Software used to process results, ii/ Instrument degradation during the campaign (e.g., likely damage to the input collection fibre) and iv/ Methodology used to calibrate the reference panel (i.e. hemispherical or goniometric illumination). These effects introduced biases into the participants' reported Reflectance factor, ρ values over the site as summarised in Table 1. These biases were most visible when the participants sampled the 100 m x 300 m sites. The biases in the participants' ρ reported values of the surface became less significant for the 1 km x 1 km sampling site which was carried out at the beginning of the campaign and before one of the instruments appeared to degrade. A change of this radiometer was also observed in the pre- and post- campaign laboratory instrument calibration checks done by NPL. The owner reported this degradation as well, based on their post-campaign laboratory calibration.

	Instrument	Panel calibration	Software
DLR	ASD, 2005	Diffuse Illumination	DLR software
	Type A ~ 0.1%	Labsphere	VNIR $\rho$ is 6% lower
	400 - 1800  nm		-
ONERA	ASD, 2005	Diffuse Illumination	ASD software
	Type A ~ 0.1%	Labsphere	
	400 - 1800  nm		
TU	ASD, 2008	Bi-directional Illumination	ASD software
	Type A < $0.05\%$	for $\theta_{\rm S} = 47^{\circ}$ , 37°, 30°,	
	400 – 1800 nm	nadir view	
		VNIR $\rho$ is 5% higher	

**Table 1**: Summary of the bias introduced in the site characterisation by the software or the instrument calibration, where DLR is German Remote Sensing Data Centre, ONERA is French Aerospace Lab, and TU is Tubitak Space Technologies Research Institute, Turkey. Visible Near Infrared (VNIR)

3) The radiometric calibration of all participants' instrumentation against a standard reference source (TSARS) with traceability to SI units through NPL and further the field cross-comparison of the instruments against a NPL reference panel proved the robustness of this methodology as a means to evaluate potential biases between instruments.

The site characterisation by DLR, ONERA and TU during the 2009 CEOS pilot comparison established the formal traceability of the spectral reflectance of Tuz Gölü standard reference test site to SI units.

4) This CEOS pilot comparison provided an opportunity to evaluate different sampling techniques used in the characterisation of test sites for vicarious calibration of land imagers and to produce an evaluation of the uncertainties associated with them. In analysing and reporting results NPL was also able to identify subtle differences in methodologies and processes used by different

participants to assess and combine uncertainties. All these results and analyses will help to inform the community and serve as input to establish best practice guidance.

5) A cross-comparison of satellite imagers and an aircraft imager using the Tuz Gölü site took place. The results are presented in a subsequent document.

# 1.3 Structure of this report

The structure of this report is as follows.

Chapter 2 describes the standard reference test site Tuz Gölü, Turkey and why it is appropriate to use for the vicarious calibration of land optical imagers during the month of August. In the same chapter details are given of the 2009 CEOS pilot land comparison listing the participant institutions and their scientific contribution to this pilot exercise. This chapter also provides the schedule for the comparison, a brief description of the cross-comparison activities and the instrumentation used.

Chapter 3 presents the details and results of the cross-comparison of instrumentation in the laboratory and on-site. This activity identified biases introduced by the instrumentation and the software. Procedures to calibrate the radiometers and reference panels with traceability to SI units are described and standard uncertainties are reported together with the measured values. The cross-calibration of the reference panels in sunlight is highly dependent on the meteorological conditions, requiring stable and constant sun irradiance that require a short time frame (minor changes in the sun zenith angle) to calibrate the participants' reference panels.

Chapter 4 describes the sampling methodologies and data analysis procedures used by each participant during the four days of field measurements. Sources of uncertainties associated with the reflectance-based method used for the characterisation of Tuz Gölü are identified and discussed. Typical values of standard uncertainties evaluated by Type A and Type B methods resulting from the site radiometric characterisation by DLR, ONERA and TU during the comparison are reported. The Bidirectional Reflectance Distribution Function (BRDF) effects of the site were measured by NPL using a dedicated gonionmeter - Gonio RAdiometric Spectrometer System (GRASS). Sources of uncertainties related to this method are identified and the typical values of the combined standard uncertainties are reported here.

Chapter 5 includes the atmospheric characterisation of the site during the comparison such as aerosol optical properties and water vapour content measured using a sunphotometer. Furthermore, meteorological data, which are required as input for the Radiative Transfer Code (RTC) to calculate the Top Of the Atmosphere (TOA) normalised radiance (reflectance), are also reported. The sources of uncertainties associated with the sunphotometry are discussed and typical values based on those reported in the literature are given.

Chapter 6 discusses the mathematical basis of the uncertainty evaluation for the cross-comparisons presented in the previous chapters. Consideration is given to uncertainty evaluation for the site characterisation, radiometric calibration, and radiometric calibration checks are presented here. The chosen methods for the uncertainty

evaluation followed those indicated by QA4EO (Quality Assurance for Earth Observation).

Finally, Chapter 7 summarises the results and makes some recommendations for the 2010 CEOS Key international comparison.

# 2 CEOS pilot land comparison 2009 Turkey

The standard reference test site used for the CEOS pilot land comparison was selected by CEOS IVOS to be a salt lake (Salt Lake in Turkish is Tuz Gölü), situated about 150 km southeast of Ankara [2]. Tuz Gölü is a permanent endorheic lake, located in the arid central plateau of Anatolia (38° 50'N 33° 20'E centre latitude, longitude), Figure 1, and it is situated well away from the influence of the sea (approx. 300 km from the Mediterranean Sea, 350 km from the Black Sea and 580 km from the Aegean Sea). It is the third largest lake in Turkey and it is a natural reserve area, though the site is well protected. It is a salt flat at an elevation of 905 m above sea level. The evaporates are mainly halite and gypsum, with minor amounts of polyhalite and coelestine [3]. There is virtually no vegetation in the salt flat but arable fields and salt-steppes surround it. There are salt mines and salt work pools operating at the margins of the lake.

The salt lake dries each year during July and August and this is the only period when it can be used as a reference target for the vicarious calibration of optical sensors.



Figure 1: Location map of Tuz Gölü salt lake, Turkey (Map courtesy of www.map-of-europe.us and image courtesy of GLCF).

### 2.1 Participants

NPL as pilot and TU as host organised the seven days CEOS pilot land comparison from 23<sup>rd</sup> August 2009 to 29<sup>th</sup> August 2009 at Tuz Gölü. The pilot land comparison had five participants: NPL, TU, DLR, ONERA and CNES (see Figure 2) with the contact details of the institutions and lead participant involved in the pilot comparison in Table 2.

One observer from the National Institute for Space Research, Brazil and two observers from the Council for Scientific and Industrial Research, South Africa participated in this pilot comparison, and provided help with some of the field measurements. In addition one PhD Student, Saber Salime, from City University London helped in the preparations and field measurements.

Contact person	Institute	Contact details	Measurement
Andrew Deadman	NPL National Physical Laboratory Hampton Road Middlesex Teddington TW11 0LW United Kingdom	Tel: +44 20 8943 6077 Email: andrew.deadman@npl.co. uk	Calibration BRDF
Selime Gürol	TU Tubitak Uzay Space Technologies Institute 06531 ODTU Kampusu Ankara Turkey	Tel: +90 312 2104600/1190 E-mail: selime.gurol@uzay.tubitak .gov.tr	Ground data Meteo data Satellite data
Martin Bachmann	DLR German Remote Sensing Data Centre - Imaging Spectroscopy Workgroup Münchnerstr. 20 D-82234 Wessling Germany	Tel: +49-8153 28 3325 E-mail: martin.bachmann@dlr.de	Ground data Airborne data
Yannick Boucher	ONERA French Aerospace Lab BP 74025 2 Avenue Edouard Belin, 31055 Toulouse, Cedex 4 France	Tel: +33 562 252605 Email: Yannick.boucher@onecert .fr	Ground data
Sophie Lachérade	CNES French National Space Agency DCT/SI/MO BPI 811 18 Avenue Edouard Belin, 31401 Toulouse, Cedex 4 France	Tel: +33 561 274 546 Email: sophie.lacherade@cnes.fr	Aerosol data

**Table 2:** Participant institutions, their contribution to the 2009 CEOS land comparison and the person responsible for the datasets provided and analysed by NPL in this report



Figure 2: Participants in the CEOS Pilot land comparison, Tuz Gölü, Turkey 2009

# 2.2 Schedule

23<sup>rd</sup> August 2009

**Laboratory measurements**: Cross-comparison of DLR, ONERA, NPL, and TU radiometers against NPL Transfer Standard Absolute Radiance Source (TSARS).

24<sup>th</sup> August 2009

**Set-up of the measurement campaign** at Tuz Gölü, the standard reference site used for the vicarious calibration of the optical sensors.

25<sup>th</sup> August 2009

Field measurements: Site characterisation according to the Land protocol.

26<sup>th</sup> August 2009

**Field measurements**: Cross-comparison of radiometers using the participants' calibrated reference panels. This day was characterised by cirrus and no site characterisation took place.

27<sup>th</sup> August 2009

**Field measurements**: Cross-comparison of the participants' radiometers against the NPL calibrated reference panel and site characterisation according to the protocol.

28<sup>th</sup> August 2009

**Field measurements**: Site characterisation according to the Land protocol.

29<sup>th</sup> August 2009

Laboratory measurements: Cross-comparison of all radiometers against TSARS.

### **Laboratory measurements**

The cross-comparison of the instrumentation in the laboratory was performed at the beginning and at the end of the measurement campaign to evaluate any biases between the radiometers used for the characterisation of the reference test site (see chapter 3.1). This laboratory cross-comparison of the radiometers used as a common reference source a lamp illuminated integrating sphere, the NPL Transfer Standard Absolute Radiance Source (TSARS), which provides traceability of the ground data to SI units.

### Field measurements

# Cross-comparison of instruments

The radiometers of the participants were cross-compared by using a reflectance reference panel calibrated by NPL for the sun illumination angles specific for this period of the year at the Tuz Gölü reference site. Another cross-comparison of radiometers used all participants' reference panels to evaluate potential biases in their primary calibrations derived either from the manufacturer or the participant institution. This procedure, the data and the results are presented in chapter 3.

### Site radiometric characterisation

On different days DLR, ONERA and TU characterised 100 m x 300 m and 1 km x 1 km sites using independent and different techniques and sampling strategies, but the same radiometer type produced by ASD Inc was used. Additionally, NPL performed a BRDF characterisation of the site at two locations near the sampled site. A detailed description of the site characterisation is given in chapter 4.2.

### Atmospheric characterisation

As part of the vicarious calibration of the site, atmospheric measurements are required. TU recorded the meteorological conditions using an automatic weather station and CNES performed measurements of the aerosols and precipitable water using a CIMEL automatic sunphotometer. These measurements and the related uncertainties are given in chapter 5.

### Aircraft and Satellite imagery

During the pilot land comparison 24<sup>th</sup> August to 28<sup>th</sup> August 2009, there were various satellite overpasses including the optical sensors: SPOT4, MERIS and AATSR on board ENVISAT, CHRIS on board PROBA, MODIS on board Terra, Beijing1, UK-DMC-1, UK-DMC-2, Deimos1, and AWiFS on board IRS-1. On 2/9/2009 DLR performed airborne measurements using the HyMap spectrometer [34]. These datasets will be used for the end goal of this process, the vicarious calibration and will be presented and analysed in another report "Satellite and Airborne imagery for the pilot Land comparison of techniques and instruments used for the vicarious calibration of Land surface imaging through a ground reference standard test site Turkey 2009", CONTROLS Deliverable 12.

### 2.3 Instrumentation

DLR, ONERA and TU characterised the site using ASD FieldSpec3 instrumentation. NPL measured the BRDF effects of the site using a Gonio RAdiometric Spectrometer System (GRASS) where the measurement device could be an ASD radiometer or any other kind of radiometer. The atmospheric characterisation was recorded by TU using an automatic CIMEL sunphotometer, a handheld MICROTOPS sunphotometer and an automatic weather station. The technical characteristics of the instrumentation used for the site characterisation and the description of the NPL calibration facility Transfer Standard Absolute Radiance Source (TSARS) are presented in **Appendix A: Instrumentation**.

# 3 Cross-comparison of instrumentation

### 3.1 Laboratory measurements: Cross-comparison against TSARS

One hour prior to the calibration of the participants' radiometers on 23<sup>rd</sup> August 2009 and 29<sup>th</sup> August 2009, TSARS was switched on in order to stabilise the source. The radiometers have an optical fiber for measurements and this was attached to a pistol grip aligned to the source centre. The alignment of the optical fiber to the central area of TSARS is the most sensitive step and a laser and mirror were used to check alignment.

The cross-comparison of radiometers was performed for 1° and 8° FOV, where the former choice is most commonly used for field measurements. The ONERA radiometer used a 5° FOV instead of 8° FOV for field measurements, and their radiometer was calibrated for 5° FOV. The DLR radiometer had no 1° FOV, and the manufacturer had not provided the instrument calibration for this for optics. The DLR radiometer measured TSARS using the 1° FOV fore optics provided by TU. This dataset was processed as if 25° FOV had been used for this calibration.

The two for optics required different positions so that the standard source with 50 mm diameter exit port overfills the FOV of the instrument. Based on NPL laboratory tests with the ASD, two distances were selected as ideal geometry for the calibration:

- 90 cm distance between the 1° FOV for optics and TSARS exit port, where the maximum distance is 286 cm
- o 20 cm distance between the 8° FOV for optics and TSARS exit port, where the maximum distance is 35 cm
- o 20 cm distance between the 5° FOV for optics and TSARS exit port, where the maximum distance is 57 cm

Black paper was used to stop the back reflections from the pistol grip and mount and to reduce the stray light. The results of this comparison not only provided information on any differences related to traceability routes but also allowed normalisation to a common reference to remove any effects of these differences from the latter comparisons.

### **Uncertainty Analysis**

The uncertainty associated with the radiometric calibration of ASD using TSARS was evaluated as below. It is calculated as the quadrature sum of the identified components. In practice this uncertainty has a spectral dependency but for simplicity we have taken the average value for 400 - 1000 nm and 1000 - 2500 nm as Table 3.

Uncertainty sources	Type	400–1000 nm	1000-2500 nm
Uncertainty associated with the	Type A	0.67%	1.14%
absolute radiance of TSARS			
Positional sensitivity for radiance	Type B	0.08%, FOV=1°	0.06% FOV=1°
measurements on TSARS		0.08%, FOV=8°	0.06% FOV=8°
Uniformity in the horizontal plane		·	
Measurement reproducibility and	Type B	0.68% FOV=1°	1.14% FOV=1°
optical fiber movement		0.71% FOV=8°	1.14% FOV=8°
Combined standard uncertainty	Type A+	0.68% FOV=1°	1.14% FOV=1
	Type B	0.71% FOV=8°	1.14% FOV=8°

Table 3: Uncertainty sources for the radiometric calibration using TSARS, NPL

### 3.1.1 Radiance and reflectance factor

### Radiance

Radiance as measured with the ASD radiometer is calculated using the formula below, the expression used by RCALC.EXE post processing software to convert digital numbers (DN) in radiance units:

$$L(\lambda) = \frac{\rho(\lambda)E(\lambda)DN_{t \text{ arg } et}IT/Gain_{instrument}}{\pi DN_{instrument}IT/Gain_{t \text{ arg } et}}$$

 $L(\lambda)$  = Spectral radiance measured with the ASD radiometer [W sr<sup>-1</sup> m<sup>-2</sup>].

 $\rho(\lambda)$  = Spectral reflectance factor of the ASD calibration Spectralon@ panel, ct. [unitless]

 $E(\lambda)$  = Irradiance of the ASD calibration lamp, ct. [W m<sup>-2</sup> nm<sup>-1</sup>].

 $DN_{target}$  = Digital Number response of the target spectrum, its value changes for each measurement [unitless].

IT/Gain<sub>instrument</sub> = Instrument Integration Time for VNIR or Gain for SW, ct.

 $DN_{instrument}$  =The instrument response in raw Digital Number to the ASD calibration lamp ct. [unitless].

IT/Gain<sub>target</sub> = The Integration Time or Gain of the target spectrum file. Its value changes for each measurement.

The above formula can be written in a more simple way as:

$$L(\lambda) = ct \frac{DN_{t \arg et}}{IT/Gain_{t \arg et}}$$

Following the cross-comparison of radiometers using TSARS, it could be determined if there is any gain (multiplication factor) between the measured value in radiance by each participant ASD and the expected radiance value of TSARS. This could be written as:

$$L_{TSARS}(\lambda) = L_{ASD}(\lambda)Gain$$

where Gain is calculated using TSARS absolute spectral radiance values and the ASD spectral radiance values measured against TSARS. The Gain has a spectral dependence over 350 to 2500 nm.

The corrected field radiance value for one participant will have the expression:

$$L^{corect}_{ASD}(\lambda) = L^{report}_{ASD}(\lambda)Gain = L^{report}_{ASD}(\lambda)\frac{L_{TSARS}(\lambda)}{L_{ASD}(\lambda)}$$

### Reflectance factor

The radiance reflected by a target is a function of the varying incident solar irradiation during the day, as well as changes from day to day owing to sky conditions. This value provides another check on the instrument primary calibrations but has no direct impact on assessing the intrinsic reflectance of the site surface. Reflectance factor  $\rho$  of the site is measured using a calibrated reference panel and is calculated using the following formula:

$$\rho_{t \arg et} \equiv \frac{DN_{t \arg et}}{DN_{panel}} \rho_{panel}$$

 $\rho_{target}$  = Reflectance factor of the target, in this case of the salt lake at nadir

 $\rho_{panel}$  = Reflectance factor of the reference reflectance panel Spectralon@. The manufacturer provides this value over 350 – 2500 nm for diffuse illumination (over a hemisphere) and for a near nadir view

 $DN_{target}$  = Digital Numbers measured over the target, the salt lake.

 $DN_{panel}$  = Digital Numbers measured over the reference reflectance panel in a short period of time after or in between measurements over the target in order to ensure similar illumination conditions.

If it is necessary to apply a correction to the reported value of radiance, this will not influence the reflectance factor measured over the site, because the correction applied to  $DN_{target}$  will be balanced with that applied to  $DN_{panel}$ , when combining equation (5) with equation (4).

### 3.1.2 Data

The files names sent by each participant, each containing the radiance value and the uncertainties of Type A and Type B associated with this value, are reported as relative values in **Appendix C**. The reported radiance is the average of the values from 3 runs, each run comprising 3 measurements.

### 3.1.3 Combined standard uncertainty

The gains were calculated for DLR, ONERA, NPL and TU radiometers from the first day 23<sup>rd</sup> August and last day 29<sup>th</sup> August 2009, when the radiometers were cross-compared against TSARS.

The calibration accuracy achieved with TSARS is better than that reported by ASD Inc. over 350 to 2000 nm as shown in Figure 3. The expanded uncertainty (k = 2) provided by ASD Inc is that reported by Optronics Laboratories in Orlando Florida with declared traceability to the National Institute of Standards and Technology (NIST), USA. In Figure 3 the ASD Inc. reported and NPL calculated combined standard uncertainty are presented for comparison.

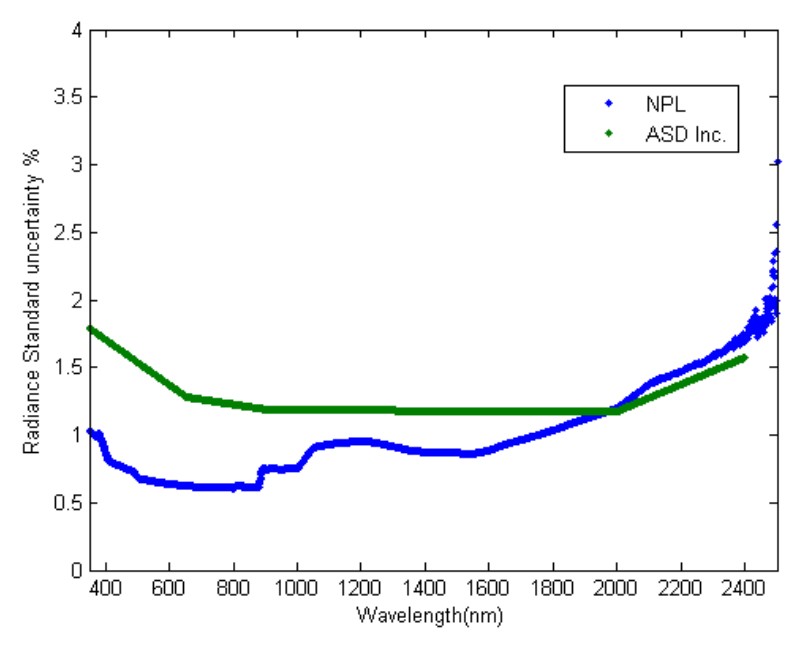


**Figure 3**: Standard uncertainty as reported by ASD Inc and NPL for radiance measurements using the ASD FieldSpec instrument

### **Type A standard uncertainty**

Type A components include the repeatability and reproducibility of radiance measurements against TSARS (the uncertainty resulting from a statistical analysis of the data). Type A values were recalculated by NPL using the datasets provided by the participants (DLR, ONERA, TU and NPL) for 23<sup>rd</sup> August to 29<sup>th</sup> August 2009 and took into account whether the measured values could be considered in groups or not (see chapter: Uncertainty estimation), allowing some uncertainty components to be removed.

The NPL Type A standard uncertainty calculated values are compared with those reported by the participants (Figure 4).

The results show some differences between the DLR, ONERA, NPL and TU values. The Type A standard uncertainty associated with the TU radiometer has the lowest values over the whole spectra, because the optical fiber and detectors of the radiometer are in the best condition compared to the others (the radiometer was manufactured in 2008 and the optical fiber of this radiometer has only been used for three measurement campaigns and so is less likely to have suffered mechanical damage than the optical fibers used by the other three instruments). This explains the lowest associated standard uncertainty Type A over the whole spectrum and especially over 1800 - 2500 nm for TU measurements against TSARS.

The DLR and ONERA associated Type A standard uncertainty have a similar range of values, where the values reported by them are higher than those calculated by NPL.

The TU reported values and those calculated by NPL have similar values over the greatest part of the spectrum with the exception of 1800 - 2500 nm spectral ranges.

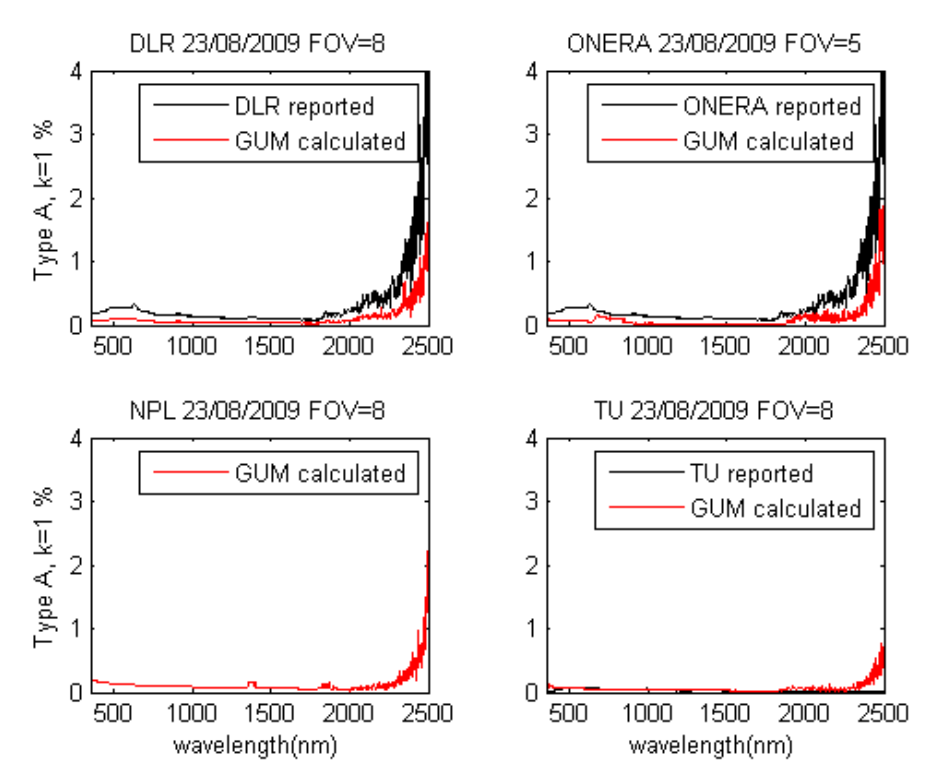


Figure 4: Type A standard uncertainty of all radiometers: the reported values (black) and the NPL calculated values using GUM (red).

The Type A standard uncertainty calculated for the NPL radiometer is higher than for all the other instruments (NPL had an instrument on loan). This radiometer, which is an old version, has the most damaged optical fibers (the optical fiber bunch was found to contain one broken fiber over SW1 and another one broken over SW2). The repeatability and reproducibility of NPL measurements using this instrument is thus relatively poor in comparison with those obtained by the DLR, ONERA and TU.

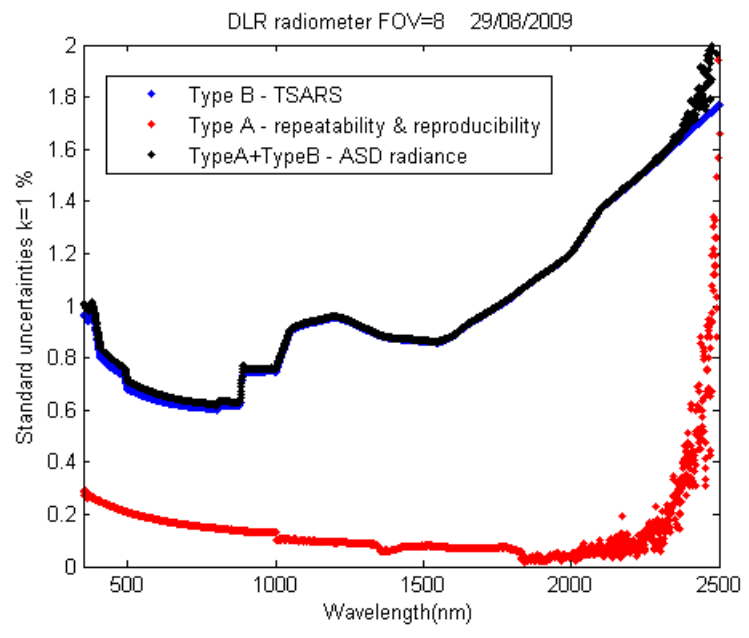


Figure 5: The combined standard uncertainty for an ASD radiometer, FOV=8°.

# Type B standard uncertainty

Type B components are related to TSARS absolute radiance standard uncertainty and covers all uncertainties related to the NPL transferable standard source calibration (see 3.1). This was the major source of uncertainty for all radiance measurements (see Figure 5 for the DLR radiometer) and therefore the combined standard uncertainty (Type A and Type B) calculated for participants' radiometers does not change significantly between them.

### 3.1.4 Calibration against TSARS

TSARS radiance values are compared with those measured by participants' radiometers. The Type A standard uncertainty is calculated as described in Chapter 6 and Type B is that associated with TSARS (see Chapter 3.1.3).

The left-hand Y-axis represents the radiance values as measured by each radiometer together with the expected value as defined by TSARS. The right-hand Y-axis shows the percentage difference between measurements made by the participant's radiometer and TSARS on 23<sup>rd</sup> August 2009. Additionally the measured radiance value by each participant is represented with the margins given by the combined standard uncertainty (eg "DLR+ Type (A+B)", "DLR – Type (A+B)" as in Figure 6.

The DLR radiometer exhibits a relatively high percentage difference (Figure 6), which may not necessarily be due to the original calibration but is thought to be caused by differences in the software used by DLR to process the results, which is different from that provided by the manufacturer and used by the other participants.

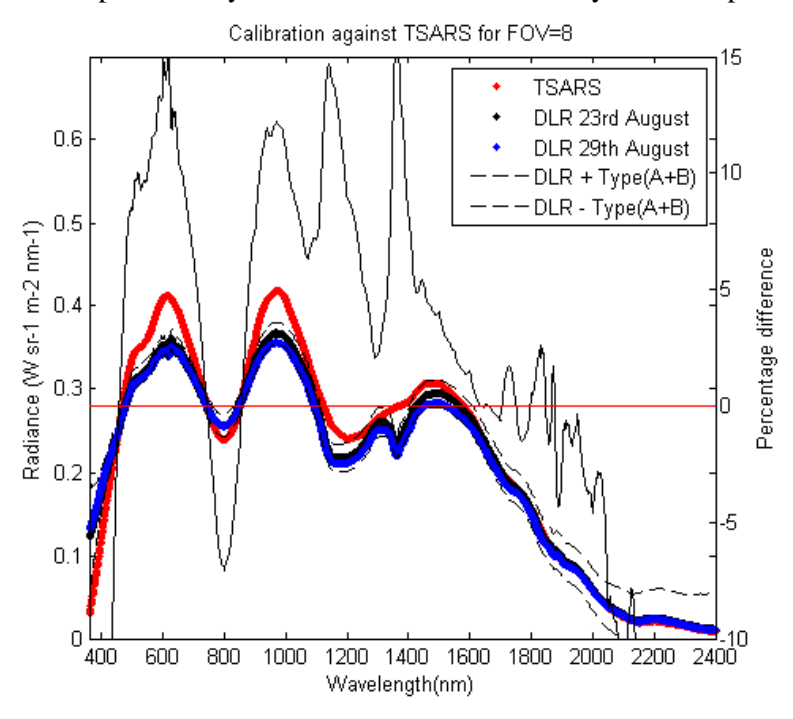


**Figure 6:** DLR radiometer calibrated against TSARS. TSARS radiance values (red) are compared with the measured values on 23<sup>rd</sup> August (black) and 29<sup>th</sup> August (blue). The percentage difference between TSARS and DLR measured values on 23<sup>rd</sup> August is represented with a black line.

A more detailed evaluation of this issue (e.g. reprocessing of data through different software) was not possible at the time of writing this report and is the subject of investigation by DLR.

ONERA's percentage difference over the visible region is within reasonable boundaries of 2 - 3% as shown in Figure 7.

The TU radiometer is also unexpectedly high, as shown in Figure 8, which is believed to be due to an error in its original calibration, which cannot be directly evaluated.

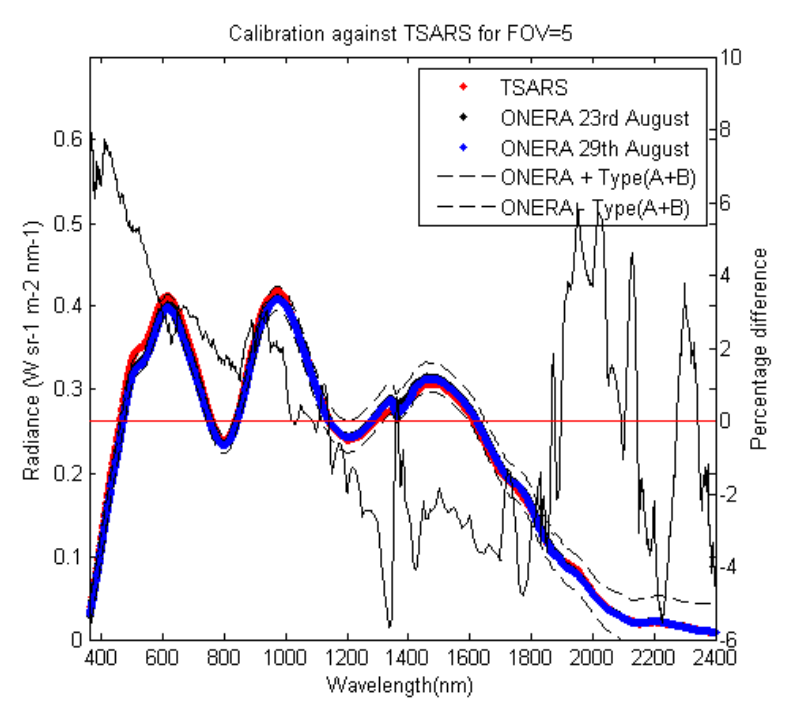


Figure 7: ONERA radiometer calibrated against TSARS

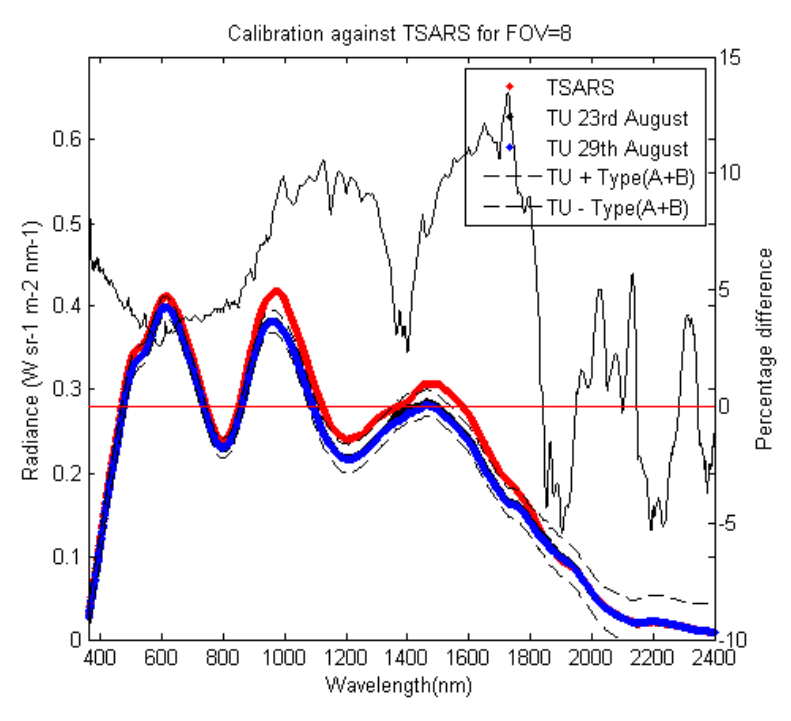


Figure 8: TU radiometer calibrated against TSARS

The cause of the offset on the fourth radiometer (NPL), Figure 9 is not fully known but again may be a function of how the calibration software developed by National Environment Research Centre (NERC) is being used to process the results. At the time of writing this report it was not possible to evaluate this potential software issue.

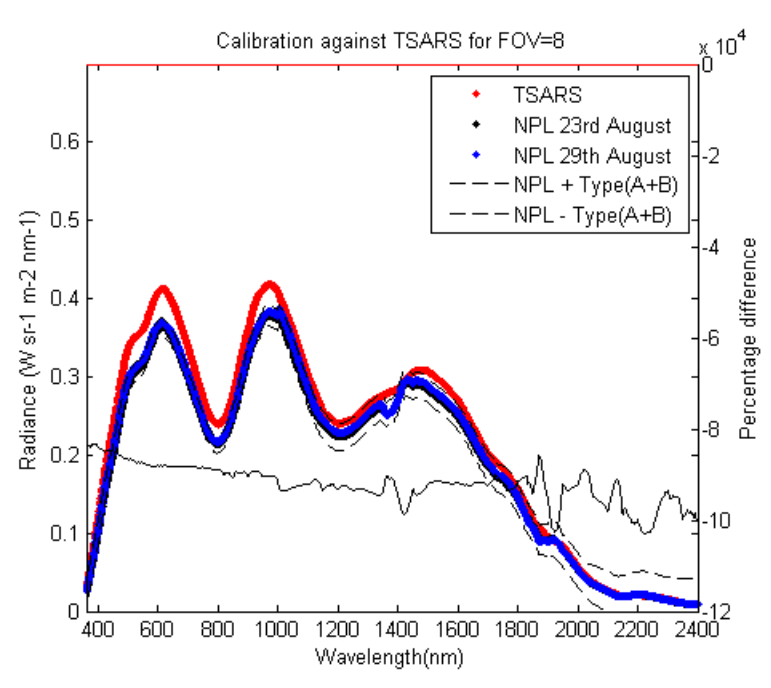


Figure 9: NPL radiometer (supplied by Durham University) calibrated against TSARS

### 3.1.5 Calibration checks

The calibrations against TSARS on 23<sup>rd</sup> August and 29<sup>th</sup> August 2009 should be consistent because the TSARS values and the associated standard uncertainties associated with the values did not change over the period 15<sup>th</sup> June 2009 to 29<sup>th</sup> January 2010. A calibration check was done using the equation:

$$\frac{L^{23}_{lab1}(\lambda)}{L^{29}_{lab1}(\lambda)} \approx 1$$

where  $L^{23}_{lab1}(\lambda)$  is the radiance measured by laboratory 1 on  $23^{rd}$  August 2009 and  $L^{29}_{lab1}(\lambda)$  is the radiance measured by the same laboratory on  $29^{th}$  August 2009. The above relation should be true within the limits of the associated Type A standard uncertainty.

The expanded uncertainty (k = 2), having a level of confidence of 95.4%, associated with the quotient in Equation (6) is calculated using the formula below:

$$u = 2\sqrt{u^{2}(L^{23}_{lab1}(\lambda)) + u^{2}(L^{29}_{lab1}(\lambda))}$$

where  $u(L^{23}_{lab1}(\lambda))$  and  $u(L^{29}_{lab1}(\lambda))$  are Type A standard uncertainties (k = 1) associated with the radiance values measured on  $23^{rd}$  August and  $29^{th}$  August 2009. A detailed explanation is given in the chapter: Uncertainty estimation.

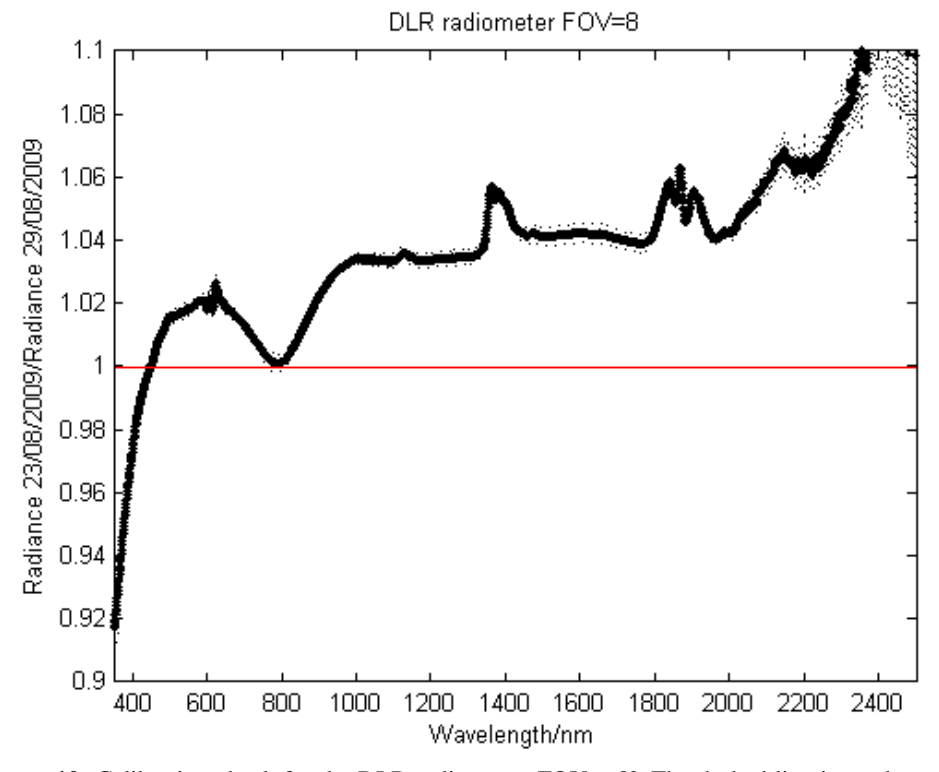


Figure 10: Calibration check for the DLR radiometer,  $FOV = 8^{\circ}$ . The dashed line is used to represent the calculated quantity +/- combined expanded uncertainty.

The calibration checks for DLR, NPL and TU radiometers (FOV =  $8^{\circ}$ ) and ONERA (FOV =  $5^{\circ}$ ) are represented in Figure 10, Figure 11, Figure 12, and Figure 13.

The DLR results show the presence of a drift in radiance-measured values against TSARS on the first and last day by their instrument. There is a spectral dependence of this difference. The magnitude of this difference is in accordance with stability estimates for this instrument of ~ 5 % (measured at DLR laboratory after the campaign).

The ONERA radiance measured on 23<sup>rd</sup> August and 29<sup>th</sup> August 2009 in the same conditions against TSARS have a small drift, however the correction will be calculated from the 23/08/2009 data.

The TU radiometer shows a non-significant change in measured values between the first day and the last day. The correction coefficients can be calculated from one of the datasets.

The NPL radiometer (on loan from Durham University) was calibrated by NERC and the raw DNs were converted into radiance values using NERC software. This software does not correct the splices at the detector junctions such as: 1000 nm and 1800 nm. This correction is not considered by NERC because it is an additional source of uncertainties. However this radiometer did not participate further in the cross-comparison against the reference panels. The NPL radiometer was used for the BRDF characterisation of the site where the correction factors required for radiance values do not affect the  $\rho$  at different zenith viewing angles (Chapter 4.2)

A feature present in all graphs is the peaks around 1400 nm and 1800 nm, which are the result of different relative humidity of the air in the lab during the two days.

The NPL radiometer calibration check (Figure 13) presents a shift in value at 1000 nm and 1800 nm, which are the wavelengths at which the different spectrometer detectors are spliced together. However the NERC software does not correct the splices at the detector junctions as mentioned previously.

The Ankara University laboratory, which hosted the radiometric calibration, had no monitoring of relative humidity and temperature in 2009. It is thus difficult to evaluate the impact of their variability on two different days of calibration. The CEOS Key comparison planned for 2010 will take into account this source of uncertainty.

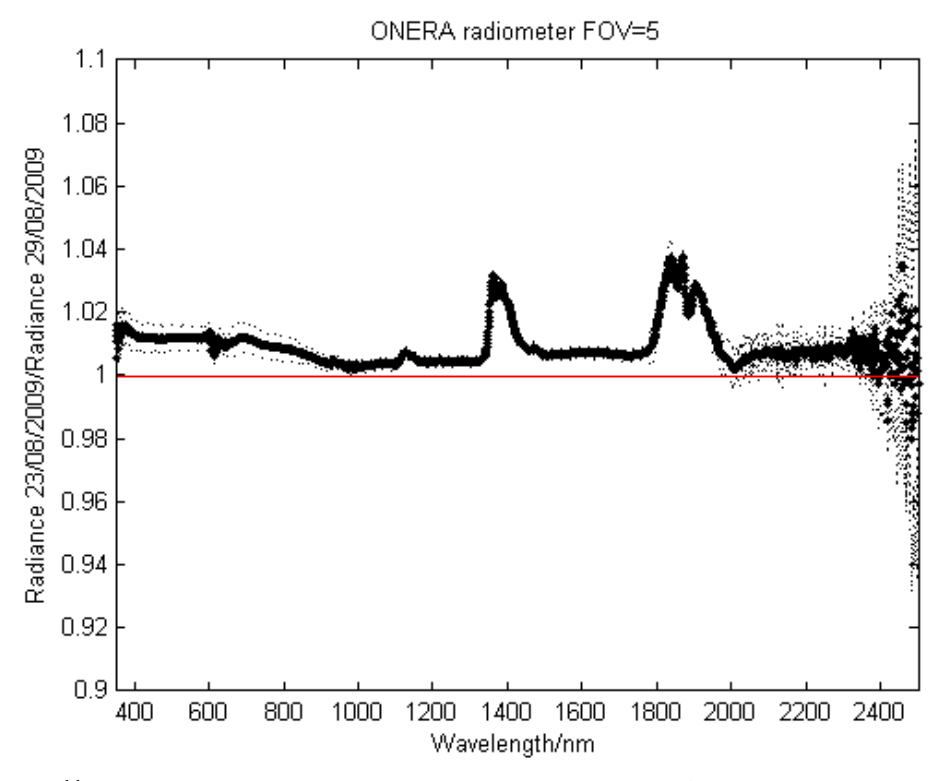


**Figure 11:** Calibration check for the ONERA radiometer,  $FOV = 5^{\circ}$ . The dashed line was used to represent the associated combined expanded uncertainty.

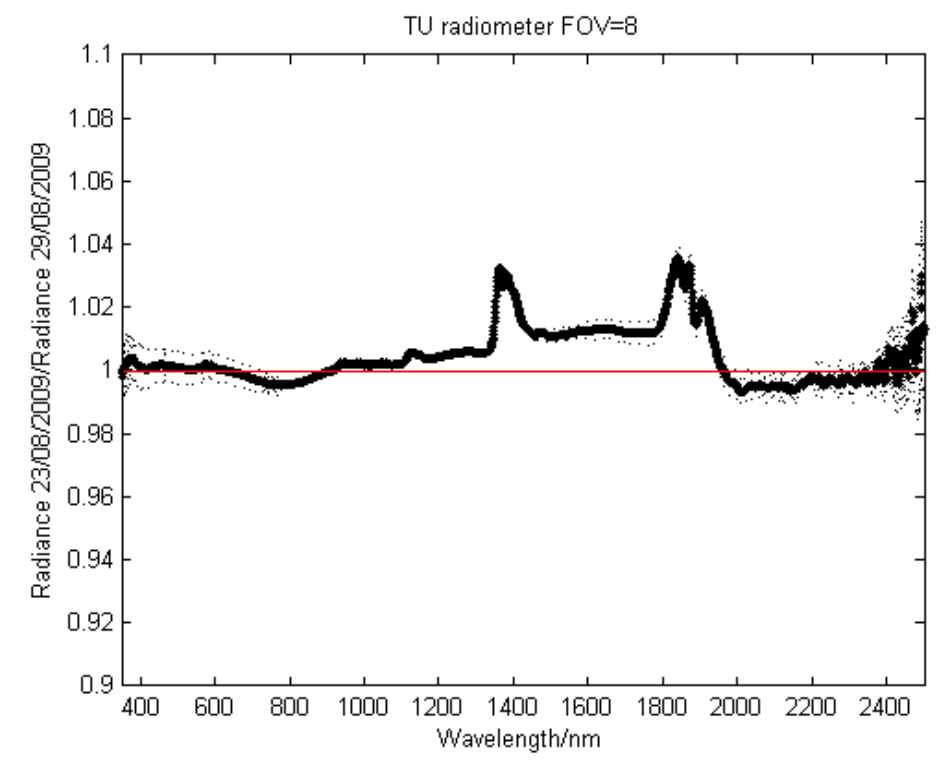


**Figure 12:** Calibration check for the TU radiometer,  $FOV = 8^{\circ}$ . The dashed line was used to represent the associated combined expanded uncertainty.

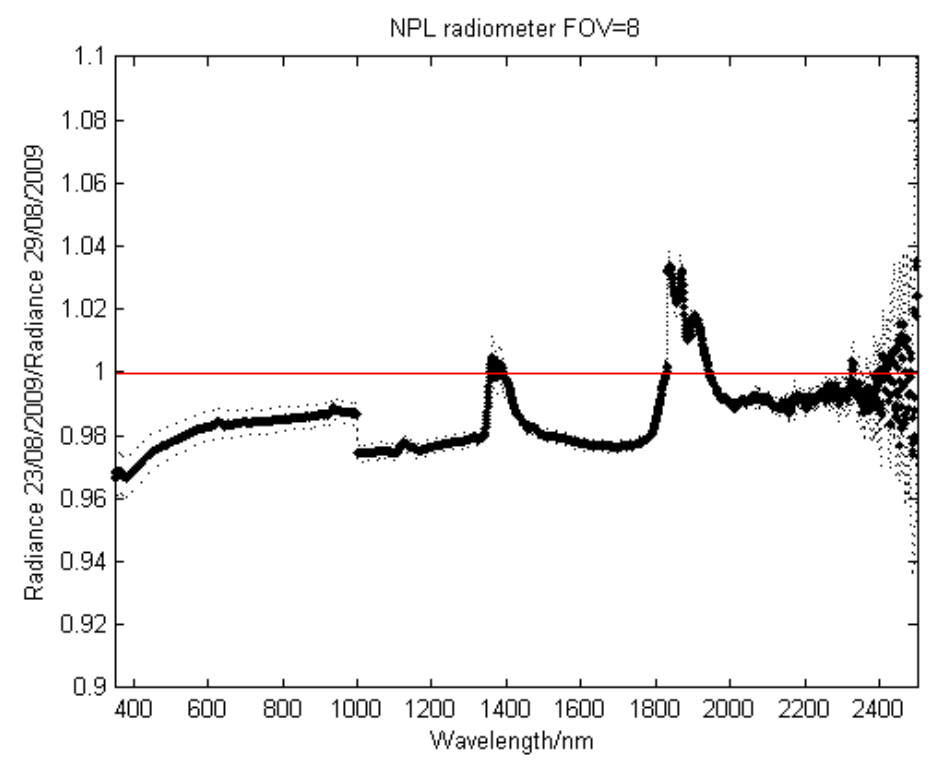


Figure 13: Calibration check for the NPL radiometer,  $FOV = 8^{\circ}$ . The dashed line was used to represent the associated combined expanded uncertainty.

### 3.1.6 Correction of measured radiance values

All radiance values measured in the field on day x require a correction as per formula:

$$L^{x}_{lab1}(\lambda) = L^{reported}(\lambda)Gain$$

with

$$Gain = \frac{L_{TSARS}(\lambda)}{L^{23\&29}(\lambda)}$$

where  $L^{reported}(\lambda)$  is the reported radiance value by the participant number 1 in the field, Gain is the correction factor which will be applied,  $L_{TSARS}(\lambda)$  is the spectral absolute radiance and  $L^{23\&29}(\lambda)$  is the radiance measured by the radiometer of the participant number 1 in the laboratory on  $23^{rd}$  August 2009 or  $29^{th}$  August 2009. The Gain is spectrally dependent and will be calculated from the first day of calibration against TSARS for the reasons mentioned in the above paragraph. The standard uncertainty for gain is expressed as follows (see chapter 6):

$$u^{23}_{gain} \equiv \sqrt{u^2 (L^{23}_{lab1}) + u^2 (L_{TSARS})}_{NPL}$$

A second check of the radiometric calibration is performed by the cross-comparison of all radiometers against the NPL reference reflectance panel on 27<sup>th</sup> August 2009. If one applies the above-calculated Gains to the reported radiance values by each lab (DLR, ONERA and TU), the resulted radiance values should be very similar for this day with stable atmospheric and illumination conditions (see chapter 3.3).

### 3.2 Field measurements: Cross-comparison against reference panels

The cross-comparison of radiometers against all reference panels took place on 26/08/2009. This unfortunately was not the best day for this comparison. There was partial cloud cover and high-level cirrus resulting in fluctuating illumination levels. The 27/08/2009 had better illumination conditions and so a new cross-comparison of the radiometers, this time only against the NPL calibrated reference panel due to time constraints, was performed.

### 3.2.1 Procedure

On 26/08/2009 the automatic sunphotometer and the NPL radiometer monitored the illumination conditions in order to discard the datasets affected by the changing illumination conditions. NPL's ASD (using the RS3 software) was used to monitor these changes by measuring the radiance from the large 60 cm x 60 cm Spectralon@ panel. The panel was measured every 2 seconds from 11:17 to 11:54 (Turkey local time). However the changes in illumination conditions could be detected in the reported datasets because they are related to much higher values of reported uncertainties. Prior to the start of the measurements each participant's laptop clock (including NPL's) was synchronised with each other's so that the time of the measurements in the files would be the same and could also be traced back to the NPL illumination monitoring measurements.

Each participant was invited to measure the radiance of all the other participants' reference panels at nadir, including the NPL's panel. There were four panels: DLR, NPL, ONERA and TU, measured by DLR and TU with the 8° FOV, and ONERA with the 5° FOV as per Figure 14.

The initial instrument measurement conditions were selected as follows: Spectrum – 50 scans averaged Dark Current – 50 scans averaged White reference – 50 scans averaged

The sampling times were increased following discussion with the participants so that they more closely reflected those used for measurements in the field.

Each participant measured the panels in a slightly different way as follows:

ONERA - had his own tripod for their pistol grip

TU - used NPL's stand to mount their pistol grip

DLR - mounted their pistol grip on the end of a rod that was held by hand.

Each pistol grip was at different height above the ground. However since radiance is independent of distance, the different heights do not affect the results.

The participants were further asked to make three independent measurements on each panel. The measurement procedure was as follow: Each participant measured his or her own panel. Again for each independent measurement three measurements were made. The panels were then moved by hand and placed under the other participants' pistol grips and aligned by eye. The fibres were not removed from the pistol grips. The three participants' panel positions were then changed a number of times so that each participant measured each of the three participant panels three times. The measurements on the three participants panels were performed between 11:17 and 11:55 local time, with sun zenith having values in the range 30.67° - 34.88°.

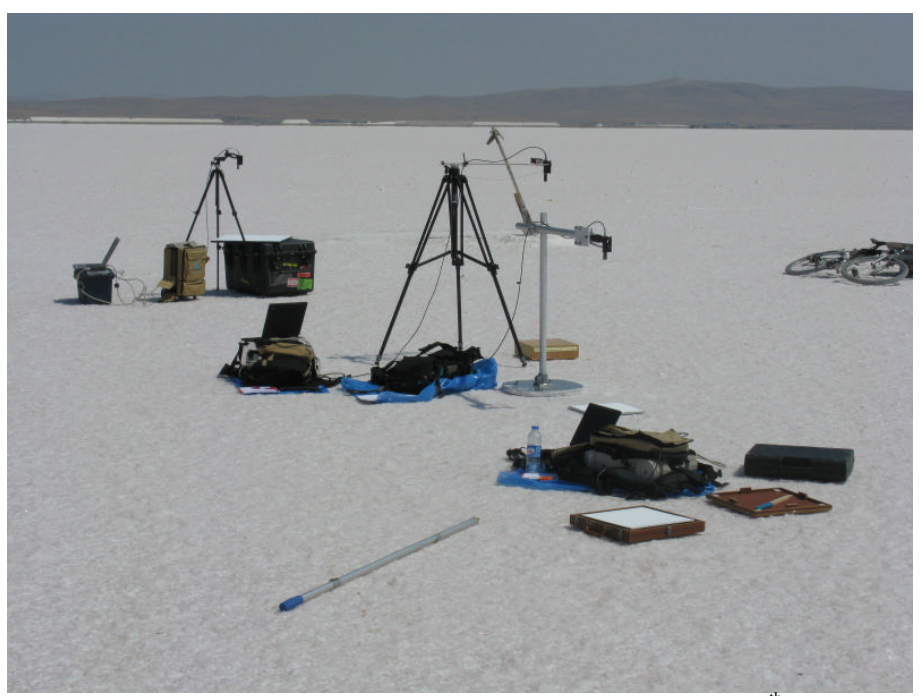


Figure 14: Participants' reference panels were measured in radiance at nadir on 26<sup>th</sup> August 2009

When this was complete, the participants measured the NPL panel again at nadir. This time all participants used the NPL stand and TU pistol grip. The NPL panel was aligned under the pistol grip by eye. Its position was not changed throughout the comparison. The first participant made three measurements before removing the fibre from the pistol grip and replacing it. This was repeated three times so that three independent measurements were made. Each participant took it in turns to measure the NPL panel.

The approximate time of the measurements of the NPL panel was as follows;

TU - 11:56 (08:56 UTC), sun zenith = 30.58°

DLR - 12:06, sun zenith = 29.78°

ONERA - 12:20, sun zenith = 28.93°

(Turkey is situated in UTC+2 zone and in summer time the local time is UTC+3.)

### 3.2.2 Reference reflectance panels

The measurement of the  $\rho$  of the site requires the use of a reference reflectance panel, often supplied with the ASD radiometer. ASD provides Spectralon@ panels, size 25 cm x 25 cm, manufactured and calibrated by Labsphere with declared traceability to NIST [28]. However even if calibrated prior to supply the Spectralon@ reference panels  $\rho$  are subject to change with time due to contamination and ageing and the supplied  $\rho$  value can be affected or depend on other factors when used as described below.

### **BRDF** effects

The Labsphere supplied Spectralon@ reference panel is characterised over 350 - 2500 nm for the nadir view again the measurement geometry is typically  $8^{\circ}$  incident illumination with collection over the entire hemisphere. However, the Spectralon@ material is not perfectly lambertian and exhibits BRDF effects (Figure 15) that can introduce additional errors in the  $\rho$  calculated value of the site if not treated appropriately.

Some authors recommend a field calibration of reference reflectance panels [8] against a primary standard using the sun as the irradiance source and having the component due to diffuse flux from atmosphere subtracted from the total sun irradiance. In such cases the calibration should use the same radiometer as for field measurements and the reference panel is compared with a primary standard diffuser. The calibration can be performed for different sun zenith angles using a goniometric system and this procedure is strongly influenced by the sky conditions. The main advantages of this technique against some laboratory calibrations are that irradiance and viewing geometry are the same as those used for the site characterisation and use the same instrumentation. In this CEOS comparison the NPL reference standard diffuser was calibrated at a range of sun and viewing illumination angles and used to cross-compare participant panels using the sun in a similar manner to that described above.

The CEOS pilot land protocol [1] called for the cross-comparison of participants' reference panels against the NPL calibrated reference panel at three sun zenith angles: 47°, 37° and 30°. These angles were related to 7:00 UTC, 8:00 UTC and 9:00 UTC for the period of 23<sup>rd</sup> to 29<sup>th</sup> August 2009 Turkey. The site was characterised in the timeframe 6:00 – 9:00 UTC (9:00 – 12:00 local time) because this was the timeframe of the most satellite over-passes. Unfortunately, 26<sup>th</sup> August 2009, the day planned for the comparison, was a day with changing illumination conditions due to cirrus clouds and so the Land protocol procedure could not be followed as originally intended.

The cross-comparison of the reference panels against the NPL reference panel was instead performed for sun zenith angles in the range 28.93°-30.58° on 26/08/2009 and for sun zenith angles in the range 52.83°- 49° on 27<sup>th</sup> August 2009. However, 27<sup>th</sup> August 2009 was a day with clear sky conditions (the diffuse background sky irradiance was less important than on the previous day) and this dataset could be used for cross comparison and normalisation of the participants' reference reflectance panels.

### **Influence of Diffuse Irradiance**

The  $\rho$  of the site is derived from the total solar irradiance, including the direct component (non-scattered radiation) and the diffuse component (the radiation scattered by the atmosphere and the surroundings of the measured target). A correction for the diffuse component is required in order to obtain the intrinsic directional reflectance factor of the target [9]. The magnitude of the error introduced by the non-correction of the diffuse component depends on the atmospheric conditions, being most important for days with poor visibility. The error decreases with the wavelength, being more important for the VNIR and it is dependent on sun zenith angle [8].

# **Contamination and Ageing**

The spectral reflectance of the reference panels could change due to the contamination of its surface during the field measurements or owing to the natural ageing of the material, with the former expected to dominate over the latter. Measurements at NPL have shown that the Spectralon@ material can age under intense UV radiation [9], which may include solar-like radiation. Further studies [11] show that Spectralon@ material can even deteriorate under low-level irradiation, with reflectance values below 450 nm being subject to the greatest change. Therefore recalibration before and after each field campaign is recommended at least to evaluate any drifts.

Some participants re-calibrated their reference reflectance panels previous to this measurement campaign as described below in Chapter 3.2.3.

### 3.2.3 Data

### 3.2.3.1 Participants reference reflectance panels

# **DLR**

The measurements were conducted after the campaign at DLR's calibration laboratory with a Perkin Elmer instrument. Different spots of the field Spectralon@ panel were measured relative to the laboratory reference Spectralon@ plate. Then these relative reflectance measurements were converted to absolute reflectance values based on the calibration coefficients for the lab Spectralon@ panel provided by Labsphere (NIST traceable). After that, absolute reflectance values were resampled to the center wavelength and FWHM of the ASD used in Tuz Gölü. Finally any remaining noise was filtered using Savitzky-Golay filtering [12].

### **ONERA**

The ONERA Spectralon@ reference reflectance panel was calibrated in house using a primary reference from Labsphere. The primary Spectralon@ reference was calibrated by Labsphere (8° – hemispherical reflectance, standard deviation <0.005 of the value of the  $\rho$  (unit less) in the range 300 - 2200 nm, <0.02 in the range 250 - 2500 nm).

### TU

Labsphere calibrated TU reference panel and the ASD software uses these values for the calculation of the target  $\rho$  at nadir. A second characterisation of the reflectance reference panel was performed by NPL using three illumination conditions and took

into account the BRDF effects of the Spectralon@ panel. The illumination angles used for the lab calibration were selected according to the illumination conditions in the field at 7:00 UTC, 8:00 UTC and 9:00 UTC ( $\theta$ s = 47°, 37°, 30°).

The  $\rho$  of the reference panels used by DLR, ONERA and TU for the calculation of  $\rho$  of the target are represented in Figure 15. It should be noted that the term  $\rho$  in this figure refers to the reflectance compared to a lambertian diffuser which explains why on first glance some values appear to be larger than unity (NPL and TU panel as measured by NPL). The DLR (green line) and ONERA (blue line) panels show ageing over the VNIR. The  $\rho_{TU}(\lambda)$  of the TU reference panel (yellow line) provided by the manufacturer shows no ageing over the VNIR. However this was the laboratory characterisation in 2008 before this panel was exposed to solar illumination. In May 2009 NPL characterised this panel and provided calibrations for 47°, 37° and 30° for nadir view (47°/0° TU panel - pink colour, 37°/0° TU panel - purple colour and 30°/0° TU panel - red colour).

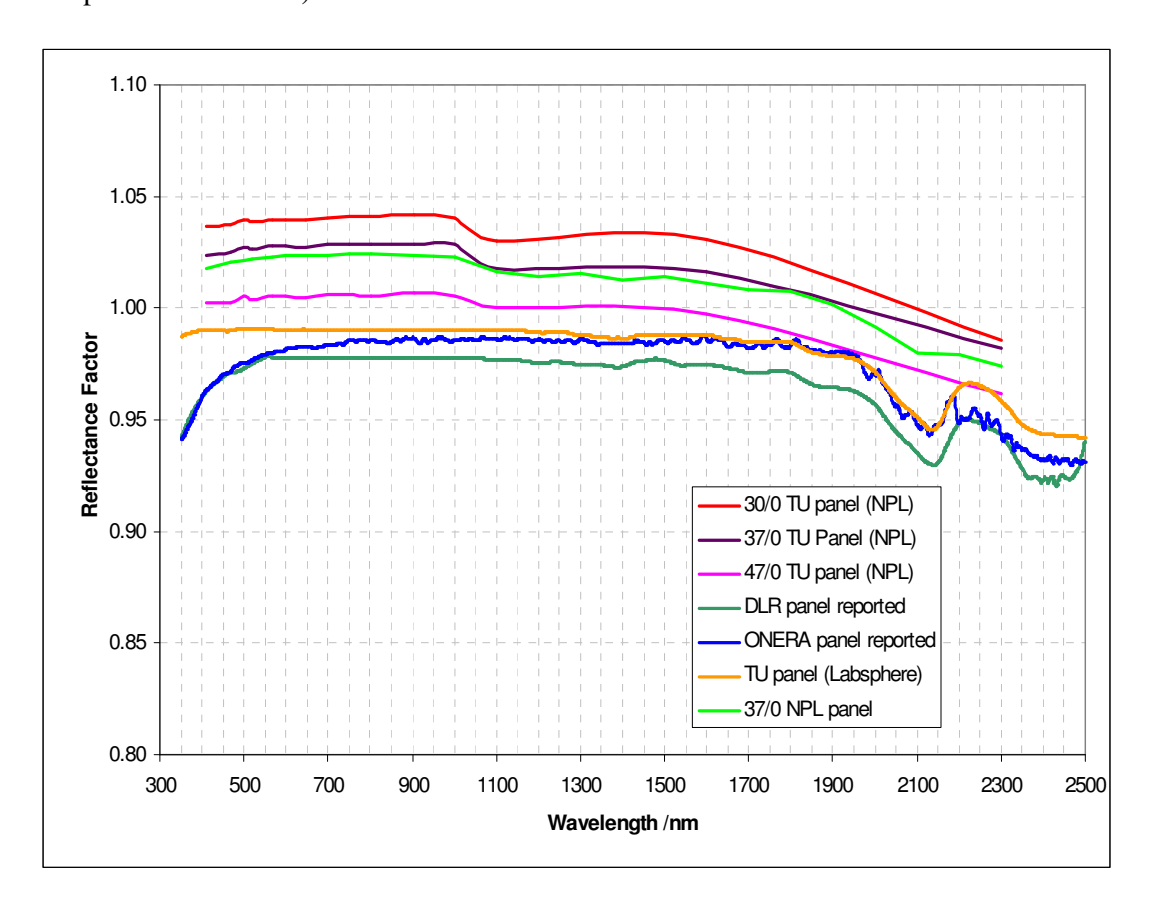


**Figure 15:** Reflectance factor of participants' reference panels

### 3.2.3.2 Field data

The data received from participants are reported in Appendix C: Participants' reported data.

### 3.2.4 Results of cross-comparison against reference panels

The 26<sup>th</sup> August 2009 was not the best day for this exercise, own to the presence of cirrus. However due to the short period of four days allocated to the field measurements, this cross-comparison took place. The standard uncertainty Type A reported by participants is relatively high, especially that reported by ONERA (Figure 17 and Figure 18). ONERA and TU reported values as well as those corrected are overlapping for all reference panels (Figure 16 and Figure 19). This was expected from the calibration against TSARS (ONERA and TU radiometers have a small difference between TSARS absolute radiance values and the measured reported values. The correction of DLR reported radiance values, using the gains from 23<sup>rd</sup> August 2009 and 29th August 2009 calibration against TSARS, increase the DLR reported values (Figure 16 and Figure 19), however there is still a difference between ONERA (TU) and DLR corrected values. For the DLR instrument note that due to the gain correction factors the spectral shapes as well as absorption features are altered; e.g. the Fraunhofer line at 430 nm is not visible. This indicates that the re-calibration factors being used are not appropriate and this is currently under investigation by DLR.

These results are similar for all reference panels: DLR, ONERA, TU and NPL and only two cases: the cross-comparison against NPL and TU reference panels are presented further.

The reported values and the corrected values are represented in these graphs. The standard uncertainty reported by participants is um and the standard uncertainty associated with the radiance as calculated by NPL following GUM is  $um^*$  as per equations below:

$$u_m \equiv \sqrt{u^2 T_{ypeAreport} + u^2 T_{ypeBreport}}$$

$$u_m^* \equiv \sqrt{u^2_{TypeAreport} + u^2_{TypeBreport} + \left(u^{23}_{gain}\right)^2}$$

# **NPL** reference panel

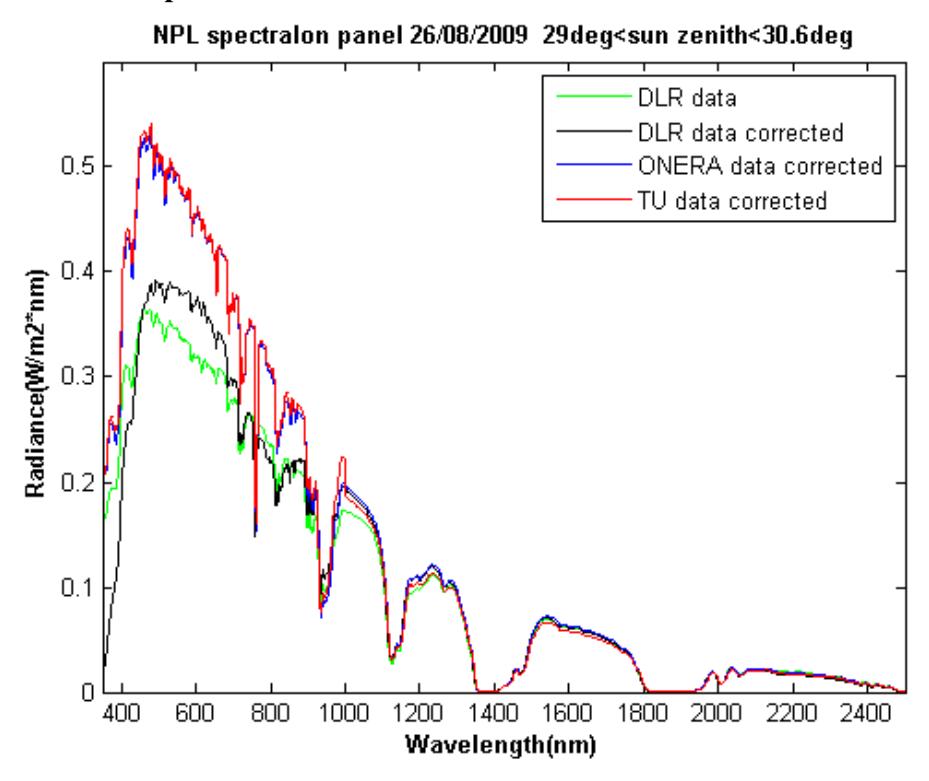


**Figure 16:** Radiance measured by DLR, ONERA and TU radiometers against NPL Spectralon@ panel, data are corrected using the gains from 23<sup>rd</sup> August 2009

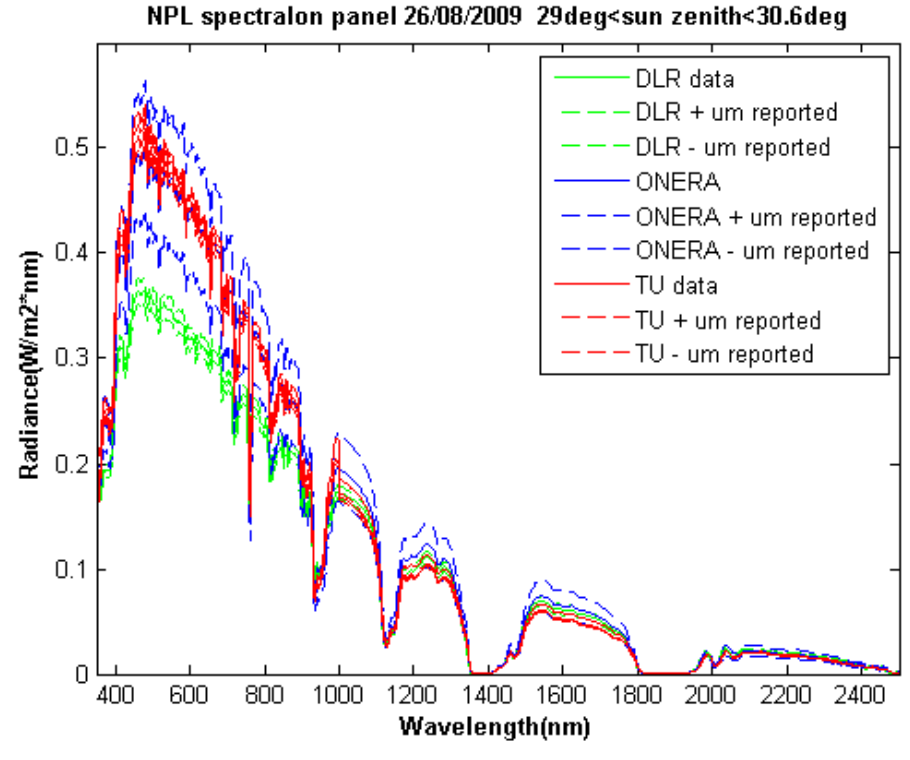
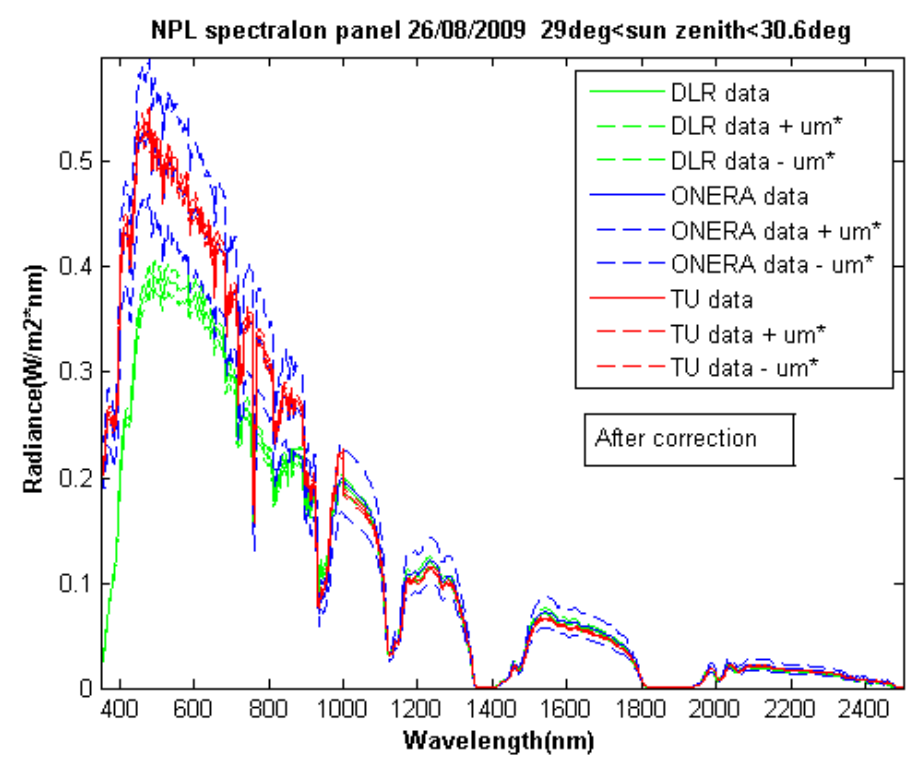
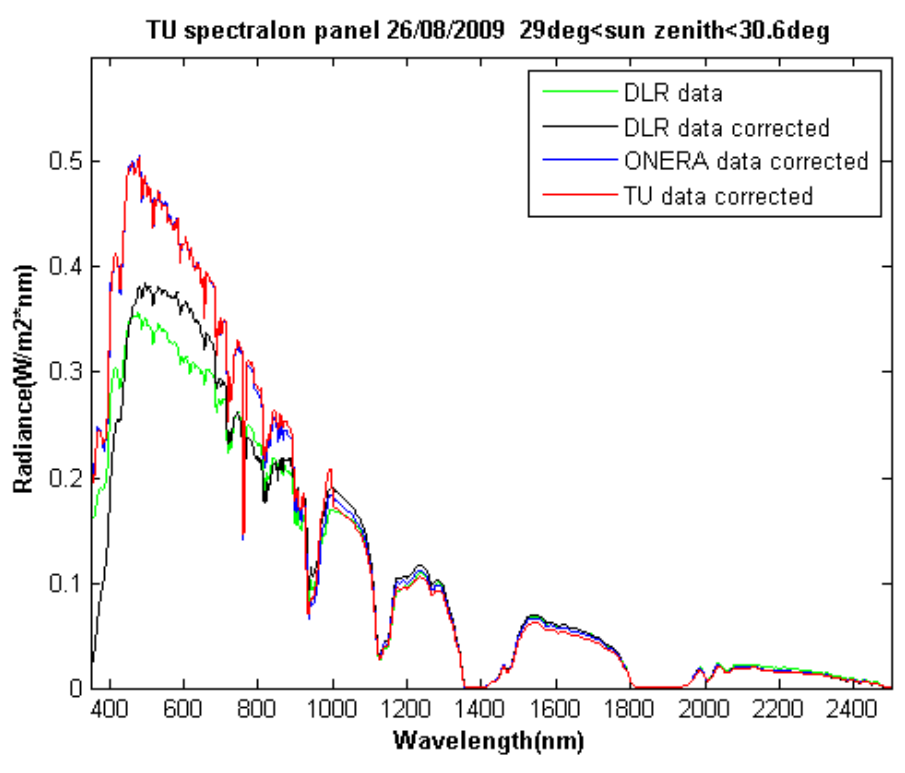


Figure 17: Radiance measured against the NPL Spectralon@ panel with the participant reported standard uncertainty



**Figure 18:** Radiance measured against the NPL Spectralon@ panel. The values are corrected using the gains from 23<sup>rd</sup> August 2009. The associated standard uncertainty (um\*) was recalculated using GUM.

### TU reference panel



**Figure 19:** Radiance against the TU panel as measured by DLR, ONERA and TU instruments Data were corrected using the gains from 23<sup>rd</sup> August 2009.

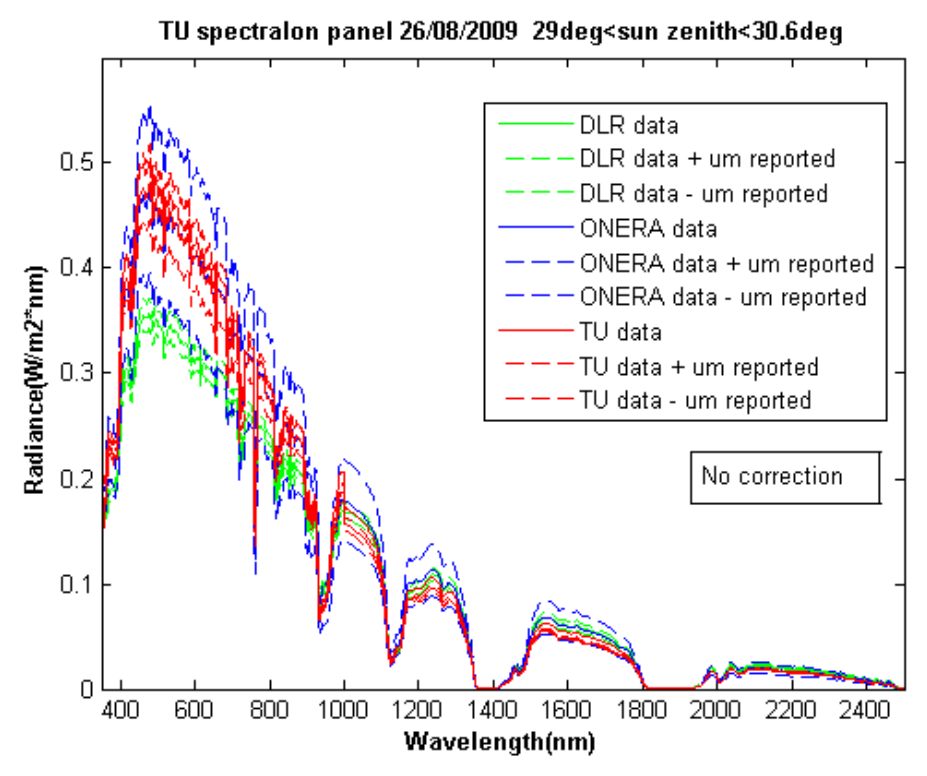
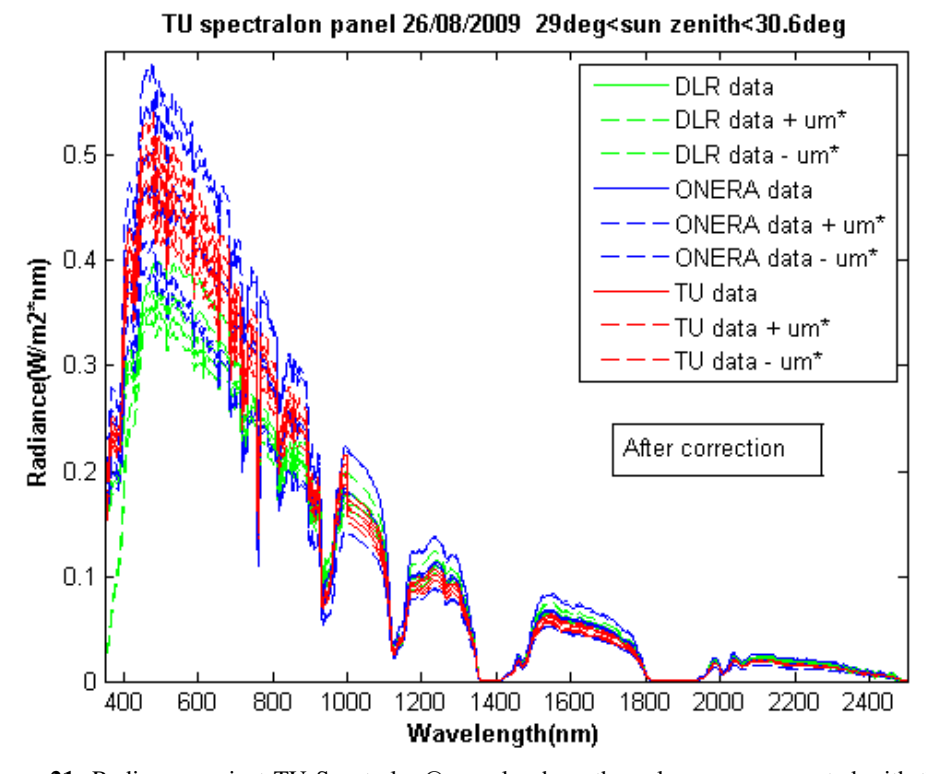


Figure 20: Radiance against TU Spectralon@ panel with the reported standard uncertainty um



**Figure 21:** Radiance against TU Spectralon@ panel, where the values were corrected with the gains from 23<sup>rd</sup> August 2009

### 3.2.5 Characterisation of participants' reference panels

The radiance values were measured over the participants' reference panels in a timeframe when the sun zenith angle varies between 29° and 30.6°. This illumination conditions were used for the field characterisation of the reference panels. In this way the participants' reference panels are characterised against the NPL reference panel and this characterisation has traceability to SI standards.

The NPL panel was characterised in the laboratory for an illumination angle of  $30^{\circ}$  for nadir view. The  $\rho$  for the lab1 reference panel will be calculated using the formula:

$$\rho_{lab1}(\lambda) = \sum \frac{1}{3} \left( \frac{L^{lab1\,panel}_{lab1}(\lambda)}{L^{NPL\,panel}_{lab1}(\lambda)} + \frac{L^{lab1\,panel}_{lab2}(\lambda)}{L^{NPL\,panel}_{lab2}(\lambda)} + \frac{L^{lab1\,panel}_{lab3}(\lambda)}{L^{NPL\,panel}_{lab3}(\lambda)} \right) * \rho_{NPL}(\lambda)$$

where lab1=DLR, lab2=ONERA and lab3=TU,  $\rho_{NPL}(\lambda)$  is the reflectance factor of the NPL calibrated reference panel measured in the lab for 30° illumination angle at nadir. (The approximate time of the measurements of the NPL panel was 11:56 to 12:20 local time that means about 9:00 UTC). On 26<sup>th</sup> August 2009 at 9:00 UTC was characterised by a sun zenith angle of 30° and  $\rho_{NPL}(\lambda)$  for 30°-illumination angle (measurement in the laboratory) was used in further calculations.

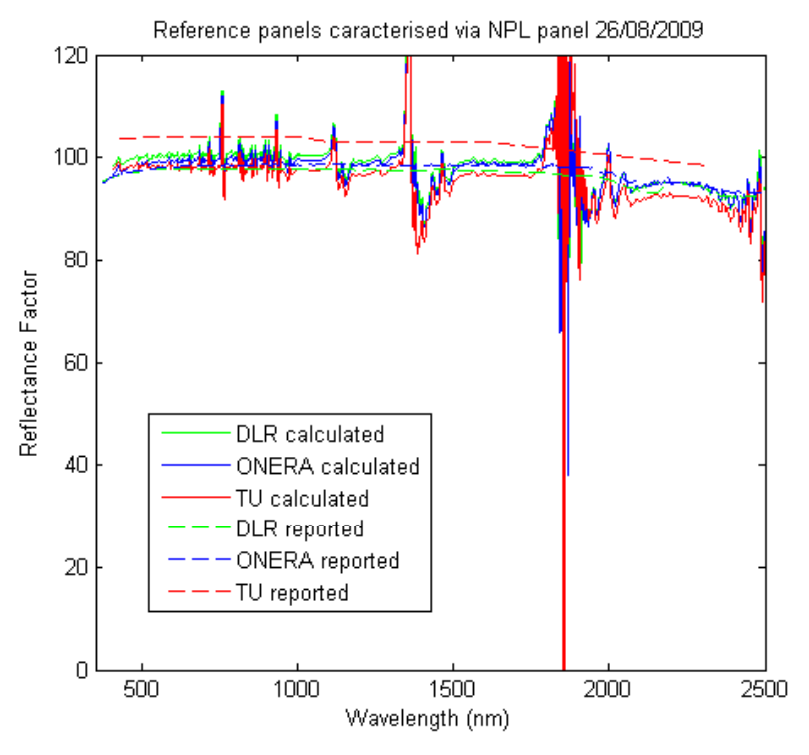


Figure 22: Reflectance factor of DLR, ONERA, TU as reported by the participants (dashed line) and after NPL calculation using the equation (solid line).

The calculated values show peaks specific to the absorption bands of atmospheric water and CO<sub>2</sub>. The atmospheric conditions changed from one to another measurement within a timeframe of 30 minutes. A further smoothing of the graphs could be applied.

These values were compared with those reported by participants for their reference panels and further used to calculate the  $\rho$  of the site. There is a small difference between the calculated values using  $\rho_{NPL}(\lambda)$  values and those reported by the three participants probably due to differences in the baseline illumination and measurement conditions during the primary calibrations, which was believed to be hemispherical for those from Labsphere and goniometric from NPL. One surprising exception is  $\rho_{TU}(\lambda)$  which represents the reflectance factor values of the reference panel as measured at nadir for 30°-illumination angle. The calculated value of  $\rho_{TU}(\lambda)$  is smaller than the  $\rho_{TU}(\lambda)$  reported values which should be based on the same calibration (Figure 23). The reason for this apparent anomaly is unknown and no indication of any error has been received from TU and so we cannot explain the cause.

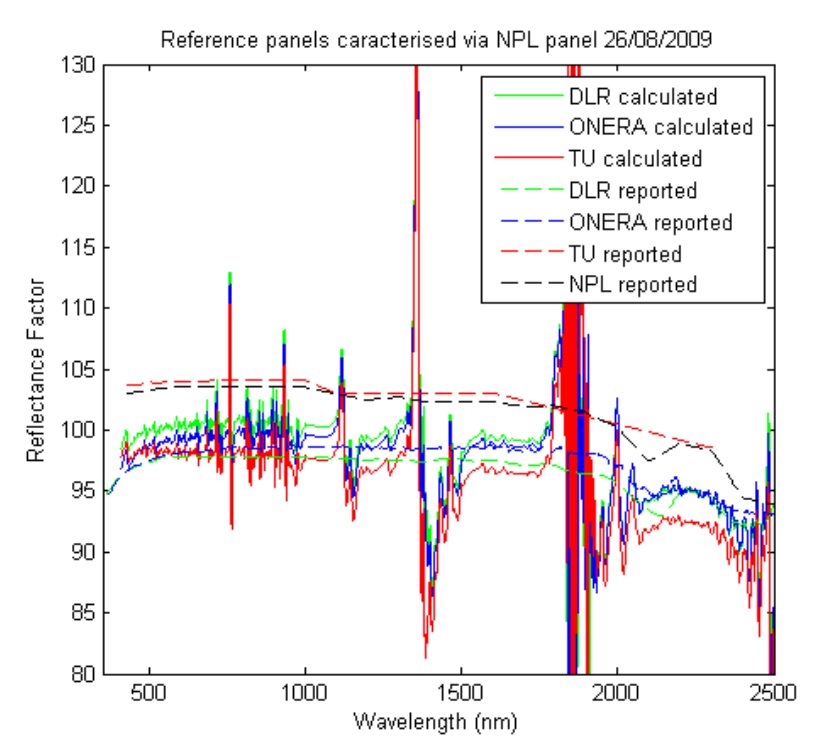


Figure 23: Zoom of Figure 22.

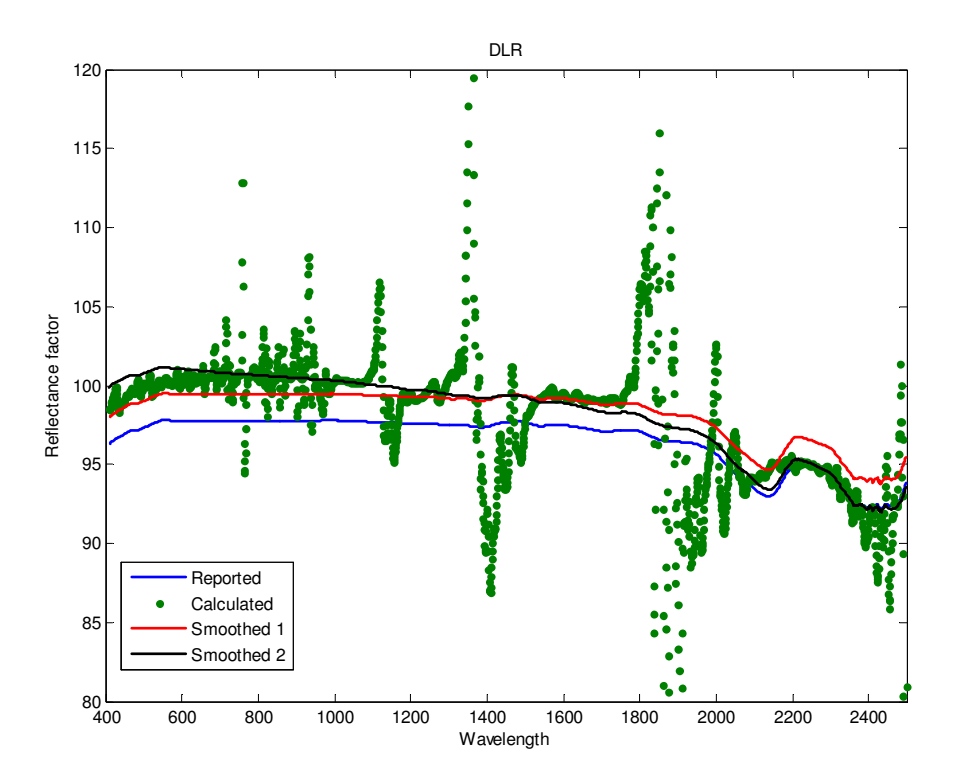
The  $\rho_{DLR}$  and  $\rho_{ONERA}$  reported values are a little bit lower than those calculated in the field using the  $\rho_{NPL}$  characterised for 30°-illumination angle.

Figure 24 illustrates some 'attempts' to use the reflectance factors reported by DLR and ONERA to 'smooth' those calculated by NPL using the NPL reference panel. This is done by 'modelling' the differences between the reported and calculated values as (1) a constant, or (2) a straight-line function of wavelength, and using the models so determined to 'correct' the reported values. The attempts are unreliable due to the significant noise and variances caused by atmospheric changes. It is noted that although the reflectance factors calculated by NPL in the two cases are not smooth, the two traces exhibit a number of common features which can be associated with atmospheric and water features. However the  $\rho$  is known to be spectral dependent and the results of method (2) are the only ones to be further considered.

A check of previous results was done using ONERA reference panel reported value of  $\rho_{ONERA}$  to calculate  $\rho$  for DLR, NPL and TU reference panels, using the above equation. Figure 25 showed consistency between the declared and the calculated  $\rho_{NPL}$  reference panel (solid and dashed black lines).

 $\rho_{DLR}$  reported values are a little bit lower than those calculated in field using the  $\rho_{ONERA}$  characterised by Labsphere for a diffuse illumination.

The calculated  $\rho_{TU}$  is smaller than the  $\rho_{TU}$  reported values as in the previous case. Another check was done using TU Spectralon@ panel as reference panel to calculate the  $\rho$  of the other reference panels (see Figure 26).



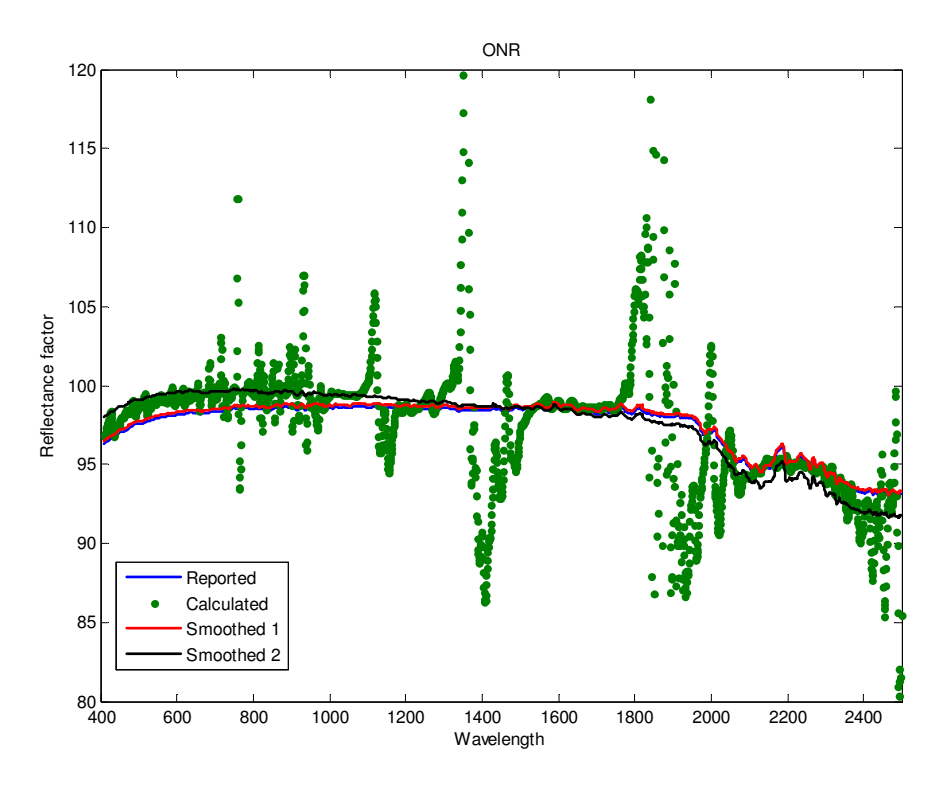
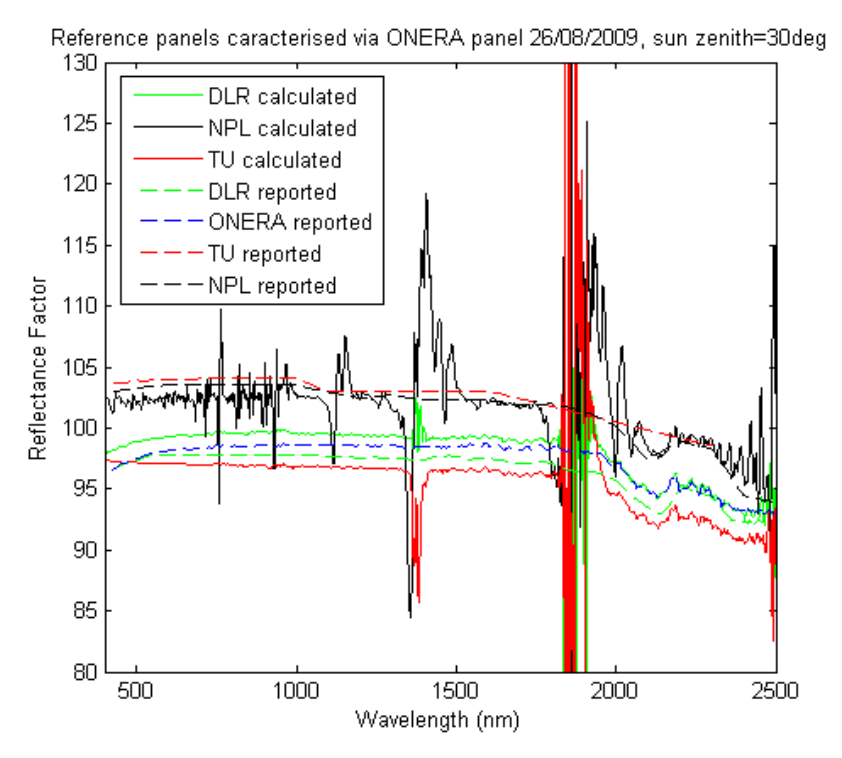


Figure 24: Matching the reflectance factors reported by DLR (top) and ONERA (bottom) to those calculated by NPL.



**Figure 25:** Reflectance factor of DLR, NPL and TU reference panels as reported and as calculated considering ONERA as white target for these measurements.

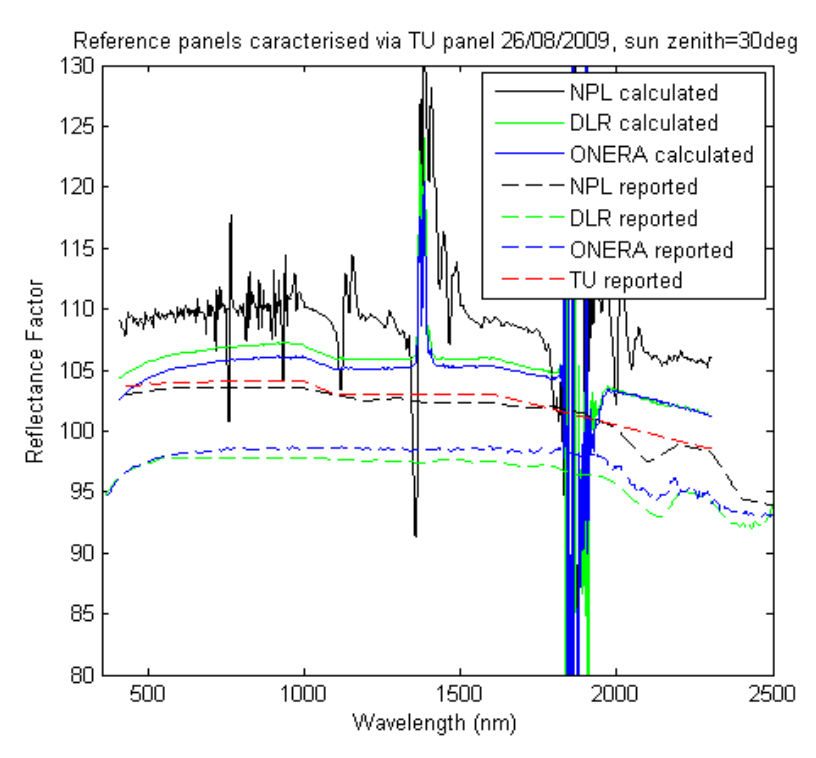


Figure 26: Reflectance factor of NPL, DLR and ONERA reference panels using TU Spectralon@ as white target.

The differences observed on Figure 23, Figure 25, Figure 26 are to be interpreted according to the poor weather conditions of 26<sup>th</sup> August 2009 (cirrus and clouds).

#### 3.3 Field measurements: Cross-comparison against NPL reference panel

#### 3.3.1 Procedure

The reflectance panel comparison on 26<sup>th</sup> August 2009 was subject to illumination changes due to partial cloud cover and high-level cirrus. As a result of this the reflectance panel comparison was repeated on 27<sup>Th</sup> August 2009 for the NPL panel and only for one illumination angle.

#### 27/08/2009

The measurement procedure was slightly different to that on 26<sup>th</sup> August 2009. The NPL stand was set up for nadir on the NPL panel. The first participant inserted their fibre into the TU pistol grip and measured the panel three times. After that the next participant inserted their fibre and made three measurements, followed by the third participant. It was done like this to try to reduce the time between the participants measurements and so therefore reduce the affects of any illumination changes. The whole sequence was repeated three times so that each participant made three independent measurements.

The instrument measurement conditions were also different. They were now the same as for TSARS measurements:

Spectrum – 10 scans averaged Dark Current – 25 scans averaged White reference – 10 scans averaged

The measurements started at 9:29 local time (6:29 UTC) at a location with 38.81 N lat 33,40 E long. The approximate times, sun zenith angles and order of the participants is resumed in **Table 4**. The sun zenith angles are calculated using the software developed by University of Oregon, *Solar Radiation Monitoring Laboratory* [13].

	First Run	Second Run	Third Run
TU	09:29, θs=52.78°	09:40, θs=50.78°	09:49, θs=49.16°
DLR	$09:32, \theta s=52.23^{\circ}$	$09:41, \theta s=50.60^{\circ}$	$09:48, \theta s=49.34^{\circ}$
ONERA	09:35, θs=51.69°	09:43, θs=50.24°	09:50, θs=48.98°

**Table 4:** The schedule of the inter-comparison of radiometers against the NPL reference panel, where  $\theta s$  – sun zenith angle, where  $\theta v$  – viewing angle was zero (measurements at nadir)

# 3.3.2 NPL calibrated reference reflectance panel

NPL and TU reference panels were calibrated following the same methodology. The main difference is that the NPL reference panel was calibrated not only for nadir view but for a series of viewing zenith angles between 10° and 50°, which are specific to the goniometric system GRASS used for the site characterisation.

#### Spectralon@ calibration methodology

The BRDF effects of the Spectralon@ reference panel were determined through measurements on a primary reference reflectometer based on a goniometer.

#### **Definition of terms**

The results reported here are specified as *Reflectance Factors*. The relationship between this and Radiance Factor and BRDF is discussed in **Appendix B**.

#### Reflectance measurement apparatus

A goniometric system was used to orient the sample and detector with respect to the (fixed) incident beam. Description of the apparatus and the measurement methodology can be found in the literature [14][15]. The source was spectrally filtered light from a tungsten filament lamp. Due to time constraints, not all filters were used in all geometries however given the relatively smoothly varying spectral properties of Spectralon@ this was not considered a significant issue. The bandwidth of the filters was nominally 20 nm in the visible and 20 - 30 nm in the IR. A silicon photodiode was used to detect wavelengths up to 1000 nm, and a liquid nitrogencooled InSb detector was used for longer wavelengths.

## **Angles**

Several angle combinations were specified. By convention, incident and viewing angles are each positive when they are respectively on opposite sides of the sample normal. As a test of alignment as well as azimuthal invariance of the sample, measurements were typically repeated with corresponding negative values of the incident and viewing angles.

# **Uncertainty Analysis**

The Spectralon@ calibration uncertainties (k = 1) are:

```
± 0.3% from 409 – 1001 nm
± 1.0% from 1100 – 2000 nm
± 1.5% from 2100 – 2500 nm
```

## 3.3.3 Data

Data are in **Appendix C: Participants' reported data**.

#### 3.3.4 Results

The reported radiance values by DLR, ONERA and TU are represented in Figure 27. The reported values for DLR were corrected using the gains and the expanded uncertainty um takes into account the standard uncertainty of Gains.

The expanded uncertainty associated with the radiance measured on 27<sup>th</sup> August 2009 is:

$$u^{27}_{lab1} = 2\sqrt{u^2(L^{23}_{lab1}) + u^2(TypeA + TypeB)^{27}_{reportlab1}}$$

where, the uncertainty Type B associated with TSARS  $u^2(L_{TSARS})$  is cancelled because it is the same for all three radiometers.

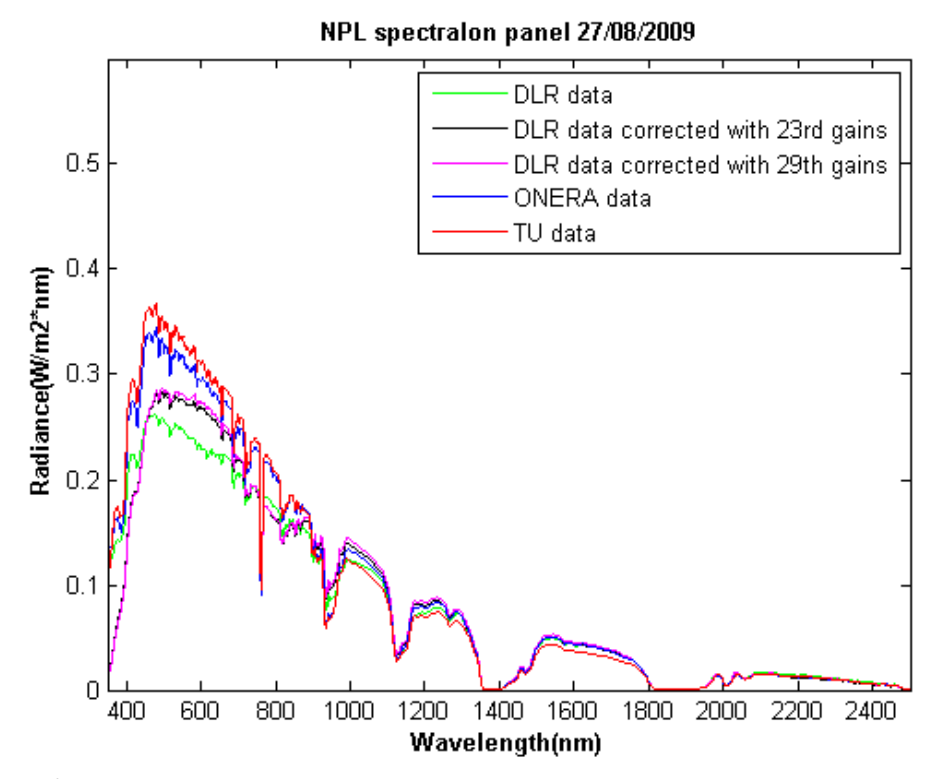


**Figure 27:** Radiance measured over the NPL reference panel by DLR, ONERA and TU on 27/08/2009 with reported values and corrected values for DLR considering the gains calculated from 23/08/2009 and 29/08/2009 laboratory calibrations.

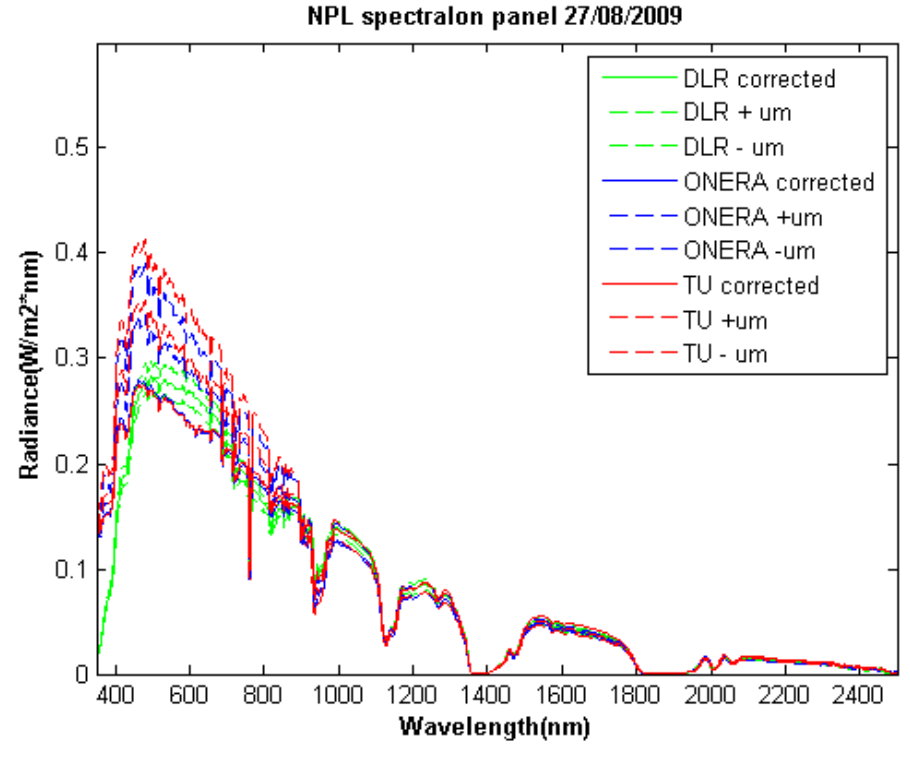


**Figure 28:** Radiance values measured over NPL reference panel by DLR, ONERA and TU on 27<sup>th</sup> August 2009, corrected with the gains from 23<sup>rd</sup> August 2009 calibration. The combined standard uncertainty um reported by participants is represented on this graph.

After the correction of all radiance values the resultant measured values are better grouped, however the uncertainties associated with TU and ONERA are important and this brings all measured-corrected values in the same range (Figure 28).

This exercise showed that with these sort of atmospheric conditions the more runs the better and thus for the CEOS key comparison in August 2010. Ideally each participant should perform five runs, where each run should consist of five measurements.

# 4 Site surface characterisation

Tuz Gölü standard reference test site has been identified as suitable for the vicarious calibration of medium and high-resolution optical remote sensors due to its large spatial uniform surface with a diameter about 20 km. The spatial uniformity was proven during the 2008 measurement campaign for the site characterisation organised by NPL and TU. It is of course recognised that the site radiometric properties (ρ) needs to be determined through a sampling strategy optimised to suit the resolution of the intended sensors and in this comparison potential variances due to differences in these strategies was under evaluation. Since the site has multiple potential uses TU selected and marked one sampling site of 1 km x 1 km for the medium resolution optical sensors, and three sites of 100 m x 300 m for the high-resolution sensors. The sampling sites for the vicarious calibration of high-resolution optical sensors had markers (black plastic sheets) of 50 m x 50 m as per Figure 29.

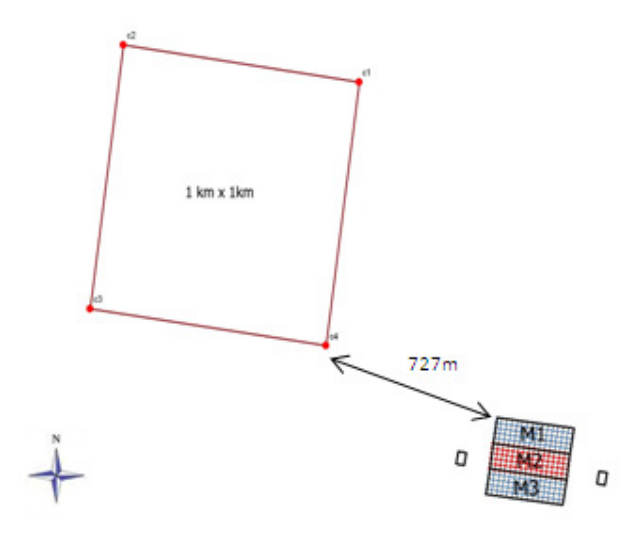


Figure 29: Sampled sites during the pilot land comparison during August 2009, Tuz Gölü.

The participants: DLR, ONERA, and TU characterised the sites by measuring the  $\rho$  and NPL measured the BRDF as presented in Table 5:

	25/08/2009	26/08/2009	27/08/2009	28/08/2009
DLR	1 km x 1 km	Radiometers cross	100 m x 300 m (M1)	100 m x 300 m (M3)
ONERA	100 m x 300 m (M1)	comparison via reference panel	100 m x 300 m (M2)	100 m x 300 m (M3)
TU	100 m x 300 m (M2)		1 km x 1 km	100 m x 300 m (M3)
NPL	Near M1		Near M1	Near M1

**Table 5:** The schedule of the site characterisation from 25<sup>th</sup> to 28<sup>th</sup> August 2009.

#### 4.1 Reflectance factor

# 4.1.1 Method and sampling

The  $\rho$  of the test site surface is calculated from the radiance measurements performed with a portable spectroradiometer. Such measurements are usually made in comparative mode by alternately viewing a lambertian reflecting panel of known reflectance illuminated by the Sun and the surface illuminated by the "same Sun". This measurement can of course only be made at specific locations at specific times and whilst some changes due to sun illumination angle variation can be accounted for by frequent cross-referencing to the panel, this requires relatively small differences in the BRDF characteristics of the panel and the surface being measured.

It is thus important to define a sampling strategy optimised to minimise variation due to temporal changes in illumination whilst maximising the area under test i.e. as short a time as possible.

In addition to the formal activities specified in the land protocol, CNES carried out a study to determine the "best practice" for the site characterisation using the reflectance based method. On first glance it appears quite easy to perform reflectance measurements (it is just a ratio between the radiance measured over a reference panel and the radiance measured over the ground) but it is also very important to be conscious of what is really measured. Some questions should be addressed before commencing any reflectance measurements:

- a) What is the best practice for reflectance measurements?
- b) Over which period of the day should these measurements be performed?
- c) Which optics is optimal to take into account of any spatial roughness of the surface?

By answering these questions, we can ensure that the spatial variability, which is measured, is only due to the surface and not a consequence of other parameters.

#### a) What is a good reflectance measurement protocol?

Surface reflectance is obtained by the ratio of two radiance measurements. Therefore, it is very important to be sure that the environment (atmosphere but also people which are around the measurement site) is the same between both measurements. If there is any cirrus (even very thin), the incoming irradiance will not be the same on the ground – it can vary very quickly and with large variation e.g. 20% is not untypical. To remove this problem, irradiance measurements should ideally be performed every second during the reflectance measurements, to be sure that the atmosphere is clear and stable.

Concerning the second point, it is very important to be conscious that the measured radiance is very sensitive to the environment and can be affected by people standing next to the measurement area. When a person stands up on a surface, it can have a number of impacts on the measured radiance compared to that when no one is present. e.g. some irradiance may be reflected by the body, some diffuse components are hidden and do not reach the ground. Of course it is only differences to how the

reference panel and surface react to these changes that matters. To evaluate these effects, ONERA and CNES performed some measurements using the ONERA ASD spectrometer on 25<sup>th</sup> And 28<sup>th</sup> August 2009. These results are presented in Figure 30. This figure highlights that the impact of the operator position is very important and the most important thing is to ensure that the same position of the operator is maintained during all the measurements.

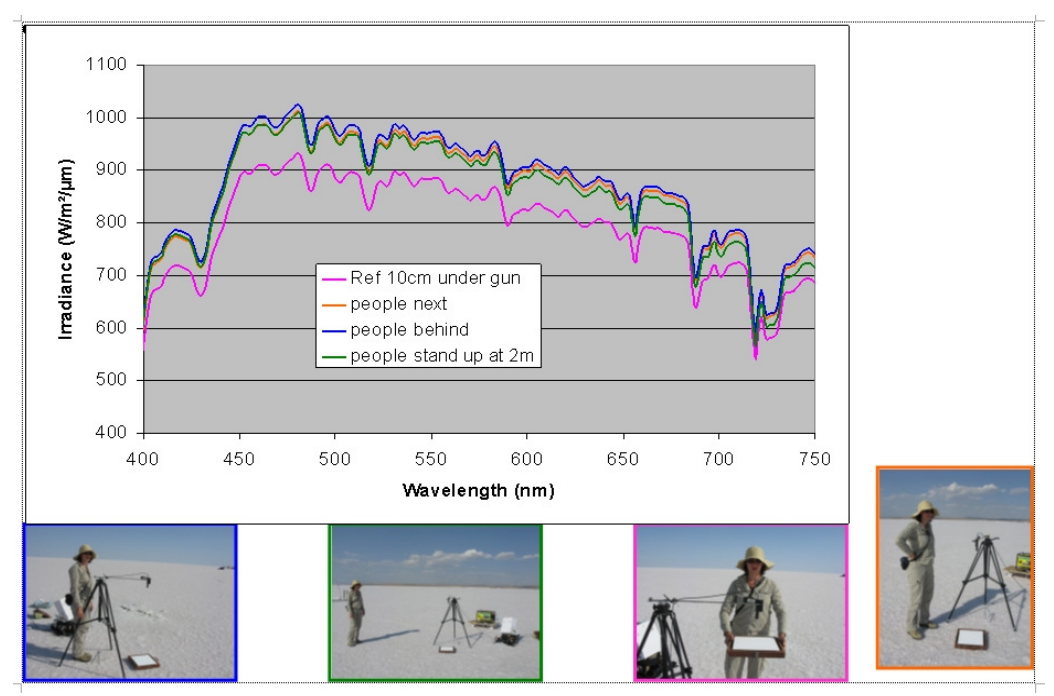
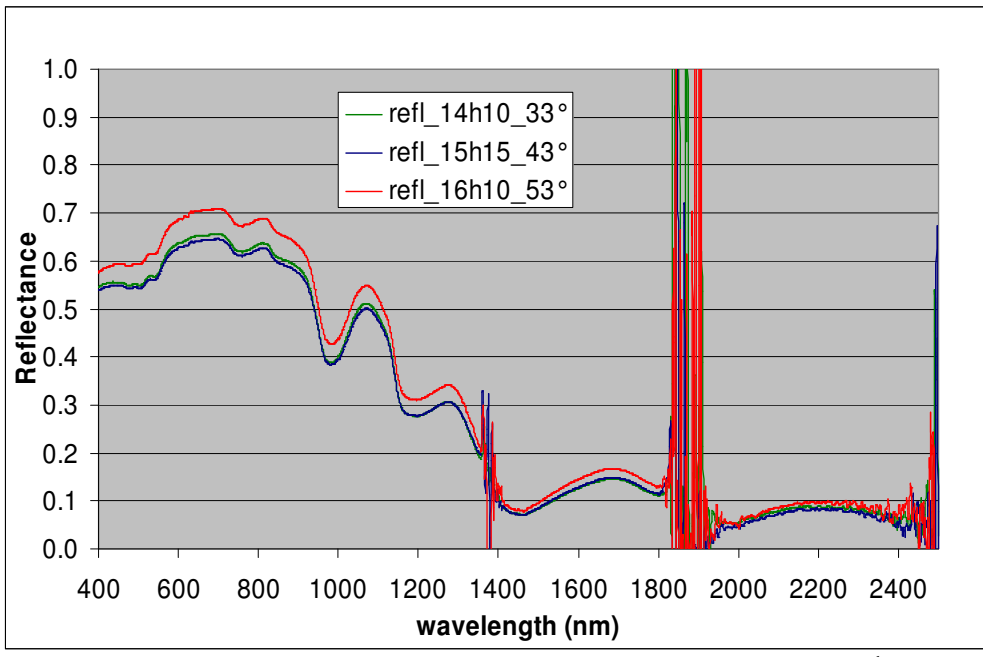


Figure 30: Impact of the operator position during measurements

#### b) Over which period of the day should these measurements be performed?

If the reflectance of the site is characterised by some directional effects, it is important to perform the reflectance measurements during a period where the sun zenith angle is quite constant. Otherwise, the bidirectional effects of the ground are significant in addition to its spatial variability. Very few surfaces have a lambertian behaviour. Therefore, it is important to take into account this parameter in particular when the characterisation of the site is targeted to match satellite measurements, which are planned early in the morning with very sensitive sun zenith angle.

Some measurements made with the ONERA's spectroradiometer showed that the Tuz Gölü site is characterised by a moderate specular behaviour (Figure 31). Therefore, to quantify the spatial variability of the site, it is better to avoid high zenith angles where the bidirectional effects are strong and to perform measurements when the sun is high.



**Figure 31:** Analysis of the bidirectional effect of the ground reflectance on 25<sup>th</sup> August 2009. The reflectance measurements were realised over the same surface.

# c) Which for optics is optimal to take into account the spatial roughness of the ground?

The goal of the campaign is to characterise the Tuz Gölü site. Several questions are then raised. For each point of measurement, how many measurements do we perform to obtain a good characterisation of the ground? As the surface of the lake is not homogeneous (Figure 32), what should be the spatial resolution of one representative reflectance measurement?

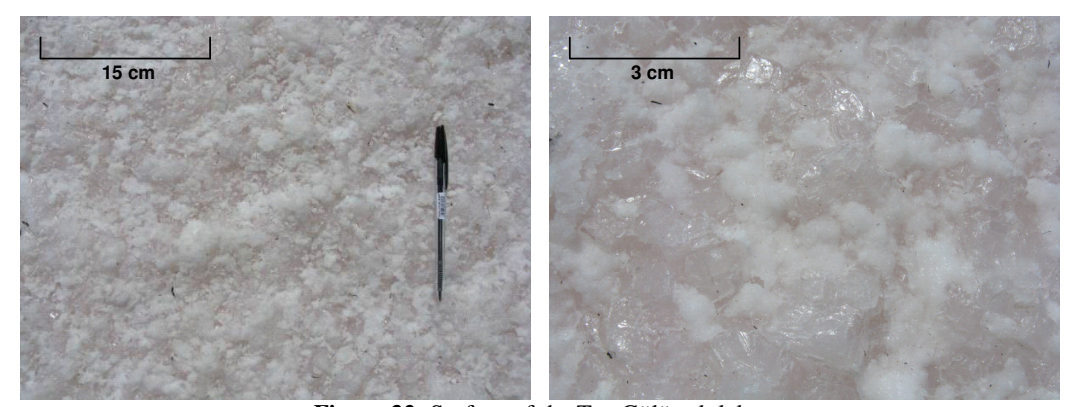


Figure 32: Surface of the Tuz Gölü salt lake.

To answer to this question, measurements were performed on the 25<sup>th</sup> August 2009 over the same point within several spatial resolutions (using different fore optics) as in Figure 33.

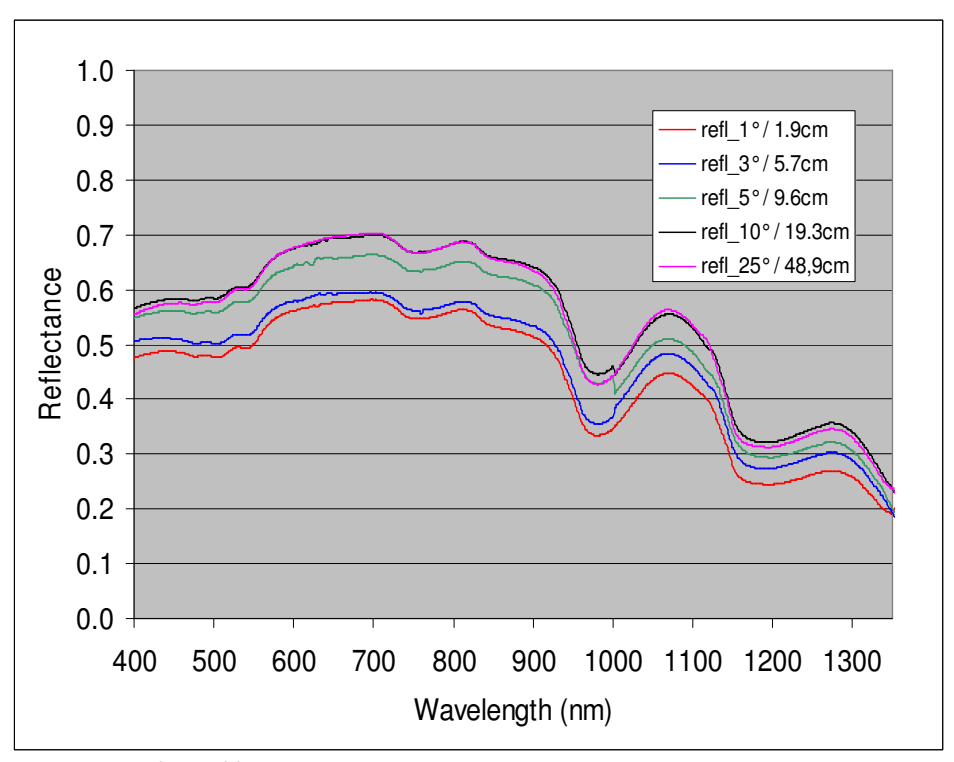


Figure 33: Influence of the spatial resolution of the measurements.

This figure shows that the best spatial resolution to characterize the ground is around 20 cm. If a smaller resolution is considered, an average of several measurements should be performed in order to obtain a representative reflectance taking into account the small heterogeneity of the ground.

# 4.1.2 Sampling patterns used by DLR, ONERA, and TU

During the pilot land comparison in Turkey 2009, there were differences in the patch size viewed by participants' radiometers at nadir (Table 6). However, the difference in patch size used should notluence the average value obtained over sampling sites of 1 km x 1 km or 100 m x 300 m.

	Height of measurements	FOV	Patch size viewed
DLR	1 m	8°	Ø14 cm
ONERA	1.45 m	5°	Ø13 cm
TU	70-80 cm	8°	98 cm2
NPL (nadir)	2 m	4°	Ø50 cm

**Table 6:** Sampling fore optics used and the patch size viewed by each participant.

Participants used different sampling strategy, and data processing as follows:

#### DLR

# Reflectance measurements and processing

#### Instrument setup and initial procedure:

- Set averaging for instrument (usually 40-40-40)
- Setting the instrument to reflectance mode
- Optimize instrument
- Take white reference
- Point towards other target, then point over Spectralon@ again & wait for display to refresh
- Check if reflectance over Spectralon@ is at 100%. If not, take white reference again.

# Measurement of targets:

- 5 nadir measurements are taken for each target at slightly different positions within ~0.5 m on ground
- All measurements are taken facing the sun & measuring perpendicular in order to minimize scattering from body into measurement
- During measurements check if reflectance measurements are similar. If not, protocol.

# Repeated check after each target:

- Point over Spectralon@ and wait for display to refresh
- Check if reflectance over Spectralon@ is within 99% 101%, and reflectance curve has no shape. If not, take white reference.
- Even if Spectralon@ reflectance is still at ~100%, white reference are taken at least every 10 minutes
- Optimization is carried out if saturation occurs (instrument message), or at least every 10 minutes

## Post-processing:

## Using DLRs IDL-Software ASTools ":

- Import ASD raw files in ENVI
- Visual check of all spectra for errors. All 5 measurements of one target should be similar -if not, discard error-prone measurement.
- Assign meaningful names to spectra
- Correct all spectra independently for "steps" between the different ASD detectors using additive approach setting the second spectrometer as reference
- Correct for Spectralon@ reflectance characteristic using the lab characterization
- Save as ENVI spectral library
- Average all 5 target measurements, calculate min, max and standard deviation as measure of spectral variability of target
- Check if standard deviation for target is unusually large. If so, check if single
  measurements are consistent. If not, discard inconsistent measure, and repeat
  averaging.
- Finally save as ENVI spectral library (i.e., mean + standard deviation for every target)

# Measurement procedure for 1 km x 1 km site (25<sup>th</sup> August 2009)

#### Setup:

- Instrument internal averaging: 30 -30 -30
- Measurements in reflectance as well as radiance mode

#### Sampling method:

- All measurements were taken facing the sun & measuring perpendicular in order to minimize scattering from body into measurement
- Large transect diagonal over the area from NW corner to SE corner
  - O Total of 143 measurements
  - O From 10:49 till 11:42
  - Bare fiber
  - O Measurements taken every ~30 m
  - O Reflectance measurements according to procedure described above
  - O Additional radiance measurements according to procedure described above
- Additional transect from point E532383 N4296052 towards center of the area
  - O Total of 36 measurements
  - O From 12:03 till 12:24
  - $\circ$  8° for optics
  - O Measurements taken every ~30 m
  - O Reflectance measurements according to procedure described above
  - O Additional radiance measurements according to procedure described above
- Additional transect from center back to the same corner
  - O Total of 20 measurements
  - O From 12:24 till 12:37
  - O Bare fiber
  - O Measurements taken every ~30 m
  - O Reflectance measurements according to procedure described above
  - O Additional radiance measurements according to procedure described above

# Measurement procedure for area M1 (27<sup>th</sup> August 2009)

#### Setup:

- Bare fiber
- Instrument internal averaging: 10 -25 -20
- Measurements in radiance mode

#### Sampling method:

- Total of 4 transects for area M1
- Spectralon@ measurements and optimization at every second flag
  - O Each Spectralon@ measurement consists of 3 single measurements
- Salt surface measurements for 17 sub-areas along transect
  - O Measurement taken close to flag location and half way in-between flags
  - O 4 locations per sub-area
  - O 3 single measurements per location within ~0.5 m on ground
- All measurements were taken facing the sun & measuring perpendicular in order to minimize scattering from body into measurement

#### Data:

- File: DLR m3 points.xls
- Average of 17 sub-areas with standard deviation

- In addition, the adjusted ('smoothed') measurements are included Notes:
  - Point 15 + 16: unusual salt surface

Measurement procedure for area M3 (28th August 2009) as per Figure 34

#### Setup:

- 8° for optics
- Instrument internal averaging: 10 25 20
- Measurements in radiance mode

#### Sequence of transects:

- Row A (start: 11:30)
- Row B (start: 11:57)
- Row C (start: 12:27)
- Repetition of row A for comparison with TU measurements (start: 13:00)

# Sampling method:

For each point marked with flag:

- 1 Spectralon@ measurement
- 8 measurements in ~1 m distance around the flag pole
- 1 Spectralon@ measurement

#### Data:

- File: DLR\_m3\_points.xls
- Average of 8 measurements and standard derivation for each of the 18 flag point
- In addition, the adjusted ('smoothed') measurements are included
- Also the data for the repeated first 6 points is included

#### Notes:

- Point 2: discarded during quality control since larger difference between Spectralon@ radiance measurements before and after target
- Point 13: unusual salt surface

Row A was repeated in order to allow a comparison with measurements by TU who started later due to technical problems



Figure 34: DLR sampling technique over M3 site on 28<sup>th</sup> August 2009

#### **ONERA**

ONERA sampling strategy is represented in Figure 35 and Figure 36. M1 (100 m x 300 m) and M2 (100 m x 300 m) had sixteen sampling points. At each sampling point ten measurements were recorded as follows:

- First reference panel measurement
- Six to eight ground measurements, usually eight (except M2 D.05: 34 ground measurements + 6 references). All measurements have been made at different places around sub-zone centre
- Second reference panel measurement

M3 (100 m x 300 m) was characterised by all participants in the last day. This site had eighteen sampling points marked previously by the organisers. At each sampling point ONERA recorded ten measurements (two reference panel measurements and eight ground measurements) as described previously Figure 36.

Data were processed using the ASD software for the parabolic correction and to convert the ASD files in ASCII (text files). Data processing was performed using Visual Basic software, which calculates all parameters related to reflectance, average, standard deviation and uncertainty. Type A uncertainty had been calculating according to the hypothesis of ground spectral reflectance regularity. This method seems to overestimate the uncertainty in water absorption bands.



**Figure 35:** Sampling of M3 site as performed by ONERA on 28<sup>th</sup> August 2009.

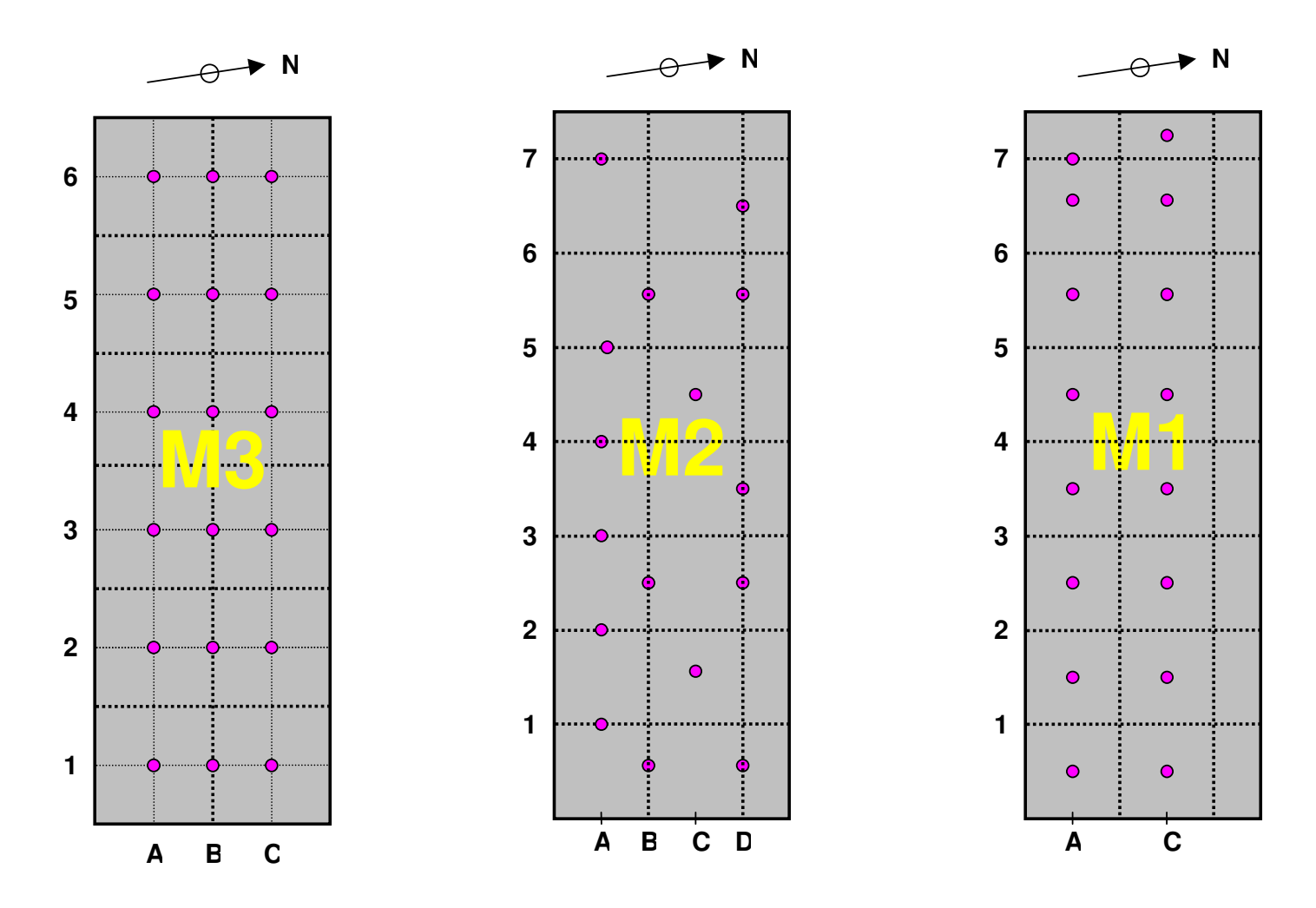
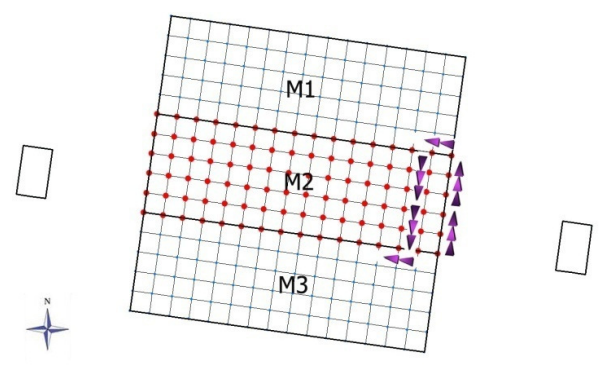


Figure 36: Sampling strategy used by ONERA for M1, M2 and M3 sites.

# **TU**

# 25<sup>th</sup> August 2009, M2 sampling site

TU performed the measurements over M2 area, which is a surface of 100 m x 300 m. The measurement strategy for M2 is shown in Figure 37. The area is sampled by 20 m x 20 m taking into consideration Beijing1, PROBA and UK DMC2 optical sensor pixel size. It is aimed to take at least one measurement for each pixel. Measurements are taken from 96 points. Outliers are eliminated and there are some missing data; therefore totally 78 points are used to obtain reflectance value of this area. Measurements are performed between 7:00 UTC and 8:00 UTC.



**Figure 37:** Measurement strategy used for M2 area. The measurements are taken over the red points and the purple arrows indicate the sampling direction.

# 27<sup>th</sup> August 2009, 1 km x 1 km sampling site

TU has performed the measurements on 1 km x 1 km area. Spiral shape of measurement sampling strategy (Figure 38) is chosen for this area. There are in total twenty-five points to be measured. The area to be walked is 4800 m. Measurements were performed between 7:36 UTC and 9:21 UTC.

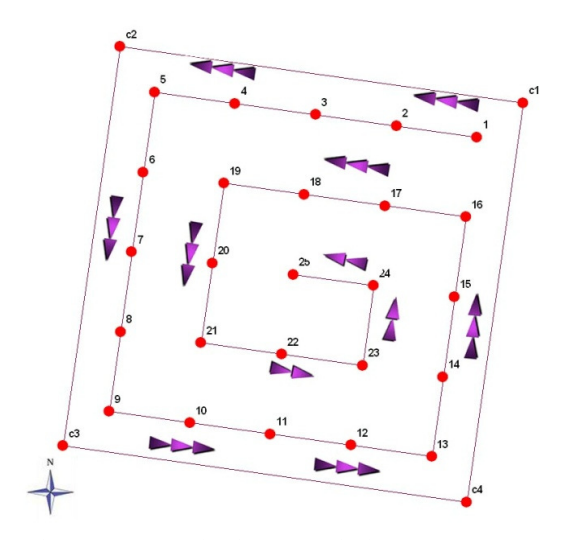


**Figure 38:** 1 km x 1 km site was sampled using the spiral measurement strategy. Red dots show the measurement points and the purple arrows indicate the sampling direction

# 28th August 2009, M3 sampling site

All teams performed measurements on the same area M3 at the same time. In total eighteen measurements were taken. At each measurement point, four different points were chosen from its surrounding. The ONERA baseline figure is represented in Figure 39, where the three TU sampling transects are marked with a blue line. The measurements took place between 09:43 UTC - 10:14 UTC.

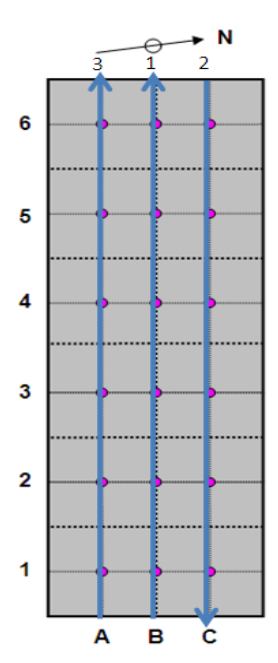


Figure 39: TU Sampling technique over the M3 (100 m x 300m) site.



Figure 40: TU team sampling M3 site on 28<sup>th</sup> August 2009

#### 4.1.3 Sources of uncertainty

There are many potential sources of uncertainty associated with measuring surface reflectance and in associating a reflectance value to a site for use by a satellite sensor. At present the best-achieved uncertainty according to the literature is around 2 - 2.5%. This uncertainty is dominated by traceability of the measurements to SI, assuming that the site is calibrated at the time of use, otherwise the value can easily double or more. The nature of most of the best calibration sites other than for very high-resolution sensors, is such that any small surface variation tends to be random in nature and so does not contribute significantly to the overall uncertainty budget.

The principle sources of uncertainty that can be ascribed to methods of measurement i.e. two different teams are:

- Reference panel characterisation; BRDF, uniformity
- Traceability of the field spectroradiometer and ensuring its calibration and usage matches the environment it is in i.e. temperature, battery power, "warm up" time, cleanliness or damage to for optics (particularly fiber optics, where bending can have a serious impact) and of course its stray light and wavelength calibration.
- Incorrect accounting for environmental scattered light, sky radiance, etc.
- Operator error in sampling the surface, due to reflections, shadowing, wrong angles, heights
- Biases due to surface variability and non-randomised sampling; missing surface features (cracks, stones, vegetation) slopes and timing sequences due to solar zenith angle variation.

# 4.1.4 Data analysis, reporting uncertainties

In reporting the results and uncertainties it was recommended that an average over a minimum of ten values collected over a similar area (1 m, 5 m, 10 m, 100 m, etc) should be calculated. As a consequence of the comparison, Table 7 now provides typical sources of uncertainty and indicative values as reported by DLR, ONERA and TU as a baseline for future comparisons.

**Table 7:** Sources of uncertainties for the measurement of the reflectance factor for FOV=8°

Source of uncertainties	Type	Typical values (k = 1)
Traceability to SI	Type B	350 – 1000 nm is 0.3 - 1.1%
(Reference panel reflectance)	Турс Б	1000 – 2500 nm is 1.5 - 3.2%
Drift from calibration	Type B	350 - 1000  nm = 0.71%
(TSARS calibration)		1000 - 2500  nm = 1.14%
Repeatability &		350 – 1000 nm is 1 - 4%
Reproducibility	Type A	1000 – 2500 nm is 1.2 - 3%
		(Excepting absorption bands)
Diffuse light correction	Type B	Not available
Spatial/Temporal stability	Type B	2 - 4%
Site characterisation time		350 –1000 nm is 1.2 - 2.3%
(If not corrected)	Type B	1000 – 2500 nm is 1.4 - 2%
		(BRDF effects of TU reference panel for
		30°, 37° and 40° illumination angles)

**Traceability to SI:** traceability in establishing the relation between the indication of a measuring instrument and the value of a measurement standard.

**Drift from calibration**: the difference between the radiance values measured before and after the field measurements with the same spectroradiometer using the same standard source in the same measurement conditions.

**Repeatability**: is the variation in measurements taken by a single person or instrument on the same item and under the same conditions. A measurement may be said to be *repeatable* when this variation is smaller than some agreed limit. (The range quoted above related to the non-uniformity of a site as measured by each group.)

**Reproducibility**: is one of the main principles of the scientific method, and refers to the ability of a test or experiment to be accurately reproduced, or replicated, by someone else working independently. (In this pilot comparison the reproducibility is the difference in value of the reflectance factor measured over different sites during different days by the same group, see further ONERA data in Figure 42)

**Diffuse light correction**: the natural irradiance is composed of a direct component (non-scattered radiation) and a diffuse component scattered by the atmosphere and the neighbouring objects of the observed area. The diffuse irradiance should be corrected before calculating the reflectance properties of the objects. Without this correction the measured reflectance characteristics are not intrinsic.

**Spatial/Temporal stability**: the surface of the test site to be characterised could be non-uniform in space and without stability in time due to changes in meteorological conditions between measurements.

**Site characterisation time**: the time required to characterise a selected surface of the reference test site could be different from one to another operator and depends on the skills and method used. The resulting value is influenced by the timeframe used to perform the characterisation due to variations in sun zenith angles.

# 4.1.5 Data

Data are in **Appendix C: Participants' reported data**.

#### **4.1.6** Results

The comparison of  $\rho$  values recorded by participants over the sampling sites (M1, M2, M3 sites of 100 m x 300 m) and 1 km x 1 km is presented here. The compared  $\rho$  values have the combined standard uncertainty added on the graph with dotted line. These are the values reported by each participant suing their methodology. NPL did not recalculate it because the provided data were insufficient ( $\rho$  averaged over the whole site and the associated combined standard uncertainty). However in chapter 6.4 we give recommendations how the standard uncertainty could be calculated and two references.

#### **DLR**

The comparison of the  $\rho$  values measured by each participant over all sites is represented in Figure 41 and put in evidence that DLR measured values are always lower than those measured by ONERA and TU, exception is made by the  $\rho$  values reported over 1 km x 1 km site. The difference between ONERA and DLR is about 6% over 600 - 1000 nm.

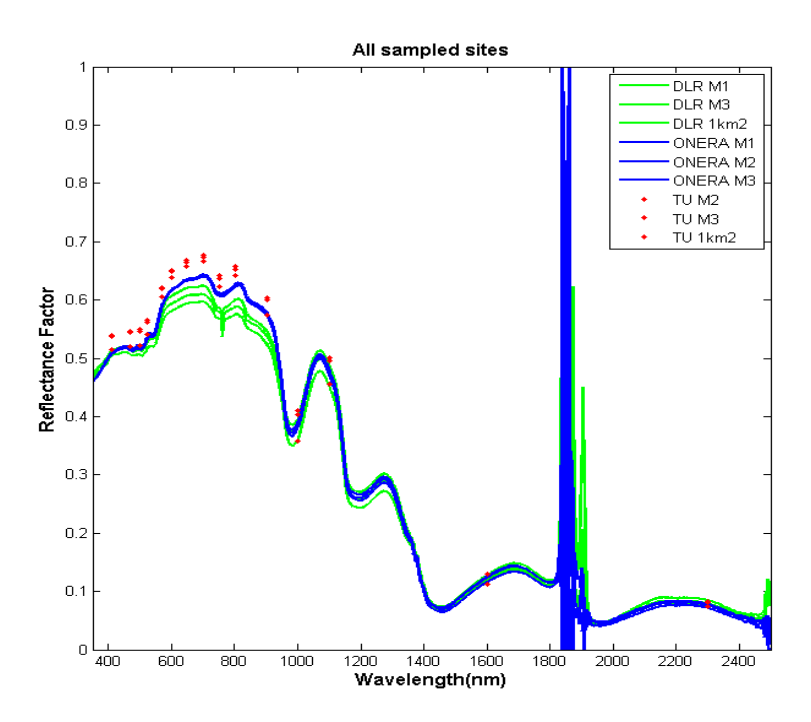


**Figure 41:** Reflectance factor as measured by DLR, ONERA and TU over M1, M2, M3, and 1km x 1km sites during the period from  $25^{th}$  to  $28^{th}$  August 2009.

Most of this difference can be explained by the DLR's post-processing procedures which aims to reduce the "step" likely to occur between the different detectors of the ASD FieldSpec Pro (i.e., silicon-based detector array up to 100 nm, single element InGaAs from 1000 – 1750 nm and from 1750 – 2500 nm) as described in [18]. For this purpose the measurements of the first detector are adjusted to the second detector altering the values up to 1000 nm. The remaining differences of DLR to the measurements by ONERA and TU are within 2% that is well within the expected range.

For the reason mentioned in the Chapter: Radiance and reflectance factor, the gains will not influence the  $\rho$  final calculated value and the  $\rho_{lab1}$  values used in this calculation are those reported by each participant (the data from  $26^{th}$  August 2009 were not good for a further correction see Chapter: Results of cross-comparison against reference panels).

The percentage difference of measured values by DLR over three different sites has a maximum of 10% over the spectral region 380 - 980 nm.

## **ONERA**

The  $\rho_{ONERA}$  reported values are very consistent and have similar values over the three sampled sites: M1, M2 and M3 as per Figure 42.

The percentage difference between all three over the spectral region 380 - 980 nm has a maximum of  $\pm$  1% well within the value given for repeatability and reproducibility in Table 6. The percentage difference above 980 nm is a maximum value about  $\pm$  7%, and is strongly influenced by the effects of water.

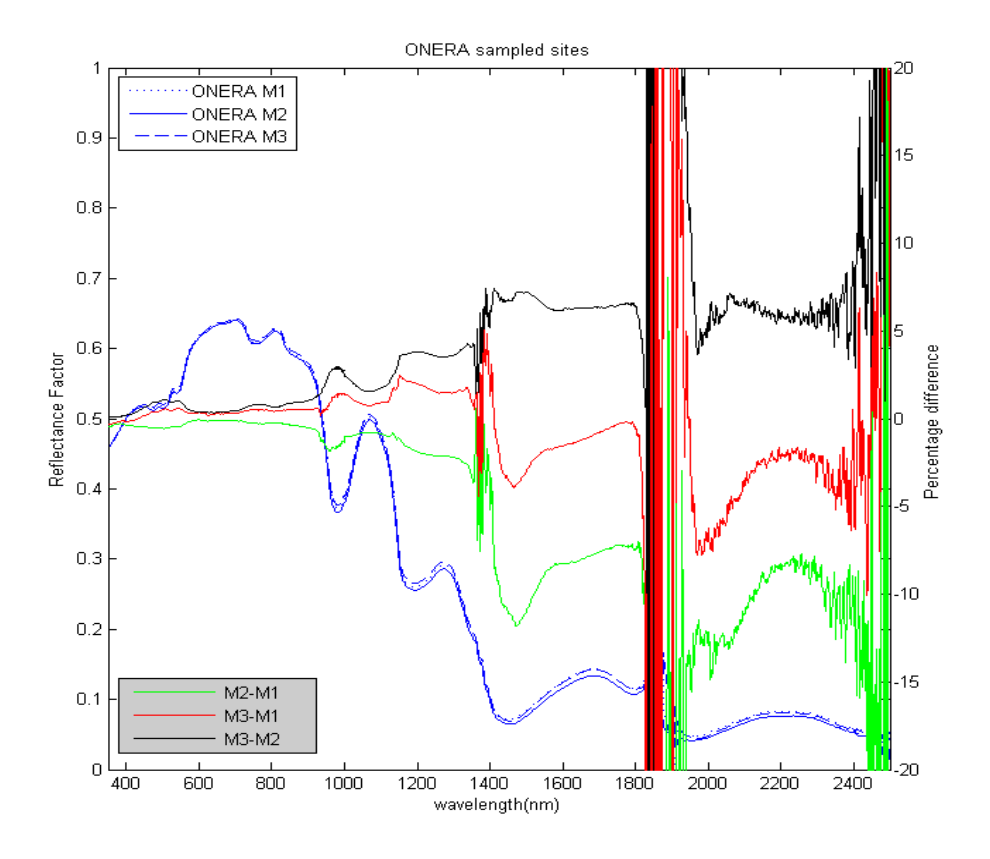


**Figure 42:** ONERA sampled sites and the percentage difference of the measured values over three different sampling sites.

#### TU

All  $RF_{TU}$  reported values are about 5% higher then those reported by ONERA over the spectral region 380 – 980 nm (see Figure 41). This is the result of the different methodology used to calibrate the TU reference panel using the bi-directional illumination and the ONERA panel is using the hemispherical illumination calibration method (Labsphere) as described in chapter 3.2.3.1. In Figure 15 are represented the reported  $\rho$  values of the participants' reference panel and there is a difference of about 3 - 6% between the  $\rho$  value of TU panel and ONERA panel. This explains the difference in Figure 41.

# Cross-comparison of participants' radiometers over M3

All participants measured the M3 site on 28<sup>th</sup> August 2009 using the same sampling points. Each participant provided the average of the measured value for each of the 18 points and the standard deviation for each measured point as per Figure 43.

In this figure are represented the TU reported  $\rho$  site values as calculated using the values of  $\rho$  panel calibrated by Labsphere (red solid line) and the TU reported  $\rho$  site values as calculated using the NPL calibration of the reference panel (red dots). The ONERA reported  $\rho$  site is represented with blue colour and the DLR reported  $\rho$  site is represented with green colour. The combined standard uncertainties are represented with dashed line (red, blue and green) for each participant.

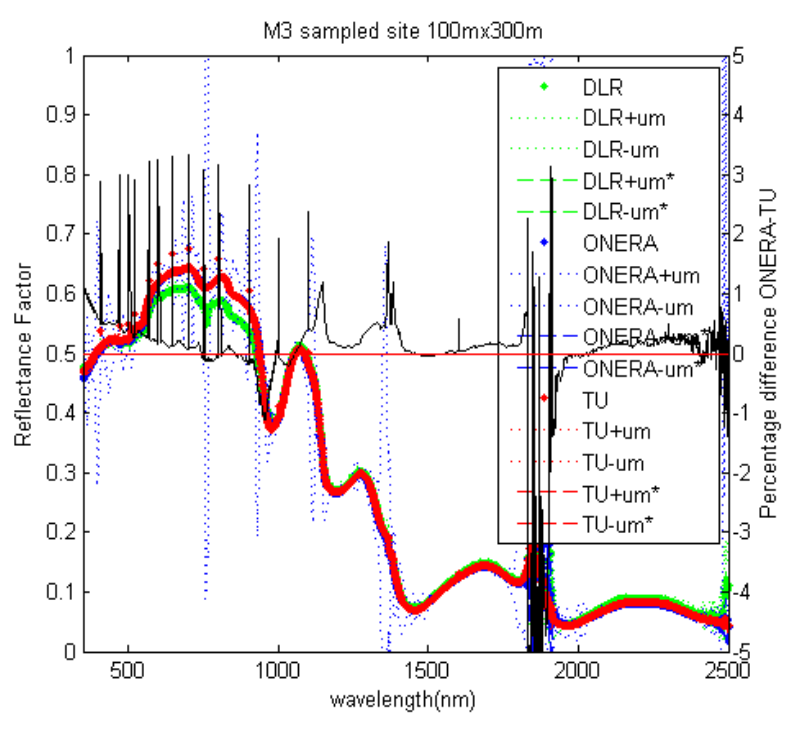


**Figure 43:** Reflectance factor of M3 as measured on 28<sup>Th</sup> August 2009 by DLR, ONERA and TU with the reported combined standard uncertainty

When TU use the  $\rho_{TU}$  panel values provided by Labsphere, the difference between the ONERA reported  $\rho$  site values and TU reported  $\rho$  site values is no more than 1% over 380 – 980 nm. That is within the spatial uniformity and temporal stability of the site as per Table 7.

#### Sampling the 1 km x 1 km site

The largest site of 1 km x 1 km used for the calibration of medium resolution optical sensors was sampled by DLR and TU on different days as per the schedule from Table 5. The reported  $\rho$  site values are within a difference of 1 - 2% over 380 – 980 nm between DLR and TU, when the  $\rho_{TU}$  panel values provided by Labsphere are used for the calculation of  $\rho$  site (red solid line for these TU reported values and black solid line for the percentage difference between  $\rho_{DLR}$  of site and  $\rho_{TU}$  of site as per Figure 44). The percentage difference is 5 - 6% when one uses the  $\rho_{TU}$  of panel resulted from the bi-directional calibration (red dots and the related black line in Figure 44). However DLR software introduced an uncertainty in the calculation of  $\rho$  site as mentioned previously. However 1 km x 1 km sampling site was carried out at the beginning of the campaign and maybe before the DLR instrument appeared to degrade (see Calibration checks).

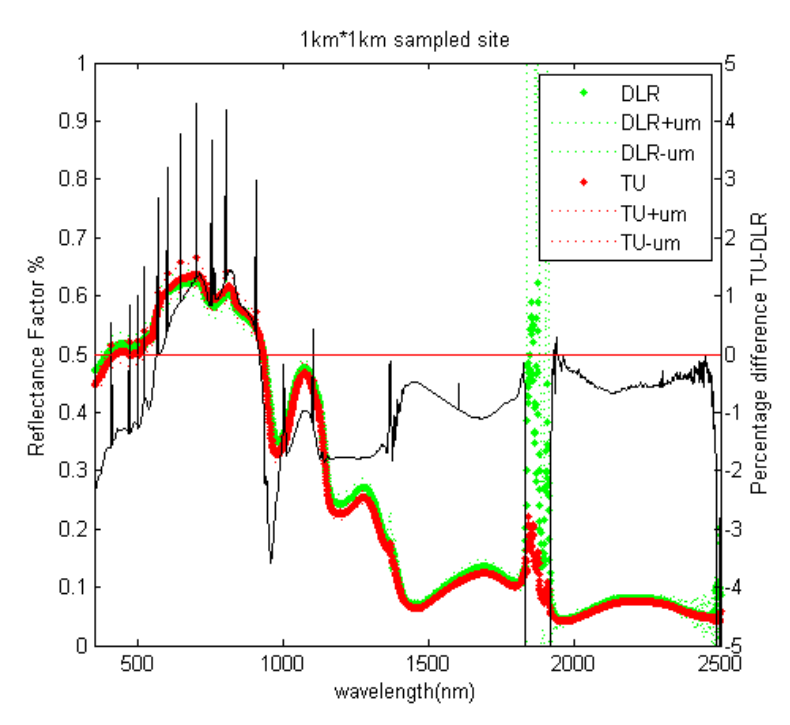


Figure 44: Reflectance factor of 1 km x 1 km site as reported by DLR and TU participants (solid lines) with the associated combined standard uncertainty (dashed line)

#### **4.2 BRDF**

#### 4.2.1 Method and sampling

The BRDF of a surface cannot be measured directly as it requires the measurement of the reflected light at infinitesimally small angles over a full hemisphere. Practically, BRDF measurements are made in the field, as measurements are usually made relative to a lambertian reflectance panel, and from these the BRDF can be inferred.

It should be noted, however, that the BRDF that can be derived from multi-angle measurements, are highly dependent on the instrument capabilities and the surface itself. A sampling method tailored to the target should be considered carefully, so that the main features of the surface BRDF are captured during such a measurement.

Most commercially available field instruments are single point sensors. Various sampling strategies and techniques to move these single point sensors can and have been devised to enable the BRDF to be inferred [19] [20] Figure 45 and Figure 46 show idealised distributions, where the horns are the enhanced forward and backscatter.

Using a fixed zenith angle method of measurement, the following sampling strategies can be used (Figure 45):

*Nadir* – For these measurements the sensor looks directly downwards. It allows direct comparison with satellite sensors, due to similar measurement geometries to air or space borne sensors [19]. It is also a simple measurement to make in the field.

Hot spot – The measurement of the hot spot requires the sensor to be at the same solar zenith and azimuth angle as the Sun. This can be difficult in the field if the sensor and target are close together because of self-shadowing. However the hot-spot can contain useful biophysical information on vegetated sites, such as the leaf angle distribution function [20].

**Solar almucantar** – The sensor scans 360° around the target at the solar zenith angle, so that it can capture the extremes of the off-nadir reflectance, which can be used to determine an 'index of anisotropy' for a surface [20].

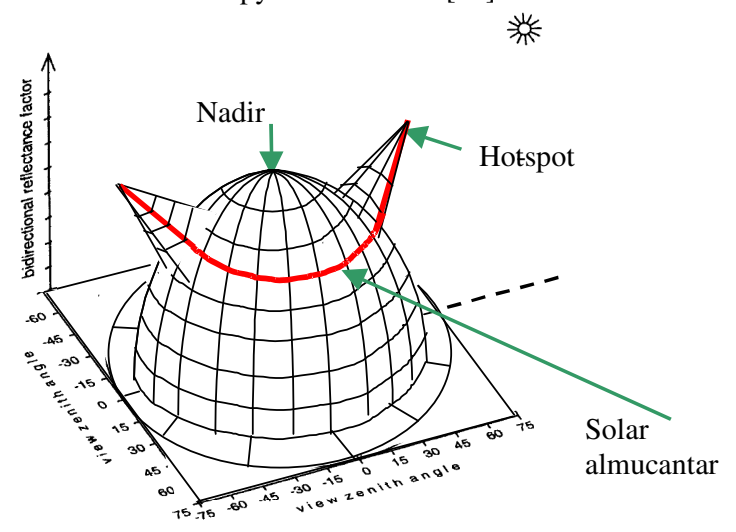


Figure 45: Fixed zenith angle sampling strategies, adapted from Milton (1995) [20].

Further sampling strategies can be developed by developing a sensor that can vary the zenith angle, at which it can measure, (Figure 46):

**Solar Principal Plane** – This method captures the greatest variation in directional reflectance for the most surfaces. It is fairly easy to set-up whilst in the field as the shadows can be used for the alignment of the instrument. It is also a useful method for airborne sensors that are performing a fly-over of a particular target [20].

*Orthogonal Plane* – The sampling geometry for this method is least likely to be affected by surface anisotropy. It is a useful method for airborne sensors, which aim to minimise view-angle effects [20].

Twin azimuthal planes at 45° to the principal plane of the Sun – The albedo can be more accurately estimated, by integrating the directional reflectance data collected in two azimuthal planes at 45° to the solar principle plane [19].

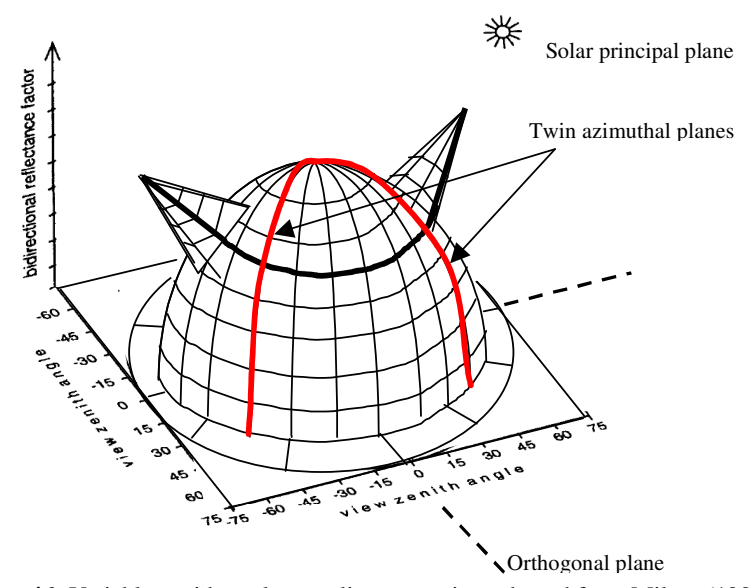


Figure 46: Variable zenith angle sampling strategies, adapted from Milton (1994) [19]

It has been shown in laboratory analysis that the angular sampling of 15° and 30° in the zenith and azimuth angles respectively is adequate to characterize the BRDF characteristics of most natural and artificial surfaces [21]. Many research teams have subsequently adapted this. However, characteristics such as the hotspot or specular peak may require a higher sampling resolution.

All the above methods make the assumption that the Sun is the source. Whilst this is true for the resultant information i.e. use of site with a satellite sensor, it does not necessarily mean that the Sun has to be used as the source for characterisation. Artificial sources can and have been deployed for such measurements most notably by ONERA who use a tungsten source at night time [22].

#### 4.2.2 Sources of uncertainty

In field based measurements of BRDF it is important to note that one of the principle sources of uncertainty relates to the timing of the experiment and not simply the instrumentation or method itself. For example, errors can be introduced due to changes in the solar irradiance over short timescales. This, therefore, means that the errors are dependent on the measurement sequence, and time-delay between successive measurements of the target and reference measurements. Careful consideration and good documentation is required to minimise these systematic uncertainties. A common approach is to restrict the field measurements to a period around solar noon when the solar geometry is changing least and when the uncertainty due to the angular response of the reflectance panel is at a minimum. Alternately the method established by ONERA using an artificial light source during night time conditions, instead of the Sun can provide the necessary data.

- Using the previous sections' sampling strategies, a single point instrument, can be used to measure the angular variability. The uncertainties associated with these measurements will arise due to the accuracy of the method of acquisition. For example, if a sensors physical location is constant, but the orientation of the sensor is changed to capture multi-angular radiance, the area of the target that is measured is assumed to be spatially and spectrally uniform. Any non-uniformity will introduce errors that can be difficult to determine. Where the sensor is mobile, the errors are associated with the mechanism of the sensor and the uncertainties associated with tilting the sensor and geolocation of the sequential measurements.
- Determining the angular reflectance characteristics of a particular surface can be difficult in the natural environment, due to effects such as the atmospheric conditions and illumination angle of the Sun, which are constantly changing. It is, therefore, critical that the time taken to perform a full set of measurements is kept to a minimum. By reducing the measurement time, the uncertainties associated with the changing environmental conditions can be reduced.
- The angular field-of-view of the sensor should also be kept as small as possible to ensure that the BRDF measured is a good estimate of the true BRDF at the specified geometries.
- A particular problem in the field is the diffuse radiation that is produced from skylight and scattered light. The light is hard to quantify as its intensity can vary over the hemisphere and with time due to atmospheric changes. These errors can be reduced if considered carefully, but crucially they should be documented, otherwise the data can be devalued and the diffuse contribution can become a significant source of uncertainty.

There are a few methods for calculating the diffuse irradiance contribution, which include conducting measurements under different conditions (e.g. clear skies/hazy skies). By occluding the solar disc, the difference between the direct and diffuse irradiance can be determined, or the complete sky irradiance can be measured.

# 4.2.3 Data analysis, reporting uncertainties

When reporting the results and uncertainties, care should be taken to include all details of the measurements, such as the illumination and measurement geometries, sampling resolution, slope of target, date of acquisition, position of the solar principal plane (SPP), altitude and surface type (see Table 8).

**Table 8:** Source of uncertainties for the BRDF measurements

Source of uncertainties	Type	Typical values (k = 1)
Two conhility to CI	Tyma D	350 – 1000 nm = 0.3%
Traceability to SI (Reference panel reflectance)	Type B	1000 – 2500 nm = 1.5%
Drift from calibration	Type B	Not available
Difft from Canoration	Туре Б	Not available
Repeatability and Reproducibility	Type A	400 - 1000  nm,  max = 0.5%
(3 days same zenith angle)		(See Appendix D)
Diffuse light correction	Type B	Not available
Angle of view, the absolute value	Type B	
0 " 11" 1 " 0 " 1	m n	N . 111
Scattered light from the	Type B	Not available
measurement system		
Solar variation during the time	Type A	The same as ρ
sequence for hemispherical data		
collection		

For the BRDF, retrieval methods such as that described by Martonchik (1994) [23] can be used. The most common way to report the results of the BRDF is through the use of three-dimensional diagrams (Figure 47), which are based on a polar co-ordinate system. Since BRDF effects are often quasi-symmetrical to the SPP, the plots are often referenced to the SPP rather than geographical north. These are highly illustrative plots, which can be used to visualise the general BRDF, however two-dimensional plots can be more suitable for quantitative analysis.

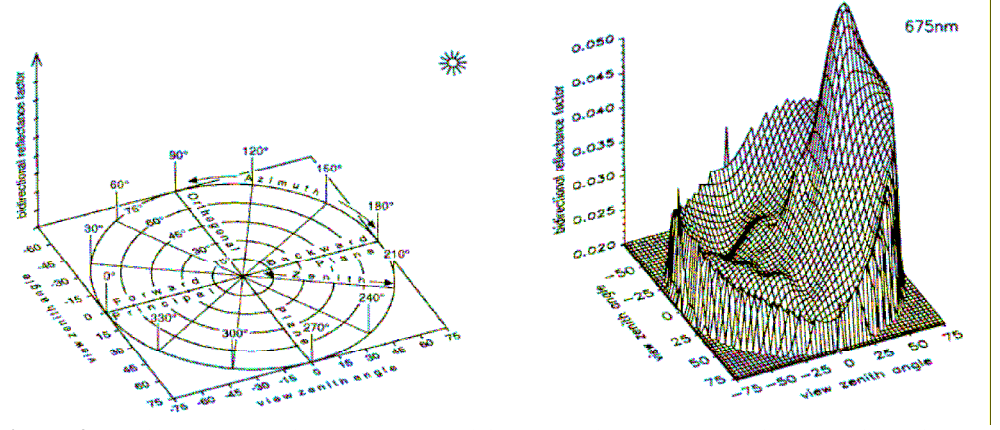


**Figure 47:** Left: Polar coordinate system used for presenting BRDF data in three dimensional plots, Right: Example of three-dimensional plot showing the BRF data of a grass lawn surface acquired with FIGOS at 675 nm under 35 source zenith angle, (taken from Sandmeier (2000))

#### 4.2.4 Data

NPL operated GRASS on 25<sup>th</sup>, 26<sup>th</sup> and 28<sup>th</sup> August 2009 near M1 (100 m x 300 m) sampling site selected for high-resolution optical sensors, at about 150 m distance from the corner of this sampling site. A second location was selected on 28<sup>th</sup> August 2009 in order to check if there is any non-uniformity of the site. The available datasets are presented in Table 9.

The data were recorded in automatic mode (Auto) using an integration time of 544 ms, excepting one measurement taken in manual mode on 27<sup>th</sup> August 2009 with a longer integration time in order to increase the Signal to Noise Ratio (SNR).

However, the manual mode introduced uncertainty as variability of the illumination conditions for the measurements taken at the beginning and at the end of the sequence. An automatic sequence over half hemisphere using 36 cameras requires 10 minutes and 30 - 40 minutes if recorded in manual mode. Another problem of the manual mode is that there is delay of about 1 hour between the measurement taken over the reference panel and over the target using GRASS and this could be critical if the atmospheric and illumination conditions change a lot in this timeframe. The BRDF data obtained in manual mode are not presented in this report.

Another solution to control the SNR is to increase the number of scans averaged for each camera. This was not possible in 2009; the operation software averaged by default 25 scans. The operation software will be modified for 2010 in order to allow the manual selection of an adequate number of scans for a better SNR depending on the illumination conditions during the day.

Lat=3848.5060 N Long=3323.8739 E

	Time	Sun		Sky		Reference		
Day	UTC	zenith	Klux	conditions	Mode	panel	Target	Hemisphere
25/08/2009	7:38	40.36	88	No clouds	Auto		X	180-000
25/08/2009	7:56	37.56		No clouds	Auto	X		180-000
25/08/2009	8:09	35.69		No clouds	Auto		X	180-000
25/08/2009	8:41	31.71	100	No clouds	Auto		X	000-180
25/08/2009	8:51	30.7		No clouds	Auto	X		000-180
	9:45		104					
27/08/2009	7:34	41.44		No clouds	Auto	X		180-000
27/08/2009	7:53	38.48		No clouds	Auto		Х	180-000
27/08/2009	8:03	37.02		No clouds	Auto	X		180-000
27/08/2009	8:26	33.98		No clouds	Auto		Х	180-000
27/08/2009	8:57	30.77		No clouds	Manual		Χ	180-000
28/08/2009	6:29	52.98	70	No clouds	Auto		Х	180-000
28/08/2009	6:39	51.14		No clouds	Auto	Х		180-000

Lat=3848.5132 N Long=3323.8484 E

Dav	Time	Sun zenith	Klux	Sky conditions	Mode	Reference panel		Hemisphere
Day	UIC	Zemui	Niux	Conditions	Wode	panei	Target	пеннарнете
28/08/2009	11:18	35.21		No clouds	Auto		Χ	180-000
28/08/2009	11:29	36.67		No clouds	Auto	Χ		180-000
28/08/2009	11:52	40.04		No clouds	Auto		Χ	000-180

 Table 9: GRASS data recorded during the CEOS pilot land comparison in 2009

#### Reference reflectance panel for GRASS

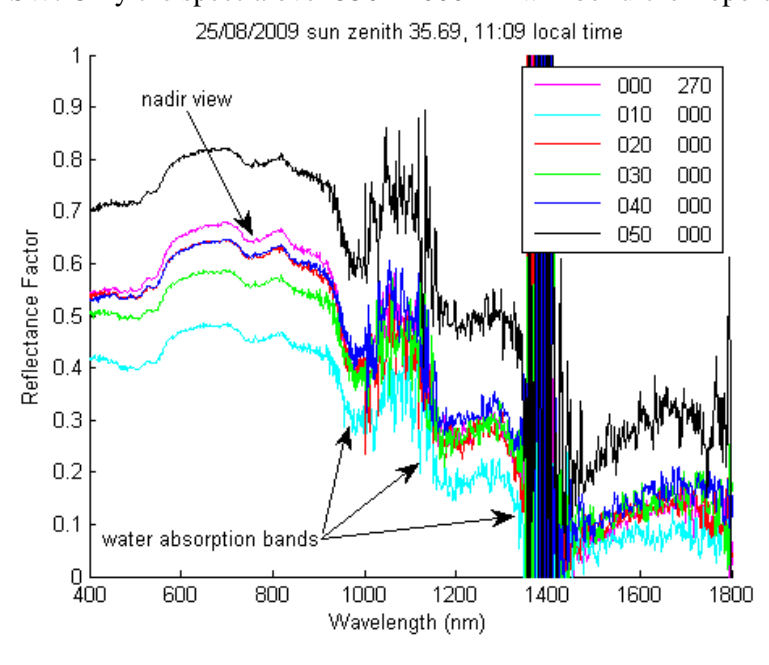
The GRASS measurements used a 60 cm x 60 cm Spectralon@ reference panel calibrated by NPL using a technique similar to that described at Chapter: NPL calibrated reference reflectance panel.

#### 4.2.5 Results

# Cross Comparison of GRASS and ASD for nadir

GRASS recorded BRDF measurements near M1 sampling site. The  $\rho$  measured at nadir with GRASS and the RF measured over M1 by one of the participants should have similar measured values.

Figure 48 presents GRASS data from 25<sup>th</sup> August at 11:09 local time. The spectra are very noisy over 1000 - 2500 nm spectral range and this is the result of the broken optical fibers over SW1 and SW2 (ASD Inc. check-up after the measurement campaign showed that there was a broken fiber). Additionally there is a miss match between the optical fibers of GRASS' cameras (400 μm core fiber Ocean Optics) and the optical fiber of the ASD spectroradiometer (a bundle of about 2 mm in diameter comprising 19 x 100 μm core fiber over VNIR and 38 x 200 μm core fiber over SW). The optical mixer provided by ASD Inc. was used to overcome this miss match and it is efficient over VNIR and not over SW. This is a second reason why the spectra are noisy over SW. Only the spectra over 350 - 1000 nm will be further reported.



Location: Turkey Date: 25/08/2009 Solar angle: 35.69 degrees Wavelength: 700 nm

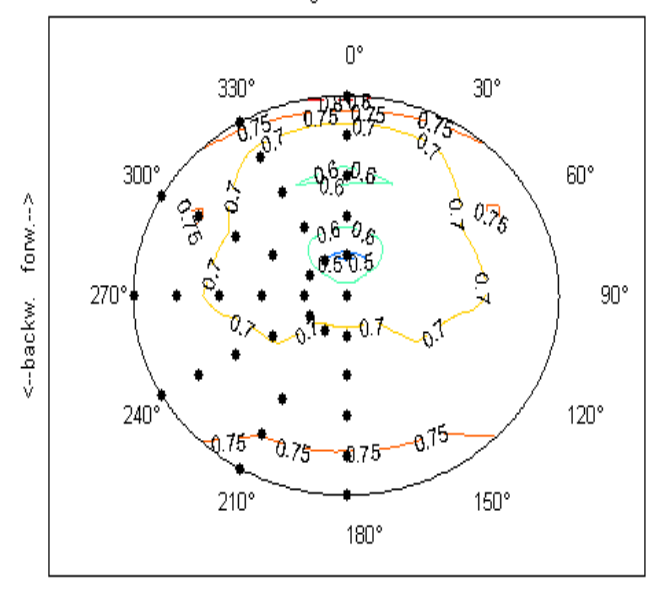


Figure 48: BRDF effects on 25<sup>th</sup> August 2009, sun zenith=35.69°, 8:09 UTC.

The representation using polar coordinates for 700 nm showed a stronger forward scattering (0.8 maximum) than the backward for this sun zenith angle. However this changes for other sun zenith angles as represented in **Appendix D: BRDF data**.

The plan 180° - 0° is the solar principal plan and the BRDF effects are symmetrical relative to this plan for uniform surfaces such as snow or desert. Tuz Gölü surface is uniform and the measurements recorded over the half left hemisphere were extrapolated over the whole hemisphere.

## Reflectance factor measured using two techniques

The average of GRASS nadir  $\rho$  recorded on  $25^{th}$  August 2009 for two sun zenith angles: 40° and 35° is compared with the  $\rho$  value over M1 site as measured by ONERA during this day and for a sun zenith angle which varies between 47° to 37° (6:29 – 8:00 UTC). There are some differences in the measurement conditions for the two instruments as it is described in Table 10.

Instrument	GRASS, NPL	ASD, ONERA
FOV	4°	5°
Sampled site	50 cm x 50 cm	100 m x 300 m
Position	Solar principal plane, azimuth000	Nadir view
Height	2 m	40 - 50 cm
Optical fiber	5 m	1.5 m
Average	25 scans	160 scans

**Table 10:** Geometry and measurement conditions for GRASS, NPL and ASD, ONERA.

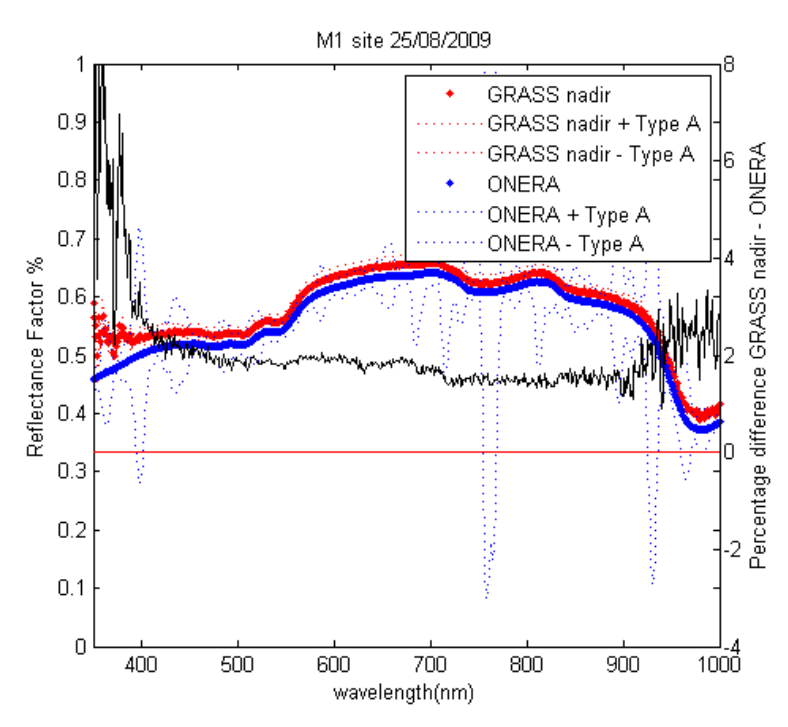


**Figure 49:** GRASS measured value at nadir compared with the  $\rho$  measured by ONERA radiometer over M1 site. Standard uncertainty Type A reported by ONERA and calculated for GRASS are represented with dotted lines.

The  $\rho$  measured values using NPL and ONERA instruments have a difference of about 2% in the absolute value (Figure 49), which is as expected based on the observed difference of 2 - 3% in their  $\rho$  absolute value for 37° sun viewing angle shown in Figure 15, chapter 3.2.3.

However the standard uncertainty reported by ONERA is greater than that of GRASS because it depends on the operator pointing accuracy over one and half hours for a 100 m x 300 m site and GRASS is a stable structure sampling a static 50 cm x 50 cm patch size.

## Type A Standard uncertainty

The Type A standard uncertainty (repeatability and reproducibility) for GRASS values was calculated considering three independent runs from 25<sup>th</sup>, 27<sup>th</sup> and 28<sup>th</sup> August 2009 for the same illumination conditions (sun zenith = 35°). Each run has 7 measurements for nadir view. The standard uncertainty was calculated in the same way as for the cross-comparison against TSARS (see **Appendix E: BRDF Type A standard uncertainty** for more details).

# Type B Standard uncertainty

It is related to the accuracy of the characterisation of the NPL reference panel used for the calculation of the  $\rho$  value for each camera (chapter 3.3.2).

#### **BRDF** effects

All BRDF measurements have the graphics: spectral reflectance for azimuth 000 and 180 and BRDF represented in polar coordinates in **Appendix D: BRDF data**.

# 5 Atmospheric characterisation

Since the ultimate aim of any test-site is to calibrate or validate the radiometric gain of a satellite, it is essential to have a full knowledge of any losses resulting from transmittance of the atmosphere. This can be calculated through use of a RTC but this in turn is highly dependent on the inputs of a variety of parameters, which are determined locally and at the time of use.

The atmospheric transmittance is measured using a "sun-photometer" to determine the aerosol optical depth, and water vapour content. These measurements can be performed in automatic mode. However, as a minimum this can be performed with the help of a handheld manual instrument sampling regularly during site radiometric measurements.

Additional input parameters required for RTC are: pressure, temperature, ozone and this is mostly achieved through an automatic weather station at ground. The instrumentation used to collect this data should be traceably calibrated and have sufficient accuracy and resolution that it does not limit the overall results of the site characterisation.

In some situations, where there may be high levels of ozone for example additional measurements may be required.

# 5.1 Aerosols optical properties and Water Vapour

# **5.1.1** Sunphotometry

The "Sunphotometers" are in essence spectroradiometers, similar to those measuring surface reflectance, but often limited to a few selected wavelengths in the atmospheric transmittance windows using spectral filters. They are used to determine the aerosol optical depth, and water vapour content, by measuring the absorption and scattering of direct sunlight. Ideally such measurements should be performed in an automatic mode and over a continuous time period (beyond that constrained by any field campaign), with the added advantage that this will also lead to a site aerosol climatology record. This is best done as part of a formal network such as AERONET [24], which has well defined operational procedures. The aerosol climatology helps in establishing a standard atmosphere containing all aerosol properties that can be used as input to the Monte Carlo simulations of the atmospheric path radiance over this site.

The pilot land comparison in Turkey 2009 used an automatic sunphotometer: CIMEL provided by CNES and a handheld MICROTOPS provided by DLR as per chapter 2.3) performing measurements with different accuracy as explained below.

#### **5.1.2** Sources of uncertainty

The dominant source of uncertainty for atmospheric transmittance comes from the aerosol optical depth measurement, and this is highly dependent on the pointing accuracy and the radiometric calibration of the instrument.

Ideally an AERONET compliant sun-photometer would be stationed near to the site and for this an uncertainty in optical depth of about  $\pm 0.01$  of the average value for wavelengths greater than 440 nm and less than  $\pm 0.02$  of the average value for shorter wavelengths can be achieved [24].

Similarly water vapour content can be determined from the 940 nm spectral band, with an uncertainty of 10% [25].

A handheld sunphotometer as MICROTOPS has an uncertainty in aerosol optical depth about ±0.01 of the average for all wavelengths and 10% uncertainty for the water vapour content (information provided by MICROTOPS as per February 2009).

## 5.1.3 Data

#### **AERONET data**

A CIMEL sunphotometer, operated in the AERONET framework, during the period of the pilot land comparison with data recorded from 25<sup>th</sup> to 28<sup>th</sup> August 2009 (Figure 50). The dataset is at Level 1.5 (Table 11, Table 12), CNES quality checked.

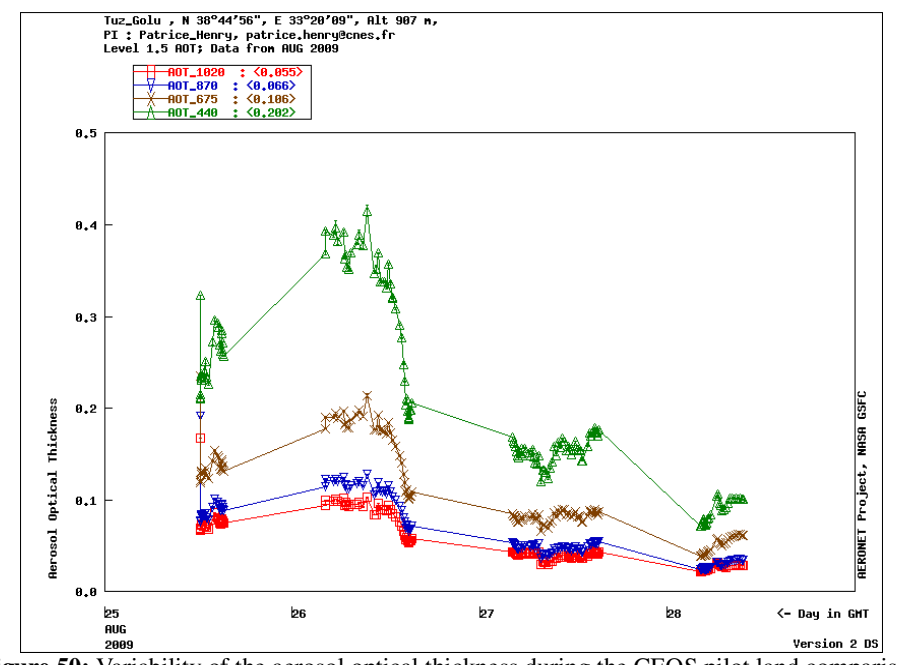


**Figure 50:** Variability of the aerosol optical thickness during the CEOS pilot land comparison (AERONET website)

## **5.1.4 Results**

## **AERONET data**

Day	N	AOT (440) daily mean Stdev%	AOT (675) daily mean Stdev%	AOT (870) daily mean Stdev%	AOT (1020) daily mean Stdev%
25/08/2009	25	$0.26 \pm 2.94\%$	$0.14 \pm 2.23\%$	$0.09 \pm 2.20\%$	$0.08 \pm 1.92\%$
26/08/2009	40	$0.32 \pm 7.40\%$	$0.16 \pm 3.51\%$	$0.10 \pm 2.07\%$	$0.08 \pm 1.69\%$
27/08/2009	57	$0.16 \pm 1.39\%$	$0.08 \pm 0.54\%$	$0.05 \pm 0.42\%$	$0.04 \pm 0.37\%$
28/08/2009	28	$0.09 \pm 1.22\%$	$0.05 \pm 0.88\%$	$0.03 \pm 0.41\%$	$0.03 \pm 0.30\%$

 Table 11: Aerosol optical thickness as recorded with CIMEL sunphotometer

Day	N	α <sub>440-870</sub> daily mean	α <sub>440-870</sub> Stdev %	PW cm daily mean	PW Stdev %
25/08/2009	25	1.55	4.69%	1.46	4.43%
26/08/2009	40	1.65	5.91%	1.82	30.67%
27/08/2009	57	1.70	5.30%	1.11	6.45%
28/08/2009	28	1.61	5.93%	0.81	8.54%

Table 12: Angstrom wavelength exponent and the precipitable water

Another dataset was recorded using the MICROTOPS (Table 13 and Table 14).

## **MICROTOPS** data

Day	N	AOT (380) daily mean Stdev%	AOT (440) daily mean Stdev%	AOT (500) daily mean Stdev%	AOT (675) daily mean Stdev%	AOT (870) daily mean Stdev%
25/08/2009	24	0.21±1.18%	0.18±1.18%	0.15±1.17%	0.10±0.94%	0.06±0.96%
26/08/2009	23	0.44±2.31%	0.37±1.87%	0.31±1.58%	0.19±1.40%	0.12±1.05%
27/08/2009	18	0.13±1.13%	0.12±0.76%	0.11±1.29%	0.07±1.58%	0.04±1.50%
28/08/2009	30	0.08±1.19%	0.08±1.02%	0.08±1.02%	0.06±1.12%	0.03±1.06%

 Table 13: Aerosol optical thickness variability using the MICROTOPS

Day	Nī	a <sub>440-870</sub>	α <sub>440-870</sub>	PW cm	PW
Day	N	daily mean	Stdev %	daily mean	Stdev %
25/08/2009	20	1.53	17.61%	0.84	3.50%
26/08/2009	25	1.63	10.65%	1.34	2.05%
27/08/2009	18	1.47	37.38%	0.60	3.85%
28/08/2009	31	1.37	38.28%	0.46	2.82%

Table 14 Angstrom wavelength exponent and precipitable water as recorded using a MICROTOPS

## 5.2 Meteorological data

Meteorological station provides ancillary data including: temperature (T), pressure (P), humidity (RH%), wind speed (WS) and solar radiation. This data were recorded with a wireless Vantage Pro2 Plus Weather Station each minute. The variability of these parameters is represented in Figure 51, Figure 52, Figure 53 and Figure 54.

### Temperature (C) 2009

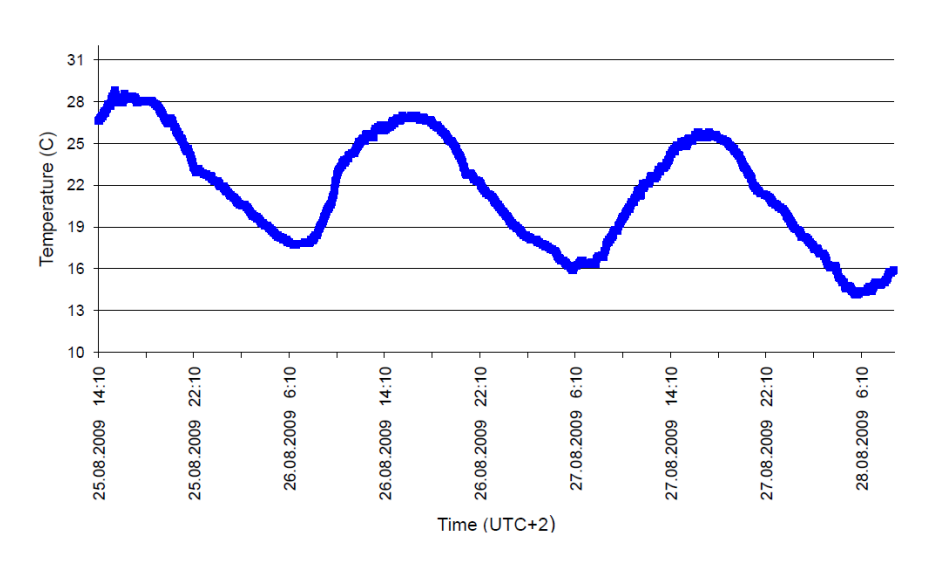


Figure 51: Temperature during the 2009 pilot land comparison

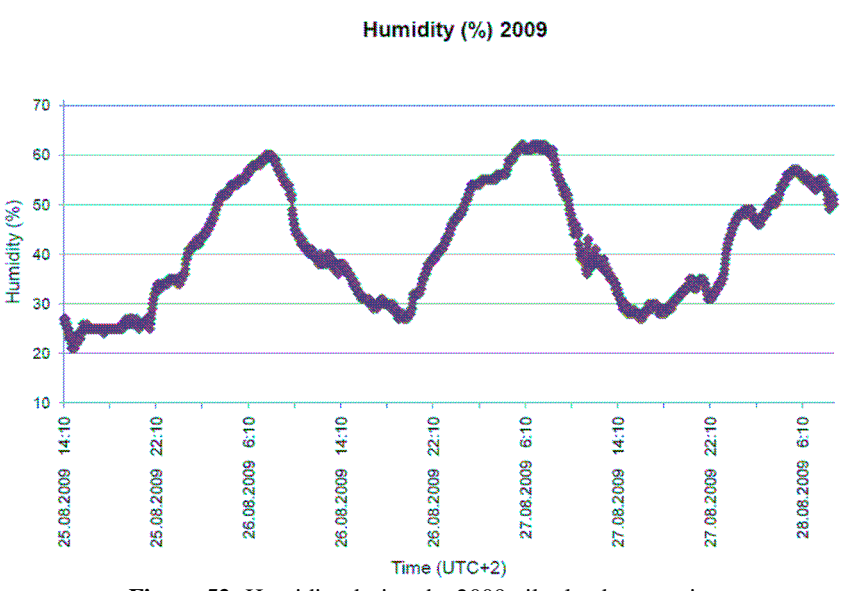


Figure 52: Humidity during the 2009 pilot land comparison

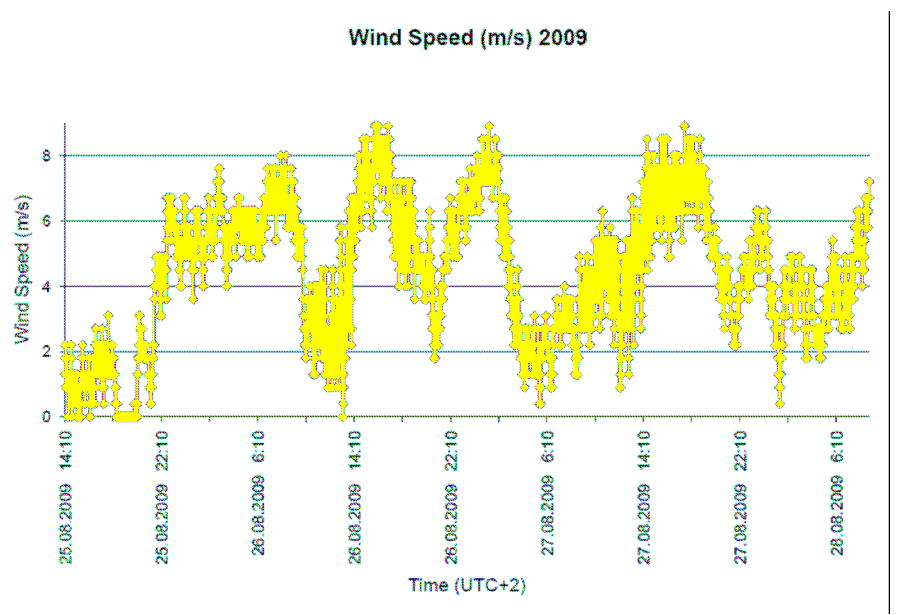


Figure 53: Wind speed during the 2009 pilot land comparison

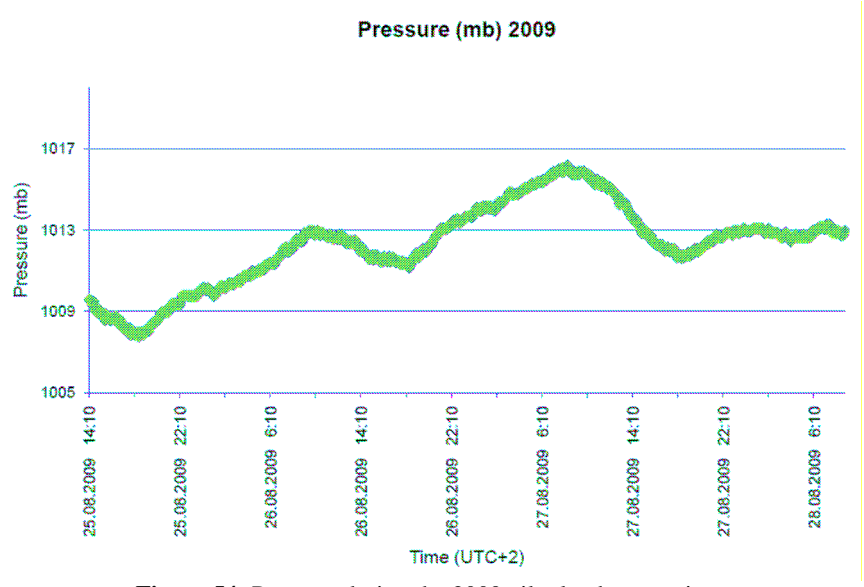


Figure 54: Pressure during the 2009 pilot land comparison

## 6 Uncertainty estimation

This chapter presents and explains the methods used in this report for the calculation of the associated standard uncertainty.

### 6.1 Experimental standard deviation for measured values of radiance

The measured values of radiance are provided as J = 3 groups with each group comprising K = 3 measured values obtained independently. Denote the measured values by  $r_{jk}$ , j = 1, ..., J, k = 1, ..., K, where index j counts over the groups, and index k counts over the values within the groups.

Define

$$r_j = \frac{1}{K} \sum_{k=1}^{K} r_{jk}, \quad j = 1, ..., J,$$

to be the group averages, and

$$r = \frac{1}{J} \sum_{j=1}^{J} r_j = \frac{1}{JK} \sum_{j=1}^{J} \sum_{k=1}^{K} r_{jk}$$

to be the overall average (equal to the average of the group averages).

The estimate of radiance is taken to be the average r of the measured values. To evaluate the (experimental) standard uncertainty associated with the average r, it is necessary to decide whether the between-group variability of the measured values is the same as the within-group variability. ANOVA ('analysis of variance') methods can be used for this purpose. The GUM [5] (in clause H.5) provides an example of the use of ANOVA methods to evaluate the standard uncertainty associated with the average of 'grouped' data. The material presented here is based on that example.

Denote by  $\sigma_w^2$  and  $\sigma_b^2$  the within-group and between-group components of variance, respectively. Under the null hypothesis that  $\sigma_b^2 = 0$ , two estimates of  $\sigma_w^2$  are given by

$$s_1^2 = K \left( \frac{1}{J-1} \sum_{j=1}^{J} (r_j - r)^2 \right),$$

based on the variance associated with the group averages, with J-1 degrees of freedom, and

$$s_2^2 = \frac{1}{J} \sum_{j=1}^{J} \left( \frac{1}{K-1} \sum_{k=1}^{K} (r_{jk} - r_j)^2 \right),$$

a pooled estimate of the within-group variance, with J(K-1) degrees of freedom.

An *F*-test is used to decide whether  $s_1^2$  is significantly greater than  $s_2^2$  and there is evidence to doubt the null hypothesis. Specifically, the null hypothesis is rejected if

$$\Pr\left[F > \frac{s_1^2}{s_2^2}\right] < p,$$

where F follows the F-distribution  $F_{J-1, J(K-1)}$  and p is a specified level of confidence (here chosen to be 0.01 or 1 %).

If the existence of a between-group effect is rejected (i.e., the null hypothesis is accepted), then the standard uncertainty associated with the average r is obtained from

$$u^2(r) = \frac{s^2(r_{jk})}{JK},$$

with JK - 1 degrees of freedom, where

$$s^{2}(r_{jk}) = \frac{1}{JK - 1} \sum_{j=1}^{J} \sum_{k=1}^{K} (r_{jk} - r)^{2}.$$

On the other hand, if the existence of a between-group effect is accepted, the variance associated with the group averages

$$s^{2}(r_{j}) = \frac{1}{J-1} \sum_{i=1}^{J} (r_{j}-r)^{2},$$

estimates  $\sigma_b^2 + \sigma_w^2/K$  (and not  $\sigma_w^2/K$ , which would be the case if the null hypothesis is accepted), and therefore the standard uncertainty associated with the average is obtained from

$$u^2(r) = \frac{s^2(r_j)}{J},$$

with J-1 degrees of freedom, which accounts for both between-group and within-group effects.

Figure 55 shows some examples of measured radiance values of TSARS provided by the NPL radiometer at two different wavelengths. In the top graph (corresponding to a wavelength of 800 nm) it is seen that the variability of the group averages (shown as circles) is large compared with the variability of the values (shown as points) within the groups. In contrast, in the bottom graph (corresponding to a wavelength of 2 000 nm) the between-group variability is small compared to the within group variability. The evaluation of the (experimental) standard uncertainty associated with the (overall) average of the values is different for the two cases.

#### 6.2 Calibration checks

Measured values of radiance were obtained independently of TSARS on two separate days. Assuming that TSARS provides a stable source, the measured values can be expected to be consistent accounting for their associated (experimental) standard uncertainties (see section 1).

For i = 1, 2, denote by  $R_i$  the quantity describing radiance measured on day i. Let  $r_i$  be the measured value of  $R_i$  with associated standard uncertainty  $u(r_i)$  and degrees of freedom  $v_i$ . The measurements can be considered to be consistent at a 95 % level of confidence if a 95 % coverage interval for the quantity  $R_1 - R_2$  contains zero, or a 95 % coverage interval for the quantity  $R_1/R_2$  contains unity.

Define

$$Y = R_1 - R_2.$$

An estimate of Y is

$$y = r_1 - r_2$$
.

Applying the law of propagation of uncertainty [1, clause 5.1.2], the standard uncertainty u(y) associated with the estimate y is given by

$$u^{2}(z) = u^{2}(r_{1}) + u^{2}(r_{2}).$$

Applying the Welch-Satterthwaite formula [1, clause G.4], the (effective) degrees of freedom  $v_{\text{eff}}$  attached to u(y) is given by

$$\frac{u^4(z)}{V_{\text{eff}}} = \frac{u^4(r_1)}{V_1} + \frac{u^4(r_2)}{V_2}.$$

Then, a 100p % coverage interval for Y is  $y \pm k_p u(y)$ , where  $k_p$  is the percentage point of the t-distribution with  $v_{\text{eff}}$  degrees of freedom such that the probability that |t| is no greater than  $k_p$  is p [1, clause G.3].

Similarly, define

$$Z=\frac{R_1}{R_2}.$$

An estimate of Z is

$$z=\frac{r_1}{r_2}.$$

Applying the law of propagation of uncertainty, the standard uncertainty u(z) associated with the estimate z is given by

$$u^{2}(z) = \left(\frac{u(r_{1})}{r_{2}}\right)^{2} + \left(\frac{r_{1}u(r_{2})}{r_{2}^{2}}\right)^{2},$$

or, equivalently,

$$\left(\frac{u(z)}{z}\right)^2 = \left(\frac{u(r_1)}{r_1}\right)^2 + \left(\frac{u(r_2)}{r_2}\right),$$

when expressed in terms of fractional standard uncertainties.

Applying the Welch-Satterthwaite formula, the (effective) degrees of freedom  $v_{\text{eff}}$  attached to u(z) is given by

$$\frac{u^{4}(z)}{V_{\text{eff}}} = \frac{(u(r_{1})/r_{2})^{4}}{V_{1}} + \frac{(r_{1}u(r_{2})/r_{2}^{2})^{4}}{V_{2}},$$

or, equivalently,

$$\frac{(u(z)/z)^4}{V_{\text{eff}}} = \frac{(u(r_1)/r_1)^4}{V_1} + \frac{(u(r_2)/r_2)^4}{V_2},$$

when expressed in terms of fractional standard uncertainties.

Then, a 100p % coverage interval for Z is  $z \pm k_p u(z)$ , where  $k_p$  is the percentage point of the t-distribution with  $v_{\text{eff}}$  degrees of freedom such that the probability that |t| is no greater than  $k_p$  is p.

It is important to account for the degrees of freedom attached to the standard uncertainties  $u(r_1)$  and  $u(r_2)$  because they are likely to be small (being equal to JK-1=8 or J-1=2 according to how they are calculated: see section 1). Consequently,  $k_p$  can differ appreciably from the value 1.96, which would be used if the degrees of freedom were taken as large (or infinite).

If the value of the TSARS source varies between the two days of measurement, an uncertainty component to describe this effect should be included in the analysis presented.

Figure 56 shows some examples of measured values of TSARS provided by the DLR radiometer at two different wavelengths and on two different days. In the top graph (corresponding to a wavelength of 800 nm) the (average) radiance values for the two days are consistent accounting the associated experimental standard uncertainties. In contrast, in the bottom graph (corresponding to a wavelength of 2000 nm) the measured values obtained on the two days are clearly inconsistent. There is evidently

a change in the instrument or the conditions of measurement or some other effect that is not accounted for in the uncertainties evaluated in terms of the measured values.

### 6.3 Correcting measured radiance values

The measurements of TSARS made by each laboratory are used as the basis of applying a wavelength-dependent correction to measurements made of an arbitrary source (reference panel) on an arbitrary day.

For each laboratory l, let  $R^l$  and  $R^l_{corr}$  denote quantities describing, respectively, uncorrected and corrected radiance. Then,

$$R_{\rm corr}^l = R^l \frac{R_{\rm TSARS}}{R_{\rm cal}^l},$$

where  $R_{TSARS}$  is the radiance of TSARS and  $R_{cal}^{l}$  describes the measurement of TSARS made by the laboratory.

Assuming (again) that TSARS provides a stable source, and the measured values of radiance for TSARS and the reference panel are obtained independently, the uncertainty associated with an estimate of  $R^l_{\text{corr}}$  is evaluated in terms of the uncertainties associated with the estimates of  $R^l$  and  $R^l_{\text{cal}}$  (either reported by the laboratory or calculated as in section 1). An effect that is common to the measurements of TSARS and the reference panel will 'cancel' in the evaluation of the corrected radiance.

If measurements of radiance are made of the same reference panel, which is assumed to be stable, by different laboratories the measured values can be corrected (as above), and can be expected to be consistent accounting for their respective associated uncertainties. If more than two laboratories make measurements, a chi-squared statistical test can be used to test the consistency of the corrected measured values provided by the laboratories, and the weighted average of the values used as an aggregate value of the radiance for the reference panel.

#### 6.4 Characterization of the site

Each laboratory provided measured values of the reflectance factor for an area of the site at a number of different locations. For example, measured values were provided for the area M3 at 18 different locations arranged on a nominally rectangular grid.

If the measured values are the only available information, and it is assumed that they relate to the same quantity, i.e., reflectance factor for area M3, and are obtained independently, an estimate of the reflectance factor for area M3 is the average (arithmetic mean) of the 18 values. The standard uncertainty associated with the estimate is the (experimental) standard deviation associated with the average, i.e.,  $s/\sqrt{18}$ , where s is the standard deviation of the 18 values.

If the measured values are provided with associated standard uncertainties, and (again) it is assumed that they relate to the same quantity and are obtained independently, an estimate of the reflectance factor for area M3 is the weighted mean

of the 18 values and the associated standard uncertainty is that of the weighted mean [26]. In this case, a statistical test (the chi-squared test) can be applied to test whether the data (measured values and associated standard uncertainties) are consistent with the assumptions made.

Finally, the assumption that the measured values are obtained independently can be relaxed. The standard uncertainty associated with an error quantity that is common to all the measurements can be used as the basis of quantifying the covariance associated with pairs of measured values. In terms of this information, the estimate of the reflectance factor for area M3 is the generalized weighted mean of the 18 measured values [27].

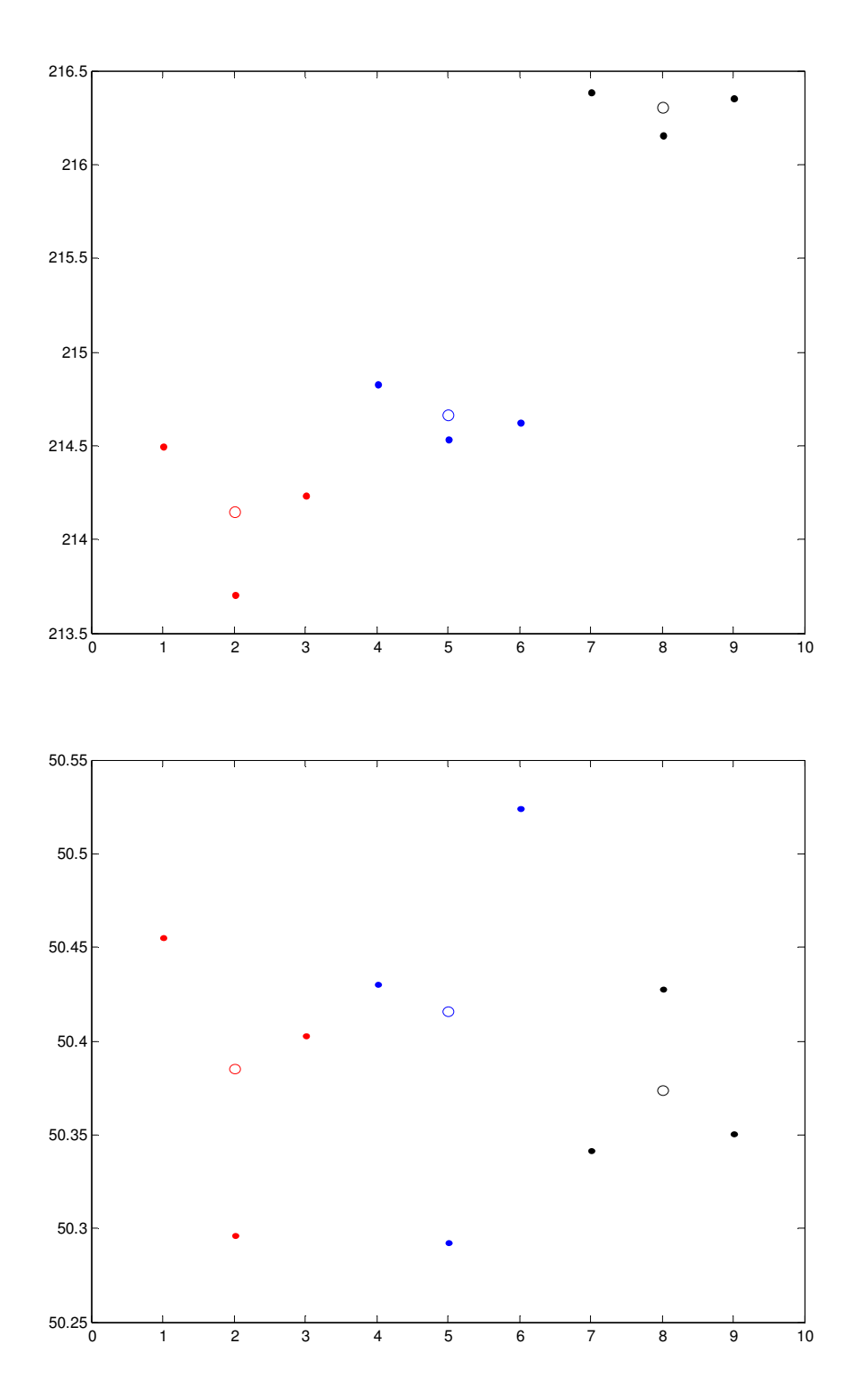


**Figure 55:** Measured radiance (points) of TSARS at 800 nm (top) and 2 000 nm (bottom) provided the NPL radiometer. The group averages are shown as circles. There are 3 runs: red, blue and black dots.

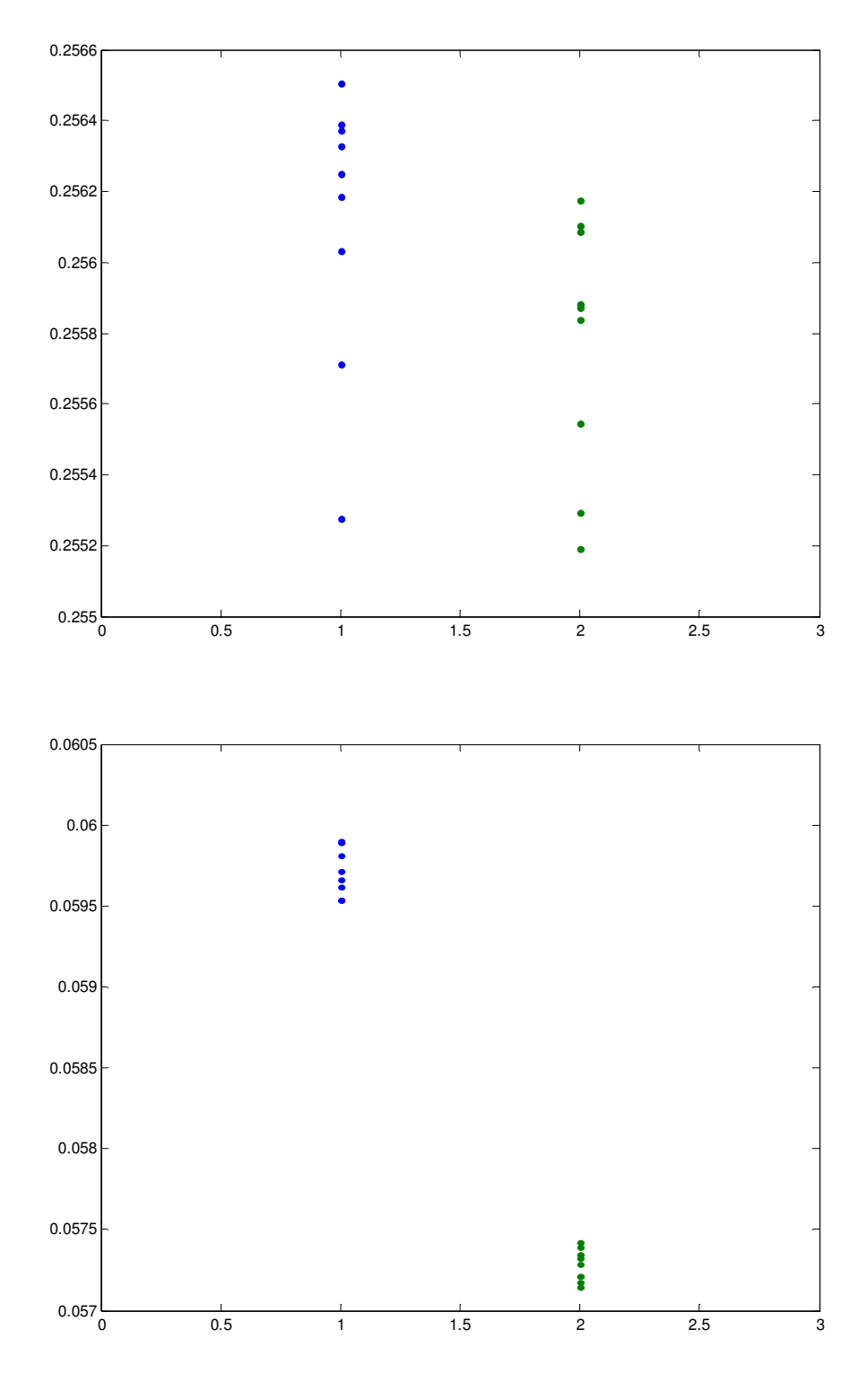


**Figure 56:** Measured radiance of TSARS at 800 nm (top) and 2 000 nm (bottom) provided by the DLR radiometer on two different days.

### 7 Conclusions

The results of the 2009 Pilot comparison of techniques and instruments used for the vicarious calibration of Land surface imaging through a ground reference standard test site demonstrated that a longer period of field measurements than four days is required to establish a best practice to characterise a land target site and to asses the sources of uncertainties.

The CEOS Key comparison in August 2010 will take place from 13<sup>th</sup> to 28<sup>th</sup> August 2010 (where nine days will be dedicated to field measurements and three days to the laboratory calibration). Ten institutions will participate in spectral reflectance measurements of the site and NPL will perform the BRDF measurements.

Bellow are summarised the lessons learnt in 2009 and how these will be addressed during the 2010 CEOS Key Comparison:

#### *a) Radiometric Calibration*

The Ankara University laboratory used for the radiometric calibration in 2009 had no monitoring of the environmental conditions. The calibration checks showed a difference of 2% in radiance for the first day and the last day of calibration for certain radiometers (ONERA). It is not clear if this change is intrinsic to the instrument or is the result of different laboratory conditions. In 2010 laboratory conditions will be monitored by NPL.

### b) Reference panel characterisation

The atmospheric conditions of the day selected for the characterisation of the participants' reference panels via NPL calibrated reference panel were inadequate (presence of cirrus) for this task. The 2010 CEOS Key International Comparison with nine days of field measurements will offer more opportunities to select an adequate day for this activity.

The 2009 results showed that illumination conditions change over a ten minutes time frame even for a day nominally without cirrus. NPL suggested a laboratory characterisation of participants' reference panels relative to the NPL calibrated reference panel prior to the field measurements. The stable floodlight source will be used for this calibration.

### c) Sampling strategy and cross-comparison

The four days of 2009 pilot comparison did not allow for the obtaining of a surface reflectance factor value over each sampled site from all participants. The nine days of site characterisation in 2010 will give participants more time to test several sampling strategies for high or medium resolution land imagers and to estimate a complete uncertainty budget. A higher variety of cross-comparisons will be helpful to understand any existing biases between the instrumentation used for the site characterisation and vicarious calibration.

#### d) BRDF

The BRDF results were used for the vicarious calibration of remote optical sensors (CONTROLS Deliverable 12). This dataset is also important information in the process of characterising a standard reference test site as Tuz Gölü.

The 2% difference in value of the  $\rho$  over the nadir camera of GRASS and the  $\rho$  measured with a similar instrument near GRASS site was explained by the difference of the absolute values of reference panel  $\rho$  used. An accurate calibration of all participants' reference panels in laboratory and in situ for 2010 would allow the correction of such biases.

2009 results showed that illumination conditions changed over ten minutes (the time required for a BRDF full sequence over 36 cameras). In 2010 the sequence will be reduced to five minutes using 18 cameras (the site is homogeneous and 36 cameras over sampled the target). Additionally BRDF measurements will be recorded during the night using a stable illumination source provided by ONERA and these dataset will be compared with the day dataset.

### e) Vicarious calibration of optical sensors

A measurement campaign over nine days will provide more opportunities for the vicarious calibration of several satellites. In 2009 five land imagers were calibrated over the four days.

## **Appendix A: Instrumentation**

#### ASD FieldSpec3 spectroradiometer

**Measurement aims:** To perform radiance/reflectance measurements over the selected target area at different times with various sampling rates to determine the spatial/temporal uniformity and to obtain the radiometric characteristics of the site.

**Instrument:** FieldSpec® 3 is a field portable, precision radiometer with a spectral range from 350 - 2500 nm and rapid data collection in the order of 1/10th of a second per spectrum. The wireless connection allows for remote control of data collection up to 50 m distance. It is designed for solar reflectance, radiance and irradiance measurements [28]



ASD FieldSpec3 with its accessories

Typical accessories with the spectrometer are as follows:

- o 2 m FS3 FR Low OH Optical Fiber Cable
- Upgrade Panasonic Toughbook 19
- o ASD FR, Accessories Package A including
  - 1 deg NIR/FR Lens for optics w/ radiance radiometric calibration
  - 5 deg NIR/FR Lens for optics w/ radiance radiometric calibration
  - 8 deg NIR/FR Lens for optics w/ radiance radiometric calibration
  - Radiance radiometric calibration of bare optic fiber input
  - ASD diffuser-type Full-Sky Irradiance Remote Cosine Receptor w/irradiance radiometric calibration
  - Auxiliary Pistol Grip w/Spotting Scope & Bubble level.
  - 10 inch x 10 inch (25.4 x 25.4 cm) calibrated white Spectralon@ panel
- o Spectralon@, Wooden Case for 10 x 10
- o Tripod, Bogen 3011 w/3025 Head

- o Battery, Aux. Panasonic Toughbook 19
- o Auxiliary Battery, NiMH High Current
- o NiMH Battery Charger
- o The instrument has 3 detectors:
  - Silicon photo-diode array for 350 1000 nm
  - TE-cooled, extended range InGaAs photo-diode for 1000 1830 nm
  - TE-cooled, extended range, InGaAs, photo-diode for 1830 2500 nm

**Spectral Resolution:** 3 nm @ 700 nm, 10 nm @ 1400 - 2100 nm

Noise Equivalent Radiance (NEdL): 1.4 x 10 -9 W cm<sup>-2</sup> nm<sup>-1</sup>sr<sup>-</sup>@ 700 nm 2.4 x 10 -9 W cm<sup>-2</sup> nm<sup>-1</sup>sr<sup>-</sup>@ 1400 nm 8.8 x 10 -9 W cm<sup>-2</sup> nm<sup>-1</sup>sr<sup>-</sup>@ 2100 nm

**Set-up time:** Approximately 90 minutes to setup and 15 minutes to be dismantled.

**Transportation:** Two packages of size 55 x 46 x 41 cm and 79 x 57 x 48 cm, total weight 47 kg.

**Power Requirements:** 12VDC NiMh high current rechargeable battery pack is required. It can be used for 4 - 5 hours. Charging time is 8 hours.

The ASD participants' radiometers were manufactured in different years and have declared traceability to NIST through ASD Inc (see Table 15).

DLR #6472 ASD	1° and 8°	- Traceability to Optronic Laboratories, USA
ONERA #6487 ASD	1° and 5°	- Traceability to Optronic Laboratories (Calibration in March 2009), USA, 2005
NPL #6401 ASD	1° and 8°	- Traceability to NERC, UK, 2004
TU #16210 ASD	1° and 8	- Traceability to NPL, UK, 2009

Table 15: ASD radiometers manufacturer numbers used during the pilot land comparison, 2009.

### Gonio RAdiometric Spectrometer System (GRASS)

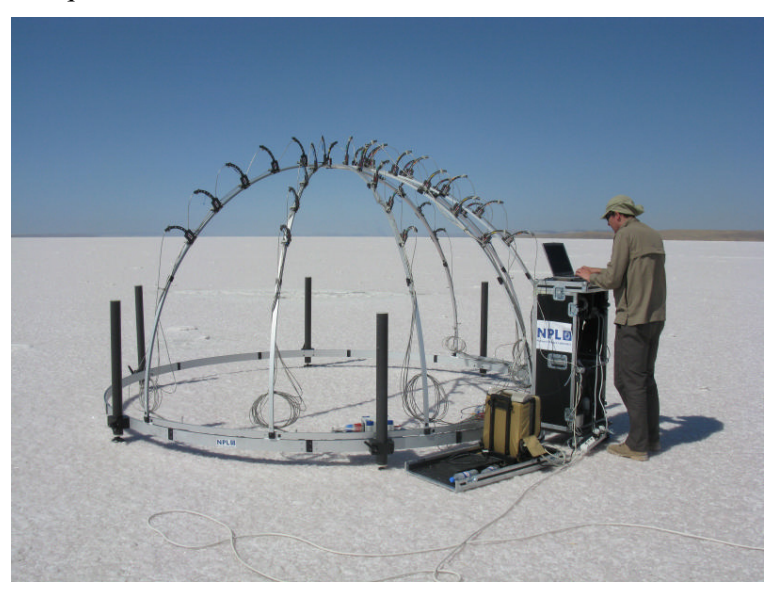
**Measurement aims:** To conduct a series of multi-angular spectral measurements of the surface, perform measurements at different solar zenith angles, perform measurements over the same surface on sequential days to determine the temporal stability and perform diffuse irradiance measurements.

**Instrument:** The instrument has been designed to be easily and quickly assembled in remote situations, be robust and able to be transported by "estate car". GRASS has been designed [29] to measure the Earth's reflected sunlight over half a hemisphere, at 30-degree intervals i.e. 0°, 30°, 60°, 90°, 120°, 150°, 180°, on a series of seven arms. Each arm has five collecting optics (referred to as a "camera"). One arm has a

sixth optic, which captures the nadir measurement. This results in 36 cameras of different measurement angles within the hemisphere. The FOV of each camera is 4°, which equates to a measurement area of approximately 50 cm in diameter, when all of them point the target.

Each camera consists of a collimating lens and an optical fibre. The fibres from the entrance optics feed to a series of multiplexers to give one optical output that can be coupled to a spectrometer. To be able to take measurements at all chosen geometries, the arms of the goniometer have been designed so that they can rotate on the circular base of the structure allowing the forward and backward scattered radiation to be measured.

The positions of the entrance optics on the arms are also designed to be moveable so that effectively any five viewing angles (up to 50°) can be chosen during each measurement sequence.



NPL Gonio Radiometric Spectrometer System (GRASS)

Another design feature of GRASS is that the lenses on the end of each of the fibers can be removed, and replaced with a cosine diffuser, and the orientation of the viewing optic rotated such that the entrance optic can then measure the down-welling irradiance. This means that the instrument can measure both the up-welling radiance and down-welling irradiance at concurrent angles.

An ASD FieldSpec Pro was used during the campaign for acquiring the spectral data from GRASS.

**Resolution**: see ASD radiometer.

**Set-up time:** about 2 hours to set-up, and similarly 2 hours to dismantle at the end of the day. The instrument was left assembled on site overnight to reduce construction time.

**Transportation:** The instrument breaks down into three boxes. 2 x (640 x 1150 x 780) mm (WxLxH) Weight - of the order of 90 kg each

1 x (425 x 500 x 1235) mm (WxLxH) Weight - of the order of 55 kg

**Power Requirements:** To run the instrument requires some power – this was achieved through the use of a petrol generator.

#### **CIMEL** automatic sunphotometer

**Measurement aims:** to determine the aerosol optical properties, water vapour content, ozone and its temporal variability over the site for various measurement conditions. The operating temperature is  $-30^{\circ}$  to  $+60^{\circ}$ C.

**Instrument:** The CE 318 automatic sun tracking photometer has been designed and manufactured [24] to be an accurate sun photometer with all the qualities of a field instrument: motorized, portable, autonomous (solar powered) and automatic. Its main purpose is to measure sun and sky radiance to derive total column water vapor, ozone and aerosol properties using a combination of spectral filters and azimuth and zenith viewing controlled by a microprocessor.



CIMEL sunphotometer used at Tuz Gölü in August 2009

The sunphotometer CE 318 is composed of an optical head, an electronics box and a robot. The optical head has two channel systems: the sun collimator 1.2°, without lens, and the sky collimator with lenses 1.2°. The solar tracker is equipped with a 4-quadrant detector with an accuracy of position better than 0.1°. The electronics box contains two microprocessors for real time operation for data acquisition and motion control. In automatic mode, a 'wet sensor' detects precipitation and forces the instrument to park and to protect the optics. The robot is moved step-by-step by motors in two directions: in the zenith and azimuth planes. The calculation of the air mass uses the sun equation [29] and is performed by two CPU cards.

For further information please refer to <a href="http://www.cimel.fr/photo/sunph\_us.htm">http://www.cimel.fr/photo/sunph\_us.htm</a>.

**Accuracy**: 0.01 - 0.02 (wavelength dependent) in aerosol optical thickness (unit less). For more information, please refer to: <a href="http://aeronet.gsfc.nasa.gov/new\_web/">http://aeronet.gsfc.nasa.gov/new\_web/</a> system\_descriptions\_calibration.html

**Set-up**: it takes approximate 3 hours to set up this radiometer.

**Transportation**: Two boxes:  $0.6 \times 0.5 \times 0.35$  mm and  $0.8 \times 0.6 \times 0.6$  mm for a total weight of 78 kg.

**Power requirements**: Internal batteries for the optical head and external batteries for the robot and the satellite transmitter which are rechargeable by solar panels.

**Traceability**: The sunphotometer was calibrated before the Tuz Gölü campaign by AERONET at Goddard Space Flight Center, NASA. This calibration was also checked and confirmed by CNES after the campaign to evaluate the impact of the salty atmosphere on the instrument calibration.

## **MICROTOPS** handheld sunphotometer

The Microtops II sunphotometer was provided by DLR for this pilot comparison.



MICROTOPS sunphotometer

The Microtops II sun photometer is a 5 channels (440 nm, 675 nm, 870 nm, 936 nm, 1020 nm), hand-held instrument for measuring the direct solar radiance using a 2.5° viewing angle.

The Microtops II has been configured with five filters for the determination of aerosol optical thickness (AOT), including filters at 936 nm and 1020 nm for the measurement of the precipitable water vapour content. Additionally it contains a non-volatile memory allowing to associate date, time, coordinates (latitude, longitude), solar angle, altitude, pressure and temperature to each measured value.

Further information on the specification and user guides can be found at: <a href="http://fsf.nerc.ac.uk/instruments/sunphotometer.shtml">http://fsf.nerc.ac.uk/instruments/sunphotometer.shtml</a>

**Measurement aims:** To determine the aerosol loading/water vapour content and its temporal variability over the target area. The aerosol data will be used as an input to the Radiative Transfer Code (RTC) for the atmospheric correction of the satellite data.

**Resolution**: 0.1 W/m<sup>2</sup>

**Precision**: 1 - 2%

**Set-up:** Location and time should be set up at the beginning of the measurements

**Transportation:** 10 x 20 x 4.3 cm and a weight of 600 gram

**Power Requirements:** 4 x AA Alkaline batteries

**Traceability:** The handheld Microtops II sunphotometers are returned to the manufacturer for annual calibration and data quality assurance.



MICROTOPS handheld sunphotometers, Tuz Gölü 2009

### **Transfer Standard Absolute Radiance Source (TSARS)**

The NPL TSARS was developed to provide a transportable radiance source for the calibration of field spectrometers and satellite instruments used for the validation of satellite data [31] [32]. The design is based around 230 mm diameter integrating sphere from Gigahertz Optik, Germany. The sphere coating is Ultralon, which is a form of PTFE based diffuser. It is illuminated externally by four dichroic lamps contained in lamp housings, which are fixed to four of the entrance ports [33].

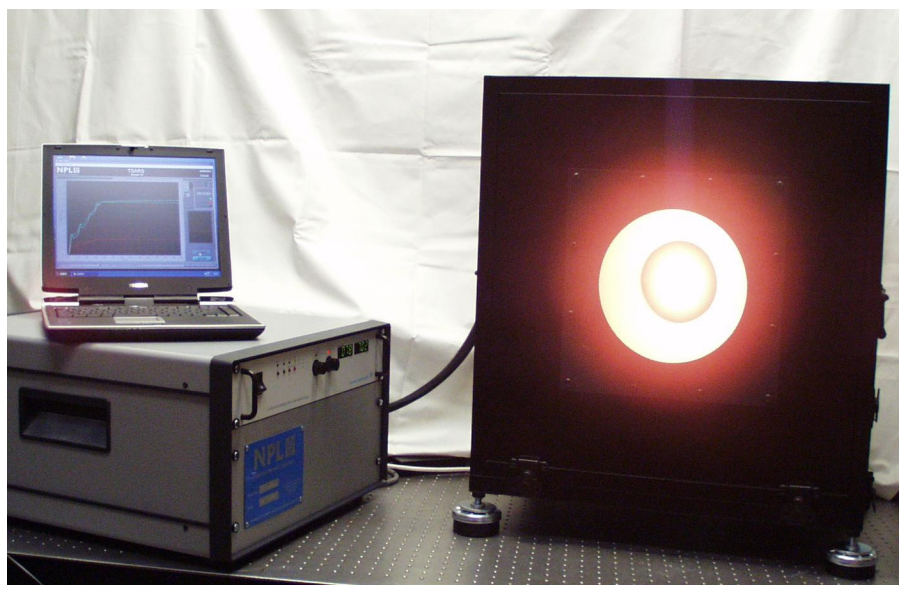
The heat generated from the lamps burn off any moisture the sphere may have absorbed during transportation, and which may affect the reflectivity of the Ultralon coating. Therefore the sphere can be used in any location irrespective of its surrounding environmental conditions.

TSARS is controlled by NPL written software. The instrument receives and records the signal from three filtered detectors mounted together on one port of the sphere. The filters have central wavelengths of 400 nm, 520 nm and 695 nm and band-passes of ~ 100 nm. The 520 nm detector provides the signal for the feedback routine, which adjusts the current to maintain stability of the lamps, while the others are monitors and can provide immediate information if the lamp output has changed outside its uncertainty limits. The user therefore has information about the current state of TSARS calibration.

### TSARS Uniformity and Stability

The key requirement of TSARS is that it provides a stable and uniform large area radiance source. Tests on the NPL TSARS were made using a uniformity measurement facility, which has a moving stage that can perform uniformity scans of large area sources in the x-y plane. The results show the uniformity is better than  $\pm 0.25\%$  across the 50 mm diameter exit port.

The stability of the NPL TSARS was also tested using an 800 nm filter radiometer. The filter radiometer was positioned to focus on the centre of the exit port of the sphere and left to monitor the sphere over a period of 5 hours. The sphere is stabilised by its own detector but the filter radiometer was used to monitor the NPL TSARS externally to verify the sphere detectors were correctly stabilising the sphere. The result of these tests revealed that the output of the NPL TSARS was stable to  $\pm 0.2\%$  over a period of 5 hours.



NPL TSARS and the detector stabilised control unit.

## **Appendix B: Definition of terms**

The results reported here are specified as Reflectance Factors. The relationship between this and Radiance Factor and BRDF is discussed in this Appendix.

Radiance factor (Raf) ratio of radiance of a surface element in a given direction to

that of a perfectly reflecting Lambertian diffuser identically

irradiated

Reflectance factor  $(\rho)$  ratio of radiant power reflected by a surface element into a

given solid angle to that of a perfectly reflecting

Lambertian surface element

BRDF ratio of emitted radiance in a given direction to incident

irradiance

#### Note that:

• Raf,  $\rho$  and BRDF are all functions of incident angles ( $\theta$ i,  $\phi$ i) and viewing angles ( $\theta$ o,  $\phi$ o)

• Raf and  $\rho$  are dimensionless; BRDF has dimensions sr<sup>-1</sup>.

• A "perfectly reflecting lambertian diffuser" is an idealised object, not a transfer standard. The quantities reported here are absolute measurements.

• For this tile the incident beam direction, viewing direction and sample normal were in the same plane, so we can set  $\phi i = \phi o = 0$ .

•  $\rho = Raf$  in the limiting case that the viewing solid angle  $\rightarrow 0$ , which is, to an excellent approximation, satisfied in these measurements

• The *BRDF* of a perfectly reflecting lambertian diffuser is  $1/\pi$  sr<sup>-1</sup>. Therefore *BRDF* and *Raf* are related by a factor of  $\pi$ .

# Appendix C: Participants' reported data

## **Cross-comparison against TSARS**

	23/08/2009	29/08/2009
DLR	B2_DLR_day1_updated.xls	B2_DLR_day6_updated.xls
ONERA	B2_ONERA_23082009_V2.xls	B2_ONERA_29082009_V2.xls
NPL	B2_NPL_23082009.xls	B2_NPL_29082009.xls
TU	B2_TU23&29082009_TU.xls	

## Reflectance factor of the reference panels used by participants

	File
DLR	DLR_Spectralon@.xls
ONERA	reflectance-reference-SRT-99-No2.xls
TU	abs162101_10A.ref.txt Labsphere characterisation in 2008
	LabsphereRF_May2009.xls calibrated at NPL in May 2009

## Cross-comparison against the reference panels on 26/08/2009

	File for 26/08/2009	
DLR	B1_DLR_Spectralon@s_updated.xls	
ONERA	B1_ONERA-Spectralon@s-intercomp-3labs_26082009_V2.xls	
TU	B1_TU_Spectralon@comparison_26082009_correction_TU.xls and	

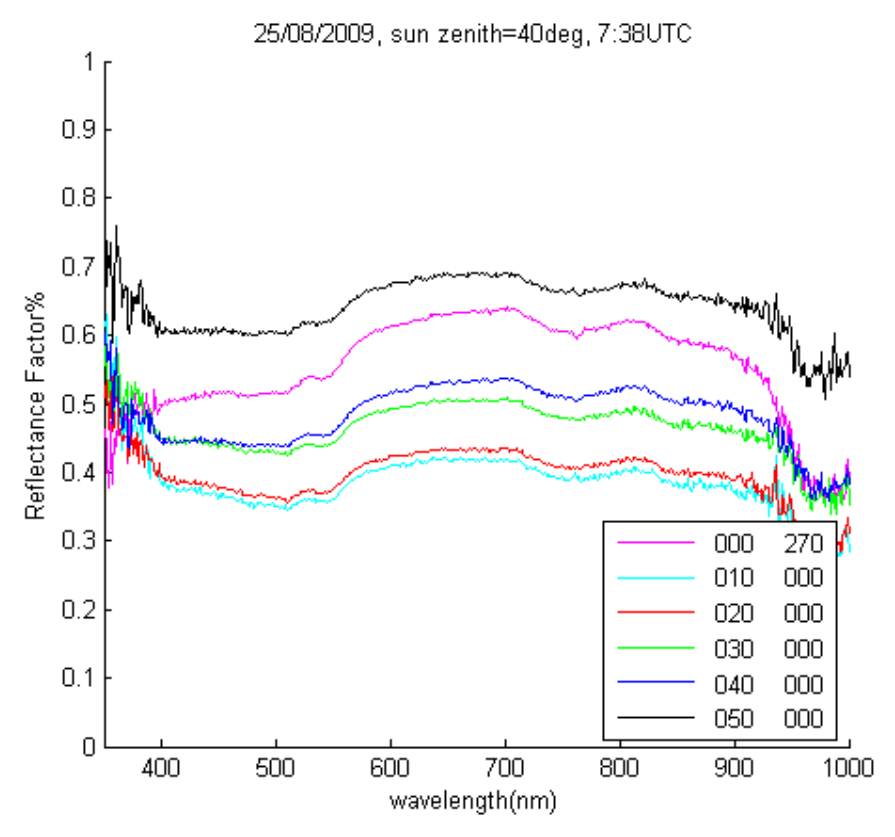
## Cross-comparison against the reference panel on 27/09/2009

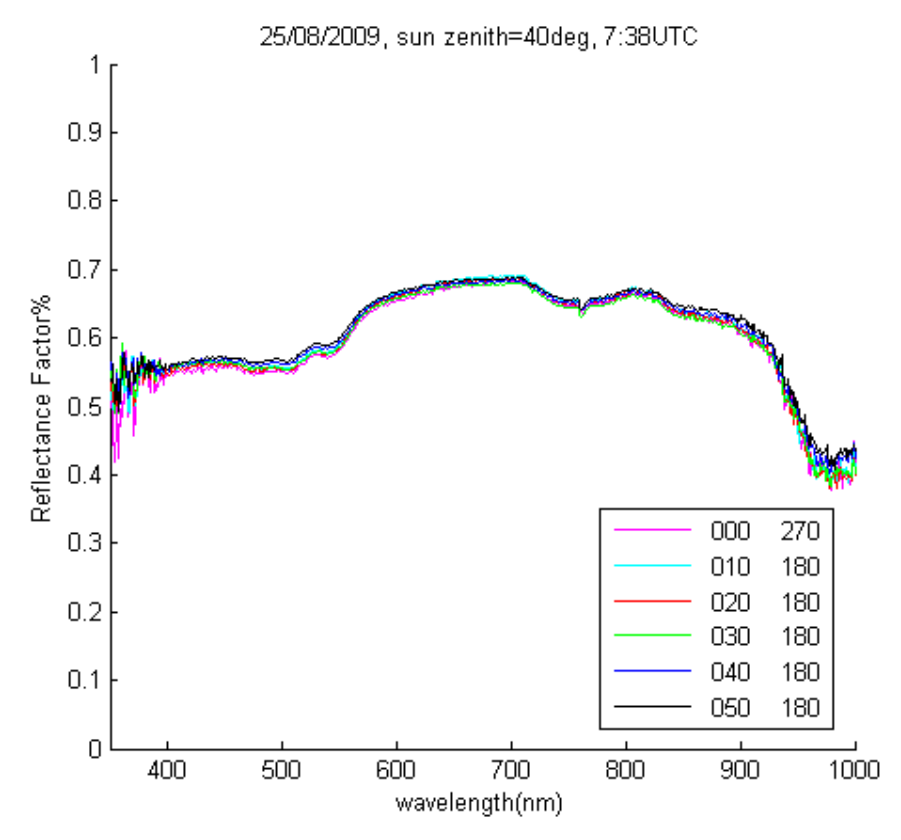
	File for 27/08/2009
DLR	B1_DLR_Spectralon@_NPL_updated.xls
ONERA	B1_Onera_asd_2009-08-27_NPL_ref_V2.xls
TU	B1_TU_Spectralon@comparison_27082009_TU.xls

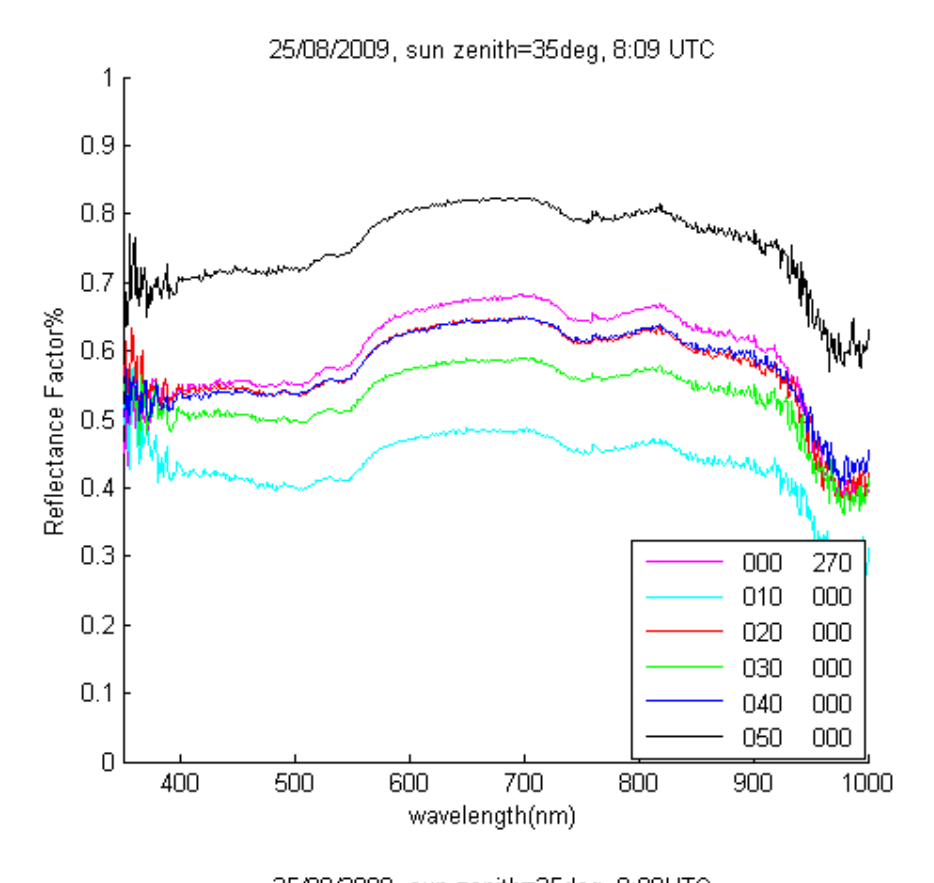
## Site characterisation

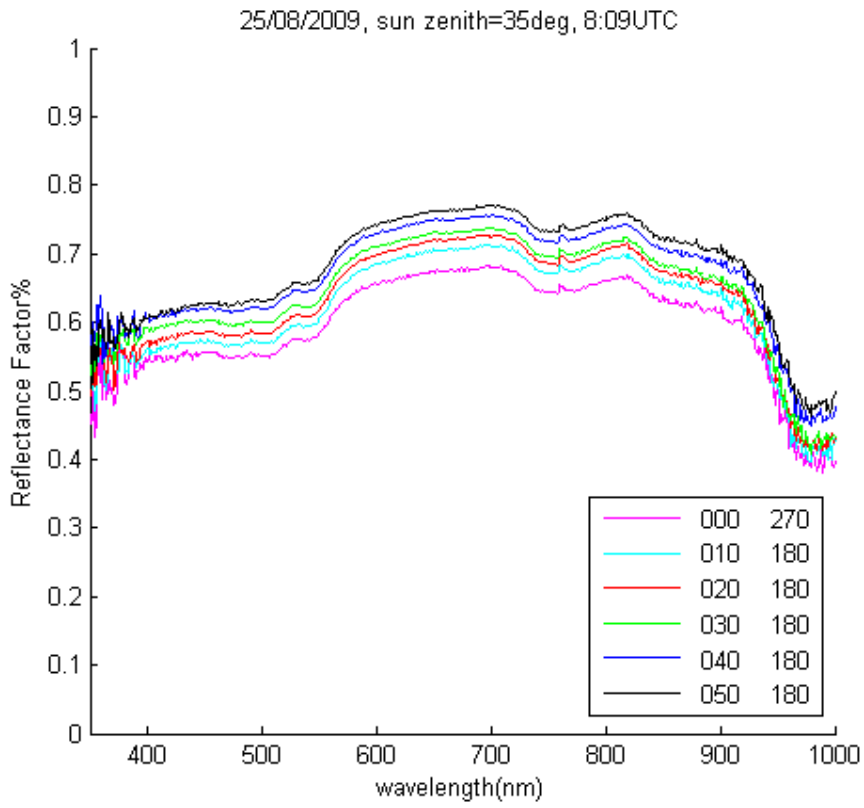
	25/08/2009	27/08/2009	28/08/2009	
DLR	1km x 1km	100m x 300m ( <b>M1</b> )	100m x 300m ( <b>M3</b> )	
	DLR_1km_overall_B3_2.	DLR_m1_points_B3_2.x1	DLR_m3_points_B3_2.xls	
	xls	s	DLR_m3_single_points.xls	
ONERA	100m x 300m ( <b>M1</b> )	100m x 300m ( <b>M2</b> )	100m x 300m ( <b>M3</b> )	
	B3_Onera_ASD_M1_V2	B3_Onera_ASD_M2_V2	B3_Onera_ASD_M3_V201	
	010-01-04.xls	010-01-11.xls	0-01-11.xls	
TU	100m x 300m ( <b>M2</b> )	1km x 1km	100m x 300m ( <b>M3</b> )	
	AppendixB3_C_TUBITAKUZAY_02112009.xls			

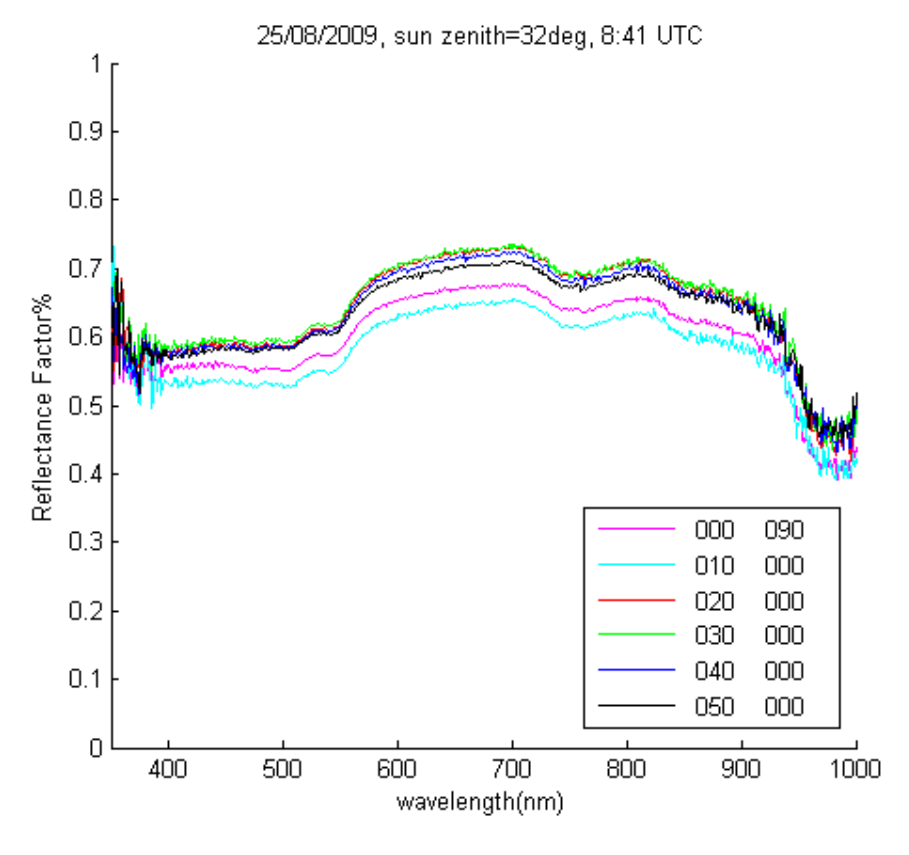
# Appendix D: BRDF data

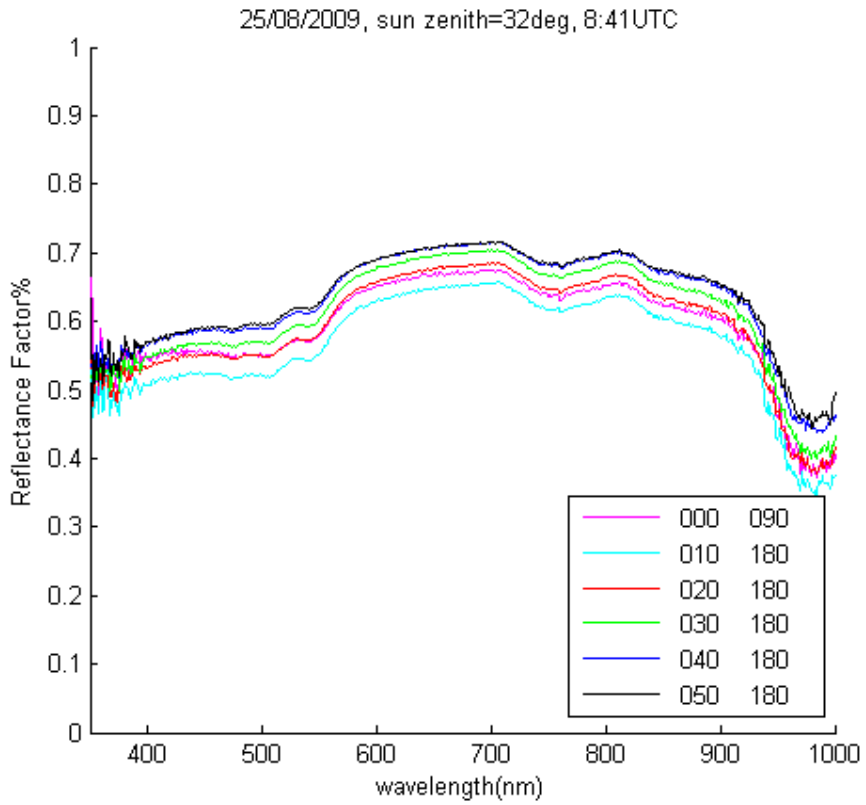


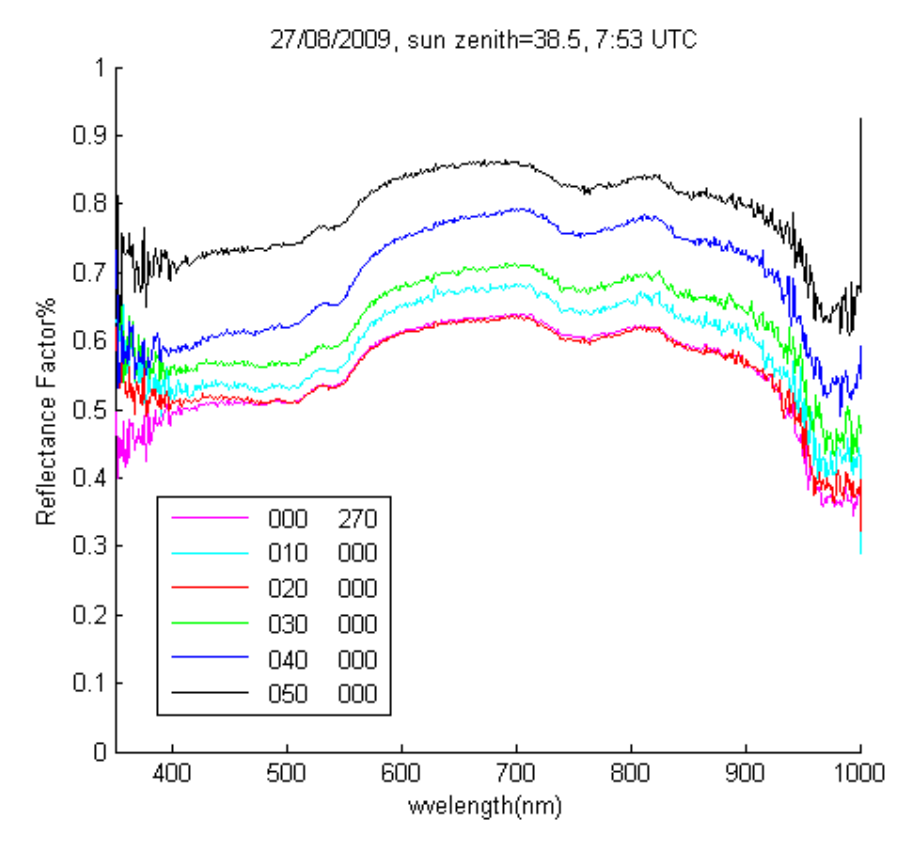


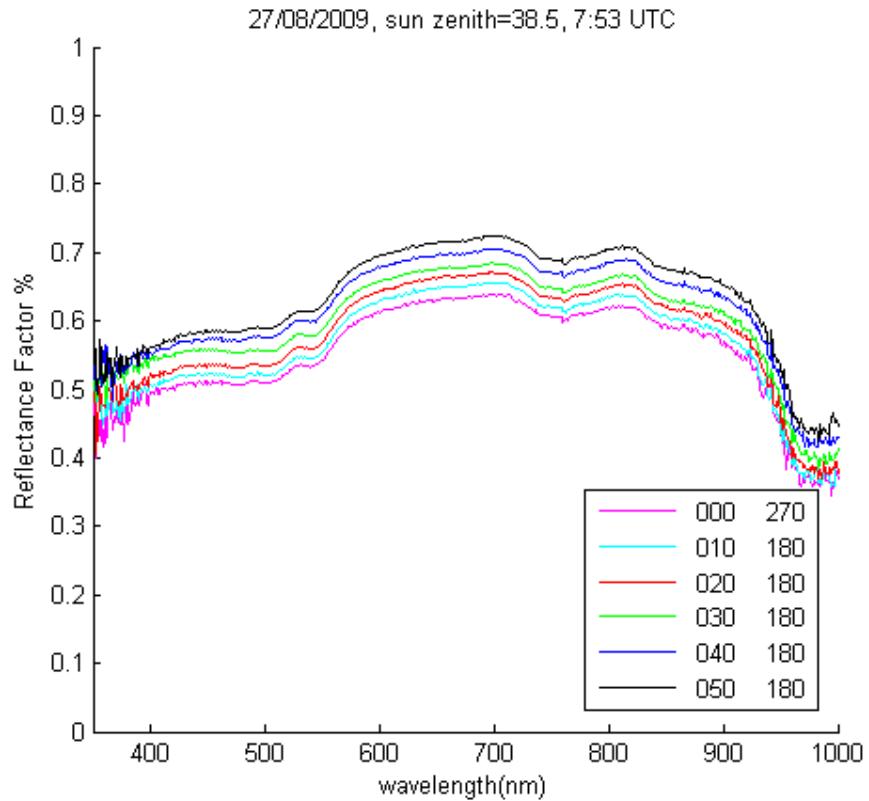


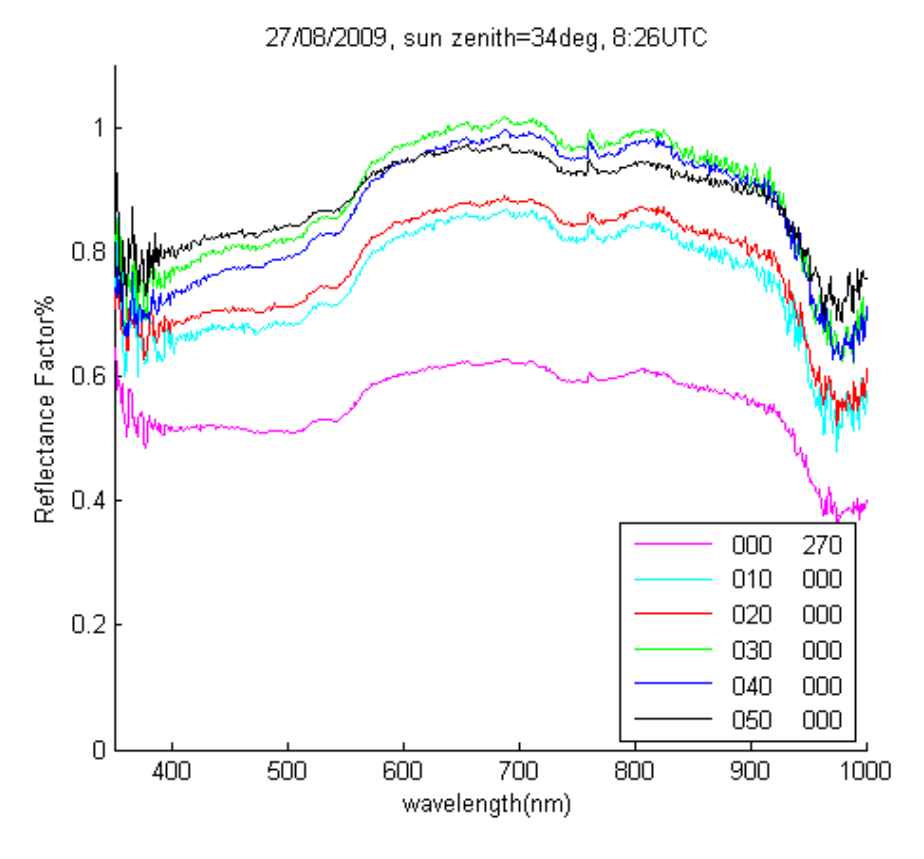


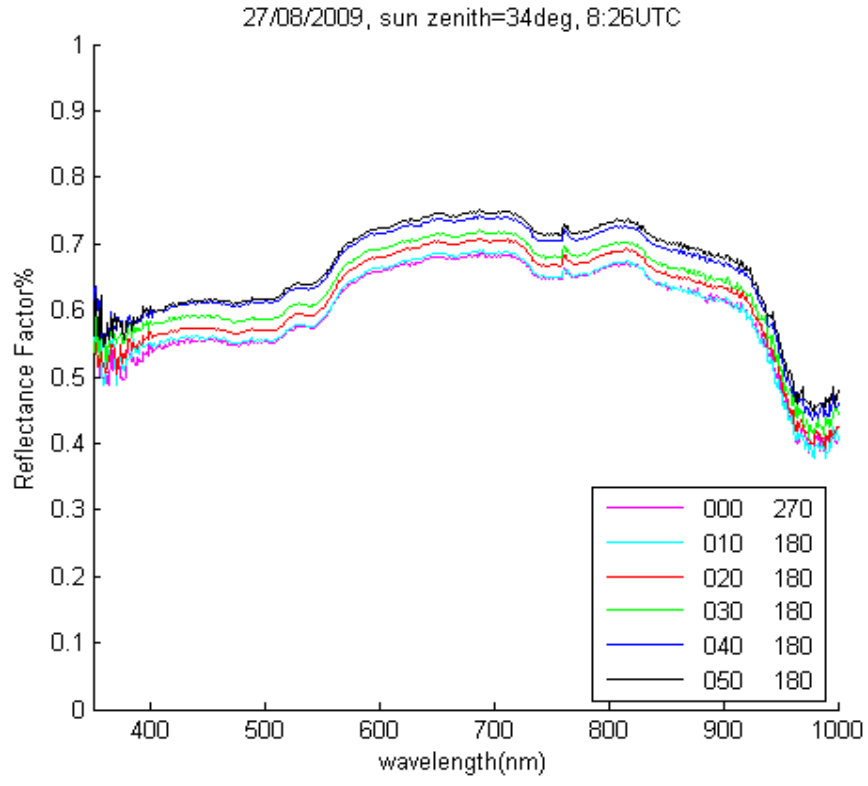


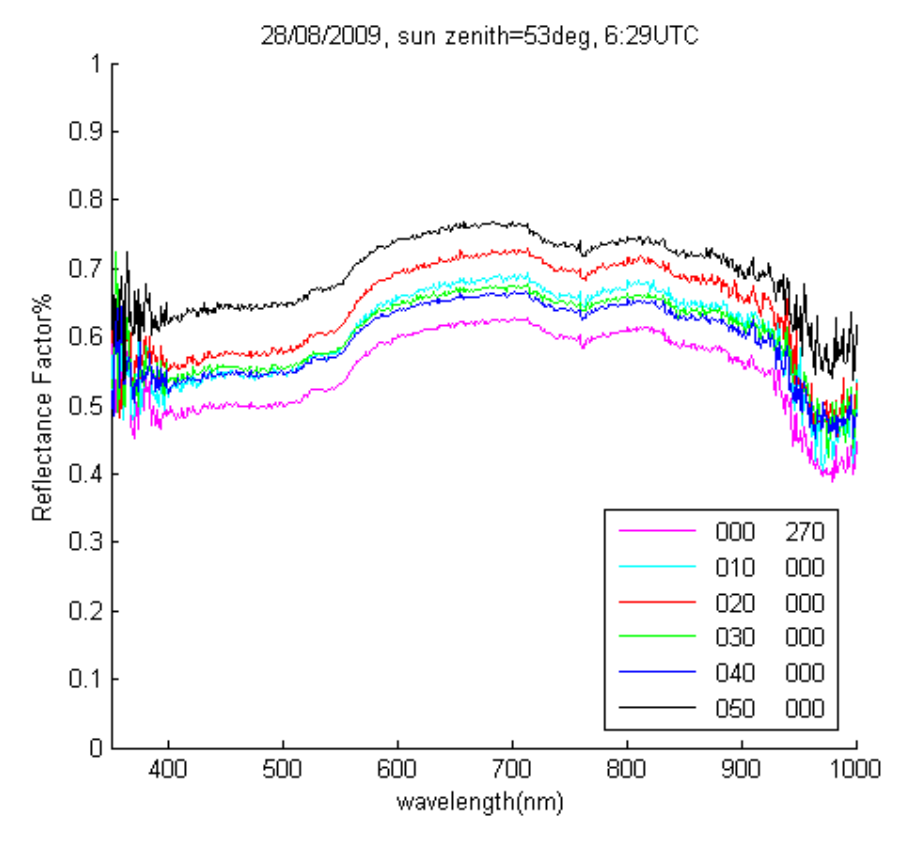


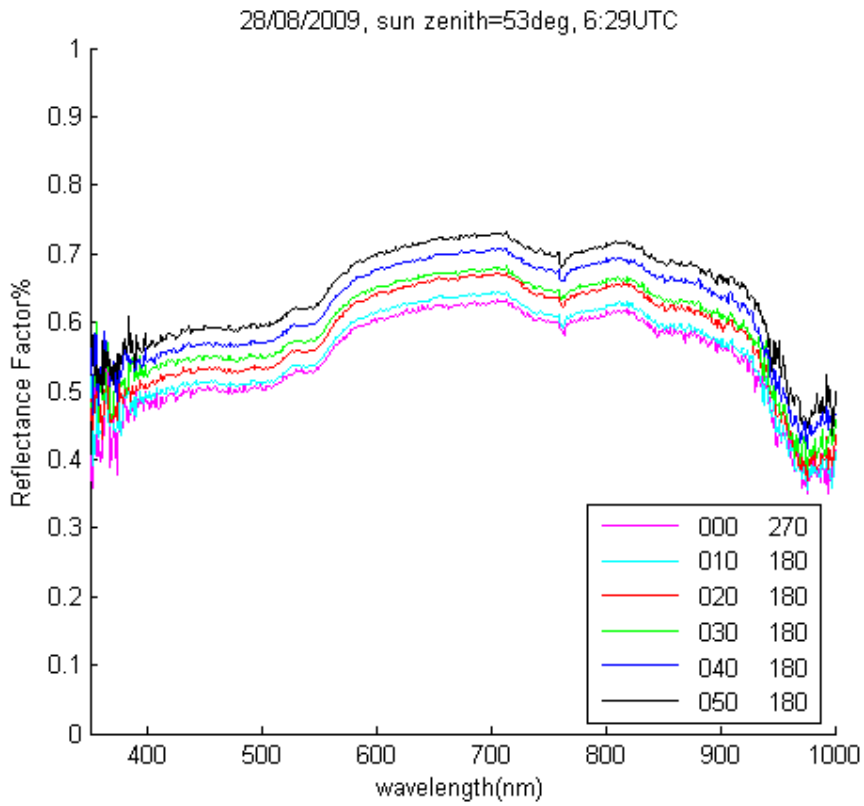


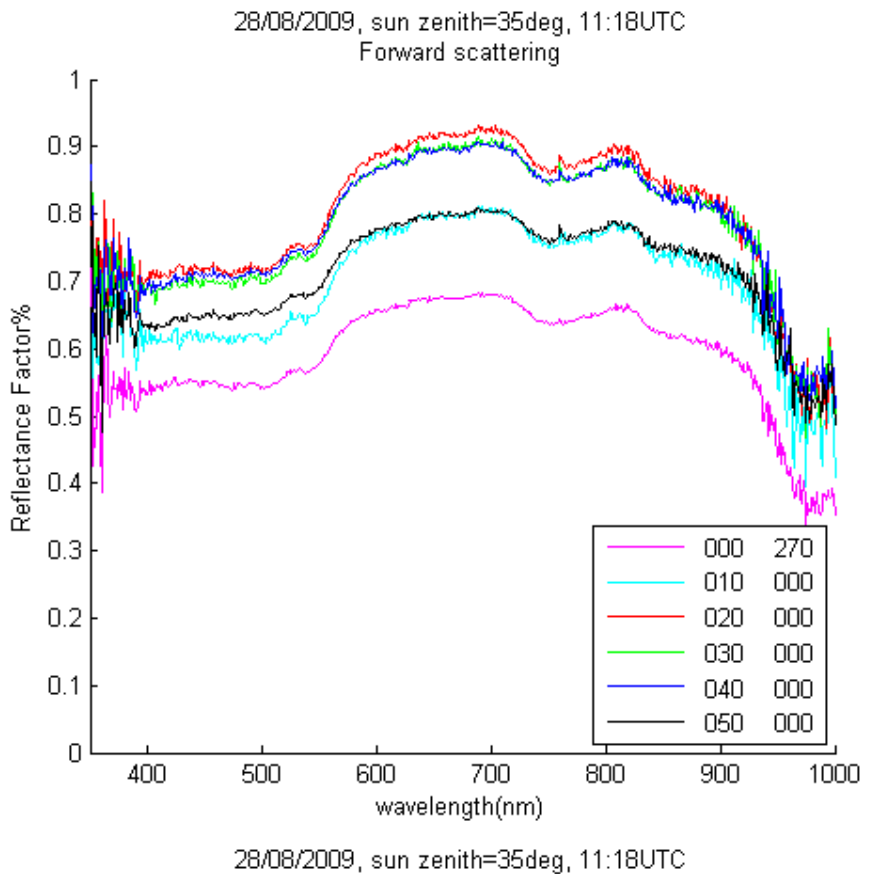


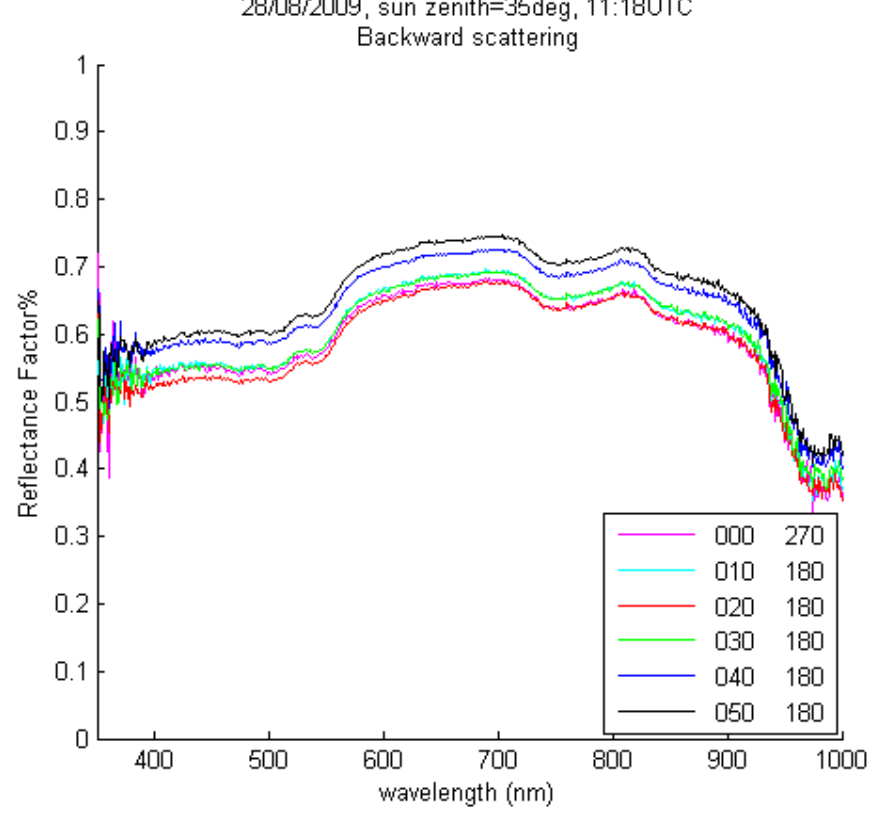






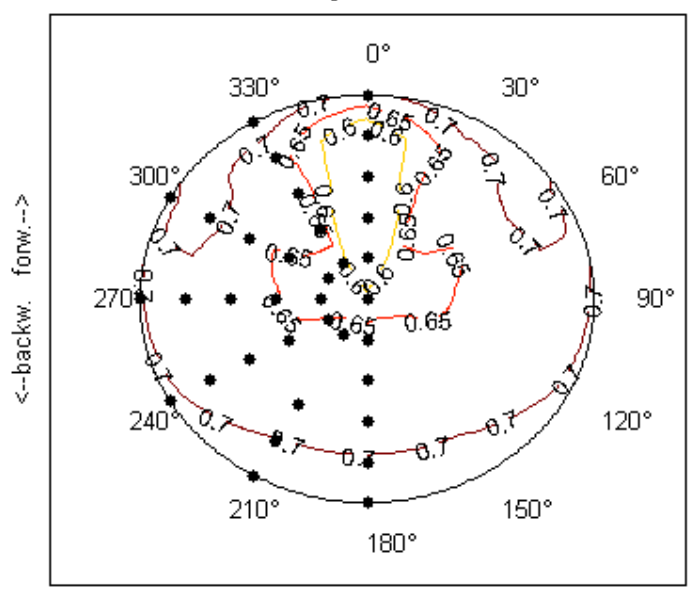




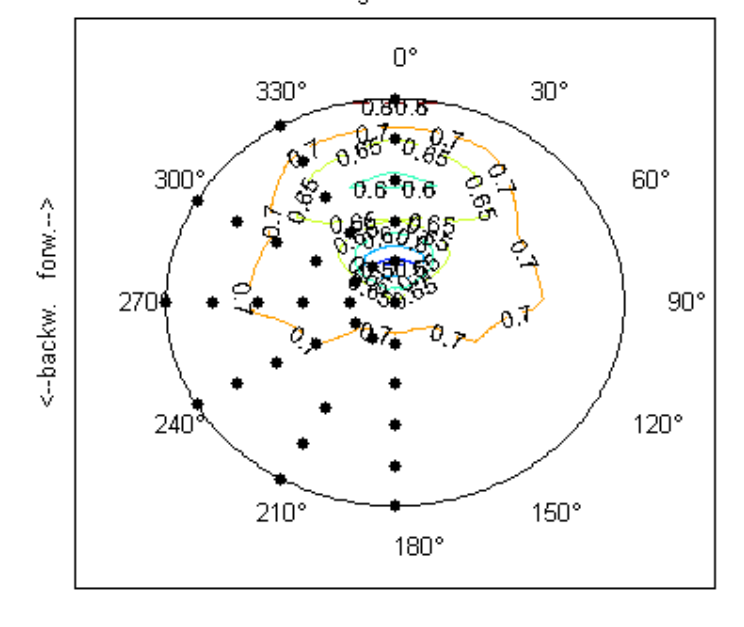


## **BRDF** in polar coordinates:

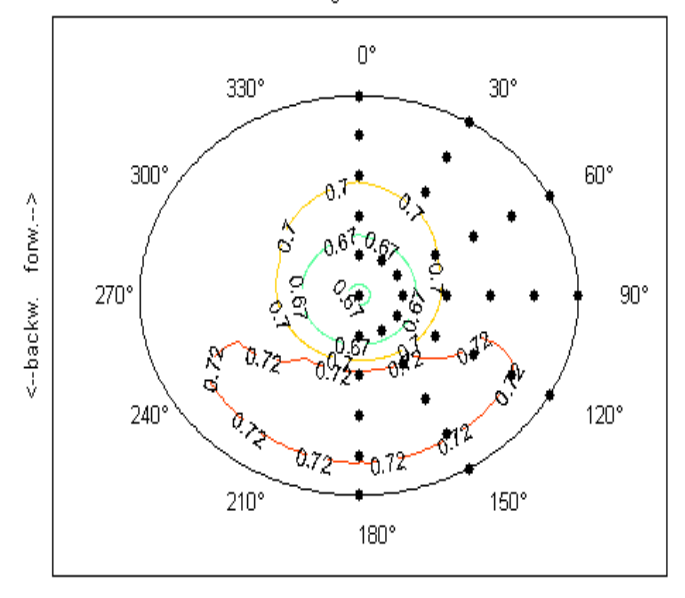
Location: Tuz Golu Date: 25/08/2009 Solar angle: 40 degrees Wavelength: 700 nm



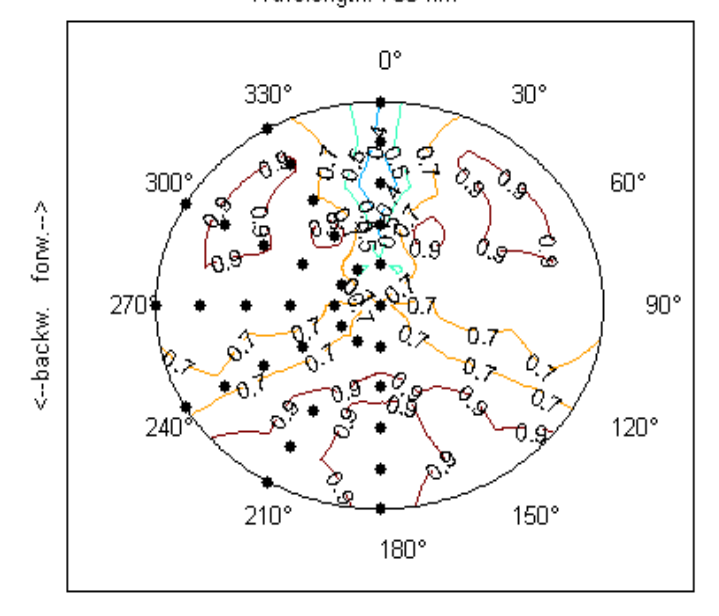
Location: Tuz Golu Date: 25/08/2009 Solar angle: 35 degrees Wavelength: 700 nm



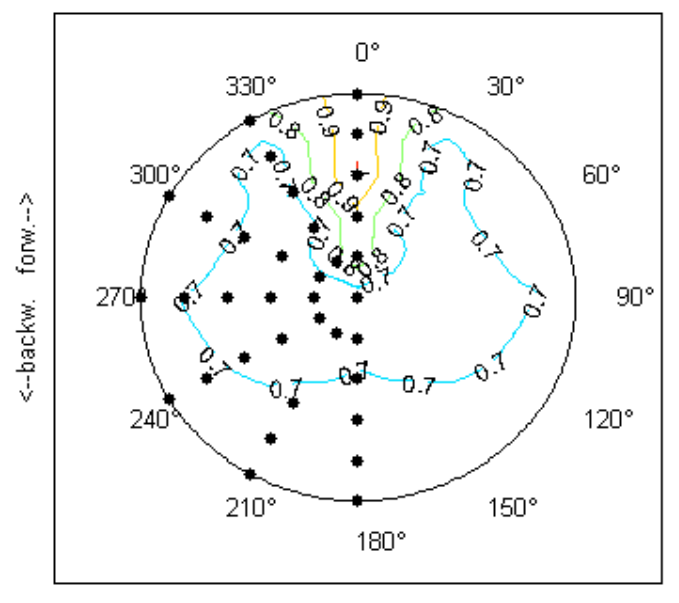
Location: Tuz Golu Date: 25/08/2009 Solar angle: 32 degrees Wavelength: 700 nm



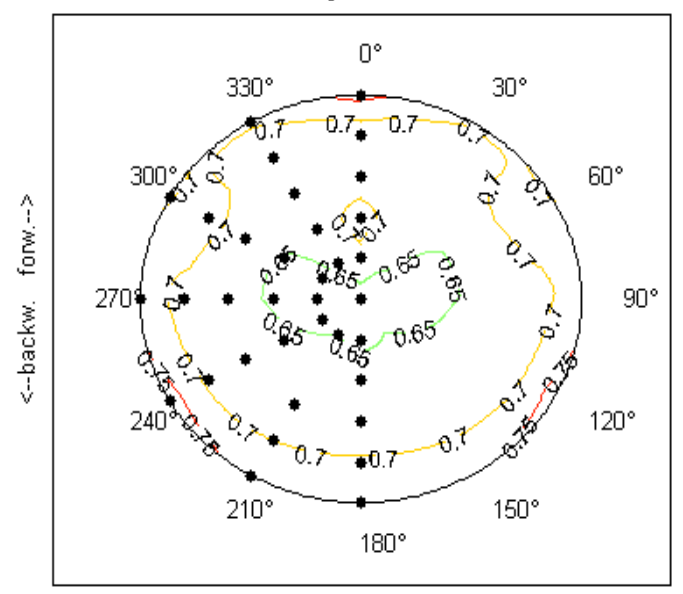
Location: Tuz Golu Date: 27/08/2009 Solar angle: 38.5 degrees Wavelength: 700 nm



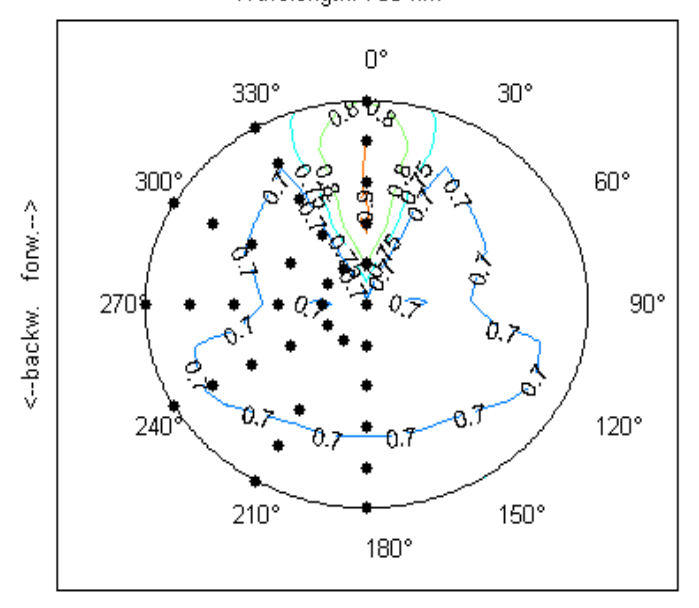
Location: Tuz Golu Date: 27/08/2009 Solar angle: 34 degrees Wavelength: 700 nm



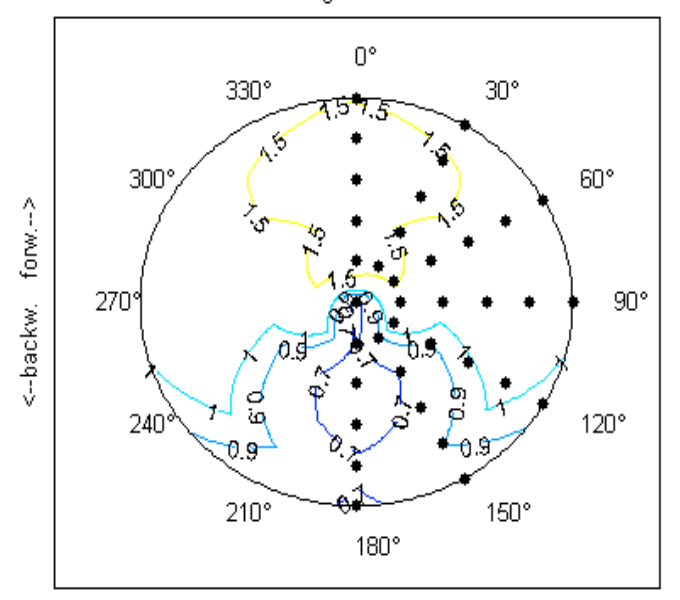
Location: Tuz Golu Date: 28/08/2009 Solar angle: 53 degrees Wavelength: 700 nm



Location: Tuz Golu Date: 28/08/2009 Solar angle: 35.21 degrees Wavelength: 700 nm



Location: Tuz Golu Date: 28/08/2009 Solar angle: 40 degrees Wavelength: 700 nm



## Appendix E: BRDF Type A standard uncertainty

Measurements were recorded with GRASS over three days: 25/08/2009, 27/08/2009 and 28/08/2009 for the same sun zenith angle: 35°. This dataset was used to estimate the Type A standard uncertainty (repeatability and reproducibility) using the same method described in Chapter: 6.1.

Over the main part of spectrum (400 - 1000 nm) the average is calculated based on replicates as a result of F-test = 0. For 400 nm the standard uncertainty is calculated based on group means (F=1).

The values at nadir for these three days at 35° sun zenith angle show a particular feature: values are decreasing with time for 25/08/2009 and 27/08/2009 (Figure 1 and Figure 2). The timeframe of a full GRASS sequence over half of hemisphere 10 minutes, however the illumination conditions could change during this timeframe. The variability of the sun irradiance was not monitored in August 2009.

Laboratory experiments using a floodlight confirmed thys hypothesis. A series of measurements using a reference panel and an artificial target proved that for stable illumination conditions the values measured over the nadir camera are constant and they do not change in value over 10 minutes (Figure 3 and Figure 4).

We consider these datasets are not enough for a complete standard uncertainty analysis. These first results (Figure 5, Figure 6, and Figure 7) will be further confirmed with the analysis of more datasets from August 2010 when the downwelling radiance will be monitored in the same time with the upwelling signal.

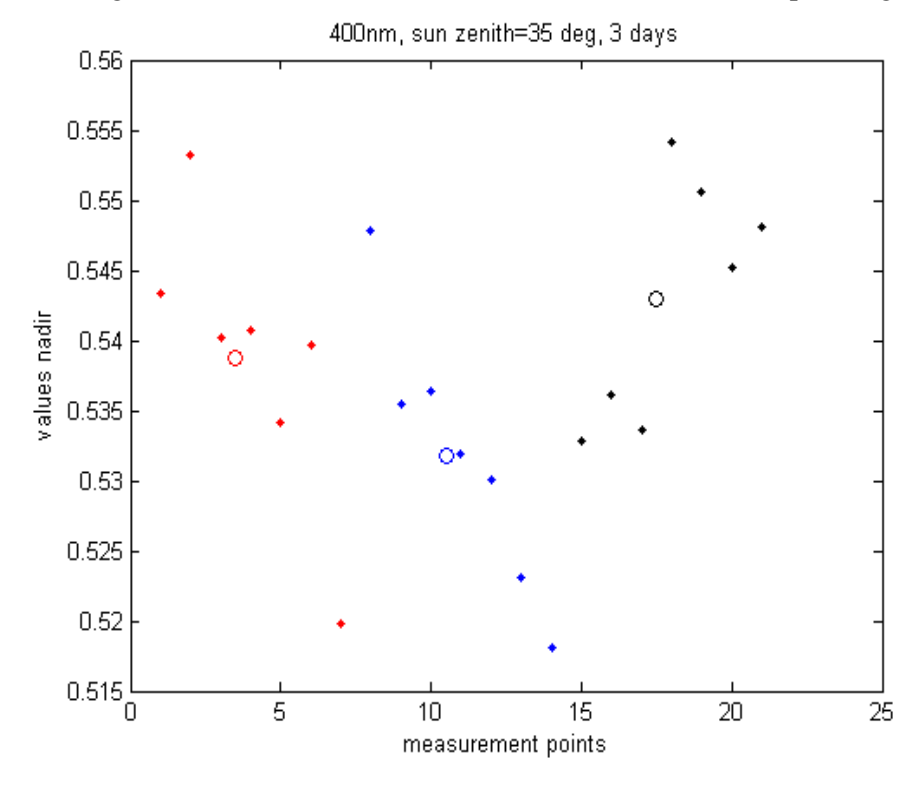


Figure 1. GRASS  $\rho$  at 400 nm recorded over nadir for three days, same sun zenith

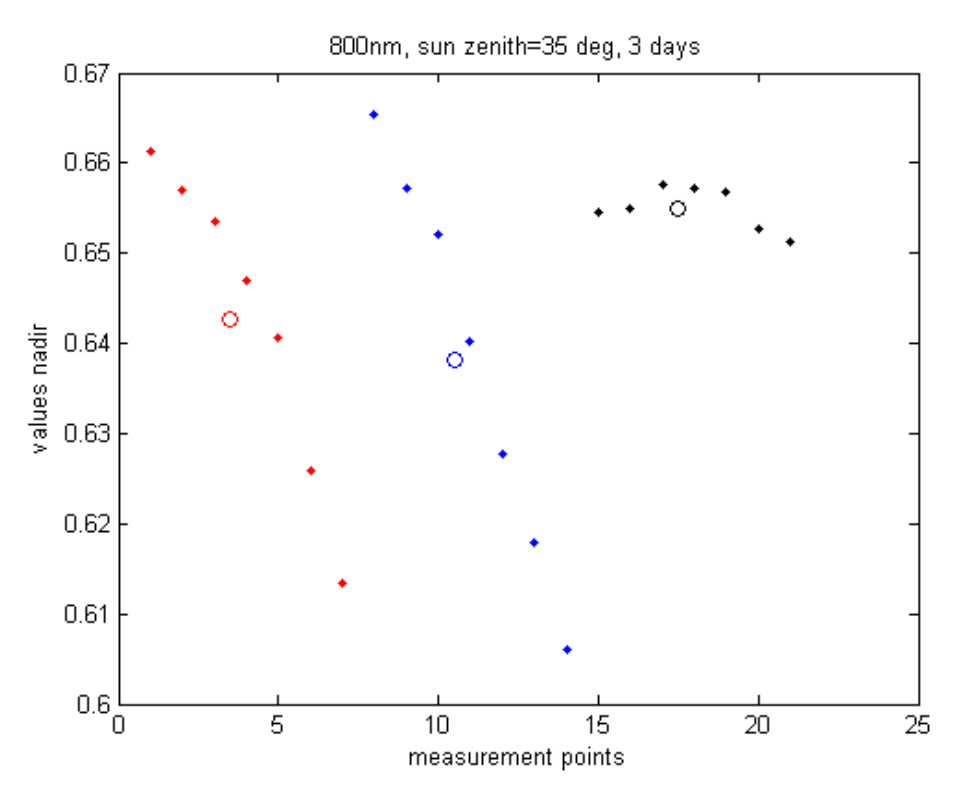


Figure 2. GRASS  $\rho$  at 800 nm recorded over nadir for three days, same sun zenith

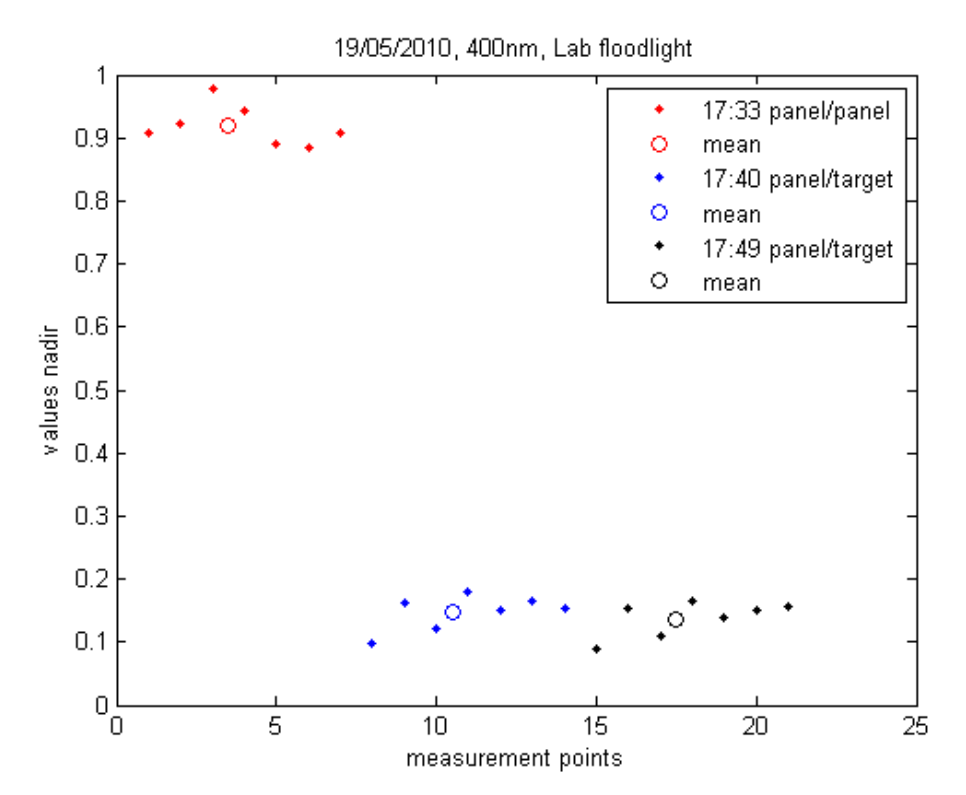


Figure 3. GRASS  $\rho$  at 400 nm recorded over nadir using a floodlight in the NPL laboratory

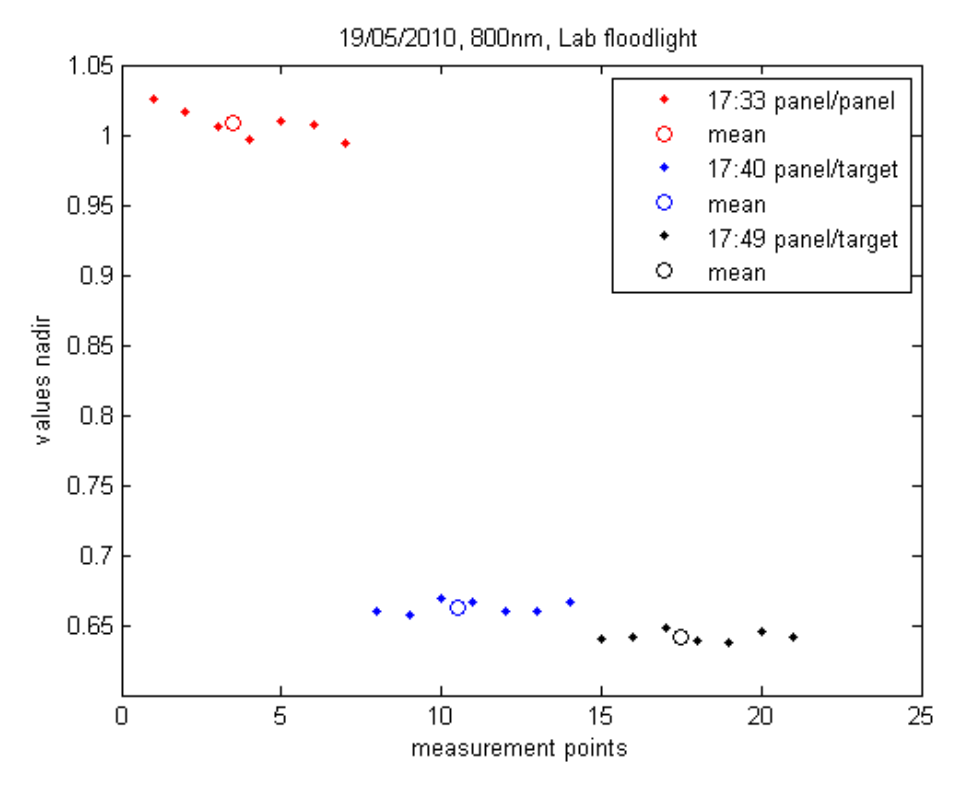


Figure 4. GRASS  $\rho$  at 800 nm recorded over nadir using a floodlight in the NPL laboratory

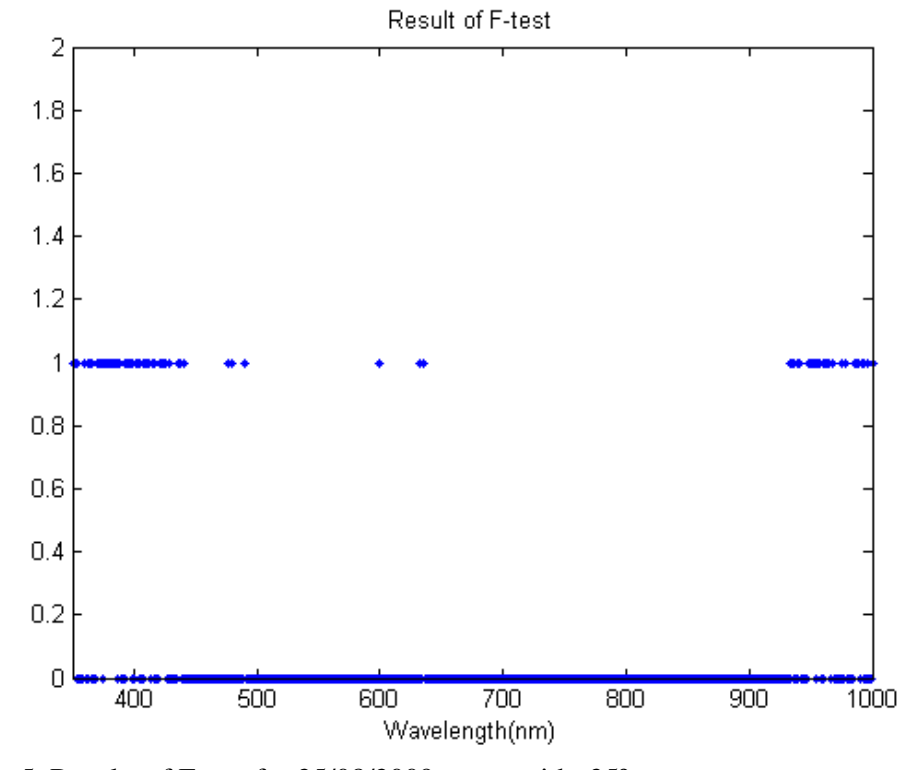


Figure 5. Results of F-test for 25/08/2009, sun zenith=35°

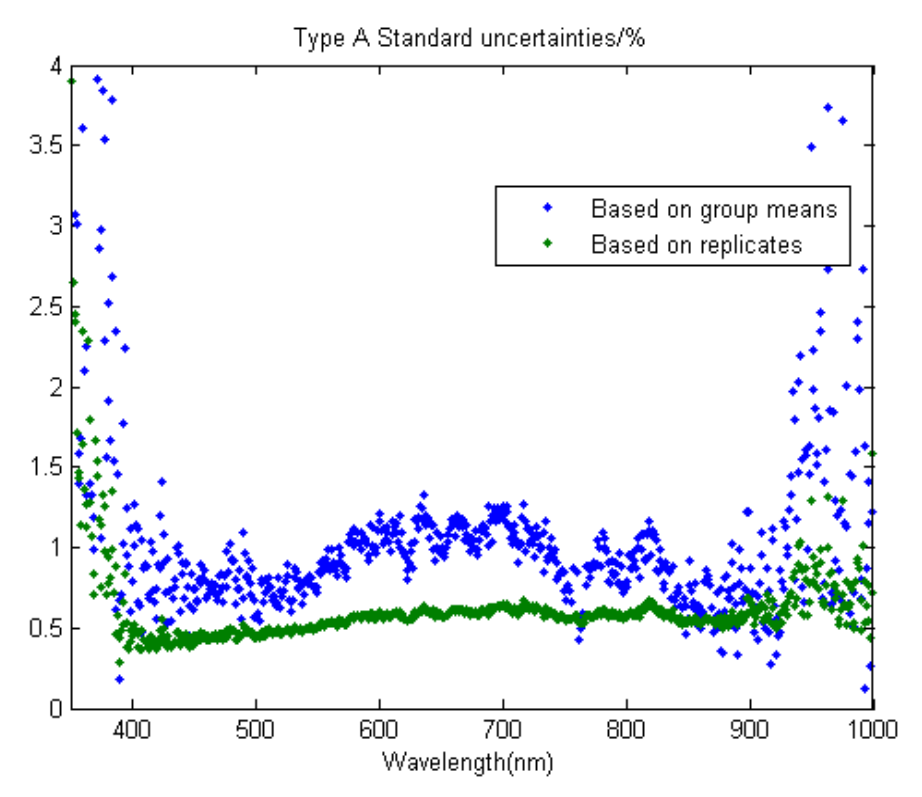


Figure 6. Type A standard uncertainty for 25/08/2009, sun zenith=35° calculated based on group means and on replicates.

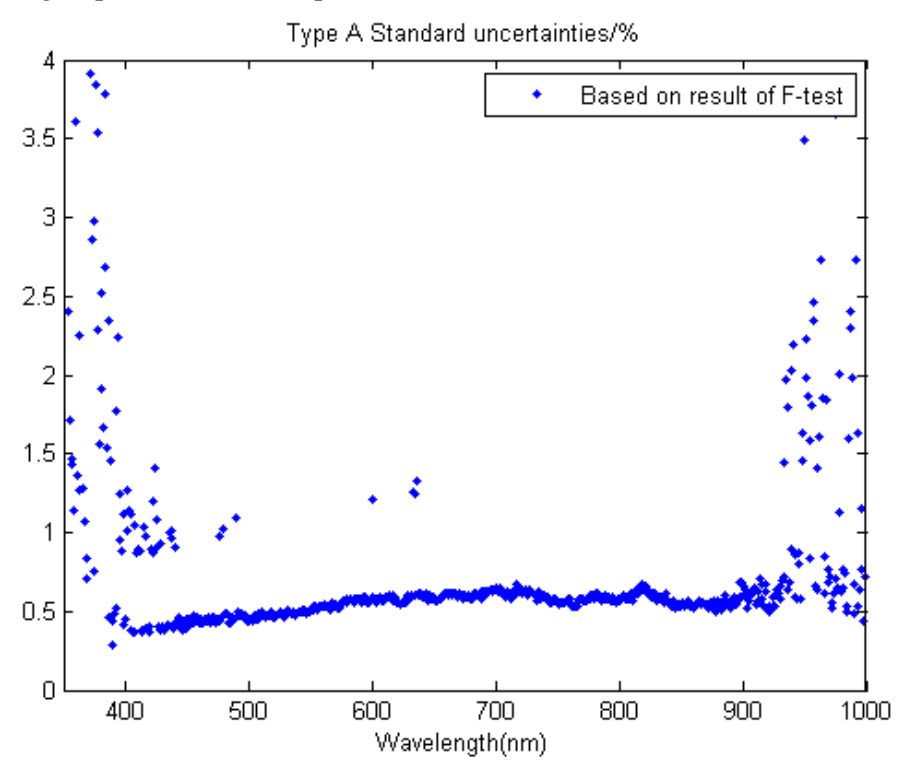


Figure 7. Type A standard uncertainty right value over each spectral region is selected using the results of the F-test

## Appendix F: Airborne hyperspectral data

As part of the HyEurope2009 campaign DLR acquired airborne hyperspectral data over Tuz Gölü using the HyMap sensor [34]. These flights took place shortly after the field campaign on 1<sup>st</sup> September 2009 during slightly dusty conditions. The system-corrected data (calibrated at-sensor radiance) will be made available to the CEOS community.

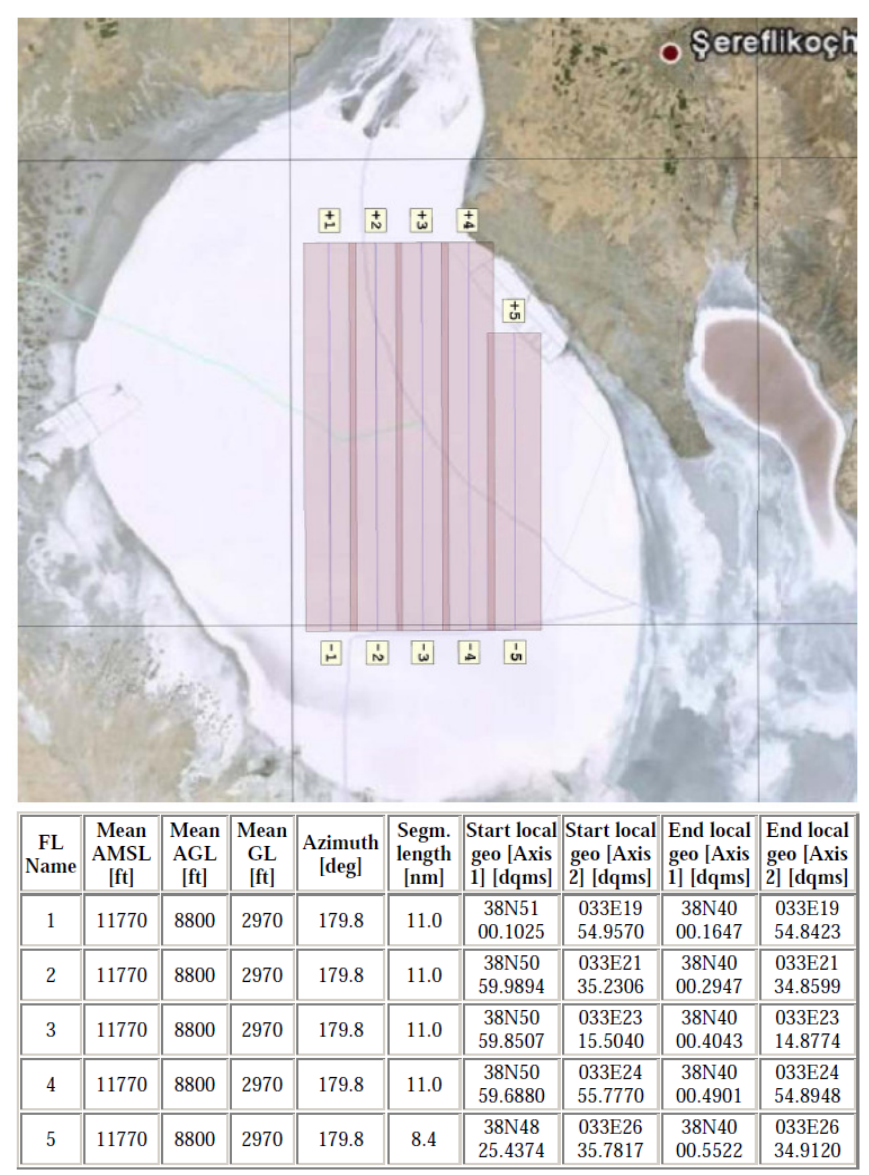


Table 16: Location and parameters of the five HyMap flight lines over Tuz Gölü

## Acknowledgements

The authors would like to thank the European Space Agency (ESA) for the financial support within the frame of "Comparison to Maintain Traceability and Equivalence for Post-Launch Optical sensors Cal/Val" project (ESRIN Contract N0. 21822/08/I-OL) and to acknowledge the financial support provided by the National Measurement Office of the Business, UK Department for Business Innovation and Skills (BIS). We thank DLR for providing airborne measurements using the HyMap system, CNES for providing an automatic sunphotometer (CIMEL) and the Field Spectroscopy Facility of NERC (National Environment Research Centre) for the loan of an ASD radiometer for field measurements with GRASS. We thank to Turkish Directorate of Mapping for giving the flight permission to DLR for airborne measurements over Tuz Gölü during the pilot comparison.

### References

- [1] Fox N.P. QA4EO-WGCV-IVO-CLP-008: Protocol for the CEOS WGCV pilot Comparison of techniques/instruments used for vicarious calibration of Land surface imaging through a ground reference standard test site, on <a href="http://qa4eo.org/documentation.html">http://qa4eo.org/documentation.html</a>, 2009.
- [2] <a href="http://en.wikipedia.org/wiki/Lake Tuz">http://en.wikipedia.org/wiki/Lake Tuz</a>
- [3] Camur M.Z. and H. Mutlu. Major ion geochemistry and mineralogy of Salt Lake (Tuz Gölü) basin, Turkey. *Chemical Geology*, vol. 127: 313-329, 1996.
- [4] ASD Technical Guide 3rd Ed. Section 18-5, 1999.
- [5] BIPM, IEC, IFCC, ILAC, ISO, IUPAC, IUPAP and OIML. Guide to the expression of uncertainty in measurement (GUM: 1995 with minor corrections). Bureau International des Poids et Mesures, JCGM 100, 2008.
- [6] "Radiometric Calibration Accuracy" document received from ASD Inc. in January 2010 and updated in April 2010 with new values for the expanded uncertainty, 2010.
- [7] FieldSpec Pro User's Guide, ASD Part # 600000 Rev C, p 118, 2005 and FieldSpec 3 User Manual, ASD Document 600540 Rev. G: 67-68, 2007.
- [8] Jackson, R.D., Moran, M.S., Slater, P.N., and Biggar, S.F. Field Calibration of Reference Reflectance Panels, *Remote Sensing of Environment*, 22: 145-158, 1987.
- [9] Schaepman-Strub G., Schaepman M.E., Painter T.H., Dangel S., and Martochik J.V. Reflectance quantities in optical remote sensing definitions and case studies. *Remote Sensing of Environment*, 103: 27-42, 2006.
- [10] Gibbs D.R., Duncan F.J., Lambe R.P., and Goodman T.M. *Metrologia*, 32, (6): 601-607, 1996.

- [11] Möller W., Nikolaus K-P., and Höpe A. Degradation of the diffuse reflectance of Spectralon@ under low-level irradiation. *Metrologia*, 40: 212-215, 2003.
- [12] <u>Savitzky, A.</u> and <u>Golay, M.J.E.</u> Smoothing and Differentiation of Data by Simplified Least Squares Procedures. <u>Analytical Chemistry</u> 36 (8): 1627–1639. doi:10.1021/ac60214a04, 1964.
- [13] <a href="http://solardat.uoregon.edu/SolarPositionCalculator.html">http://solardat.uoregon.edu/SolarPositionCalculator.html</a>
- [14] Chunnilall C.J., Deadman A.J., Crane L. and Usadi E. *Metrologia*, 40: 192-195, 2003.
- [15] Williams D.C. Anal Chim Acta 380: 165-172, 1999.
- [16] Kuester M., Thome K., Krause K., Canham K., and Whittington E. Comparison of surface reflectance measurements from three ASD FieldSpec FR spectroradiometers and one ASD FieldSpec VNIR spectroradiometer, International Geoscience and Remote Sensing Symposium, Sydney, Australia, 2001.
- [17] Thome K. Sampling and uncertainty issues in trending reflectance-based vicarious calibration results, in Earth Observing Systems X, SPIE 5882: 397-407, 2005.
- [18] MacArthur A., MacLellan C., and Malthus T. Determining the FOV and directional response of field spectroradiometers. Proc. 5<sup>th</sup> EARSeL Workshop on Imaging Spectroscopy, 2007.
- [19] Milton E.J., Blackburn G.A., Rollin E.M., et al. Measurement of the spectral Directional Reflectance of Forest Canopies: A Review of Methods and a Practical Application, *Remote Sensing Reviews*, 10: 285-308, 1994.
- [20] Milton E.J., Rollin E.M. and Emery D.R. Advances in field spectroscopy, In: Advances in Environmental Remote Sensing, F.M. Danson and S.E. Plummer (editors), John Wiley & Sons, Chichester, UK, 1995.
- [21] Sandmeier, S.R. Acquisition of bidirectional reflectance factor data with field goniometers, *Remote Sensing of Environment*, 73, 3: 257-269, 2000.
- [22] Xavier Briottet, ONERA personal communication 2008.
- [23] Martonchik, J.V. Retrieval of surface directional reflectance properties using ground level multiangle measurements, *Remote Sensing of Environment*, 50, 3: 303-316, 1994.
- [24] Holben, B.N., Eck, T.F., Slutsker, I. et al. AERONET A federated instrument network and data archive for aerosol characterization. *Remote Sensing Environment*. 66: 1-16, 1998.

- [25] Halthore, R.N., Eck, T.F., Holben, B.N., Markham, B.L. Sunphotometric measurements of the atmospheric water vapour column abundance in the 940 nm band. *J. Geophys. Res.* 102: 4343-4352, 1997.
- [26] Cox, M.G. The evaluation of key comparison data. *Metrologia* 39: 589–595, 2002.
- [27] Collett, M.A., Cox, M.G., Esward, T.J., Harris, P.M. and Sousa, J.A., Aggregating measurement data influenced by common effects. *Metrologia* 44: 308–318, 2007.
- [28] FieldSpec 3 User Manual, ASD Document 600540 Rev. G, 2007.
- [29] Pegrum-Browning, H.M., Fox, N. and Milton, E. The NPL Gonio Radiometric Spectrometer System (GRASS), in Proceedings of the Remote Sensing and Photogrammetry Society Conference, University of Exeter 15-17 September 2008.
- [30] Kasten, F., and A.T. Young, Revised Optical air mass tables and approximation formula. *Applied Optics*, 28 (22): 4735-4738, 1989.
- [31] Pegrum, H.M., Woolliams, E., et al. Calibration of the NPL Transfer Standard Absolute Radiance Source (TSARS) and its use with GOME 2 FM3 Spectral Radiance measurements, 11th International Symposium on Remote Sensing, Sensors, Systems, and Next-Generation Satellites VIII, Proc. SPIE. 5570-72, Maspalomas, Spain: 503-514, 2004.
- [32] Woolliams E., Hunt T.M., N. J. Harrison, S. A. Windsor, N. P. Fox, J. R. Mountford, L. J. Rogers, and H. M. Pegrum. Improved Transfer Standard Sources for Calibration of Field Spectrometers Used for Earth Observation Applications. SPIE Conference Sensors, Systems, and Next Generation Satellites VIII, Crete, Proc SPIE 4881: 386-394, 2002.
- [33] Hunt, T. M. "Development of Sphere Sources with High Radiance Uniformity and Enhanced UV" Engineering Doctorate Thesis Brunel University and National Physical Laboratory UK, 2001.
- [34] Cocks T., Jenssen R., Stewart A., Wilson I. and Shields T.. The HyMap airborne hyperspectral sensor: the system, calibration and performance. Proc. 1st EARSEL Workshop on Imaging Spectroscopy, Zurich, 1998.